A PHOTOELECTRIC STUDY OF THREE SOUTHERN δ SCUTI STARS

Steven L. Morris

A thesis submitted as
partial requirement
for the degree of
Master of Science
from
Saint Mary's University

Department of Astronomy
Saint Mary's University
1979

TABLE OF CONTENTS

TABLE OF CONTENTS Continued

ACKNOWLEDGEMENTS

I would like to thank, first and foremost, Dr. David DuPuy for suggesting this research topic and acting as my thesis supervisor. My thanks also go to Rick Crowe for serving as my night assistant at the telescope while I was down at Las Campanas, and to the University of Toronto for providing the observing time. Thanks go also to Gary Collins for diligently rooting out the information needed to run UCLA's non-linear least-squares fit software package, which greatly improved the accuracy of my results. And finally, I would like to collectively thank Drs. David DuPuy, George Mitchell and Gary Welch for purchasing the Tektronix hardware (with National Research Council of Canada Operating Grants) that facilitated production of the diagrams in this thesis.

ABSTRACT

Differential photometric observations of the three δ Scuti stars AI, WZ and XX Sculptoris were obtained on ten nights during October 1978. None of these three stars had been extensively observed before, and the detailed nature of their variability was therefore unknown. The data obtained were then carefully examined for periodic behaviour. For AI Scl, no strict periodicities were found, although a tendency to pulsate with a period of 134 minutes was found. For WZ Scl, periods of 94.69 and 138.16 minutes were found and for XX Scl, periods of 70.413 and 73.944 minutes were found. Because the periods for XX Scl lead to a beat period of almost one day, the entire light curve could not be observed and there remains some ambiguity about the correct values of the periods. For all three stars, the periods and colours were interpreted using theoretical studies of δ Scuti stars. Based on this study, it is suggested that all three stars are pulsating in overtone pulsation, and not the fundamental mode. For XX Scl the two periods may be caused by a degenerate non-radial mode splitting into two distinct modes, due to rotation.

CHAPTER ONE

INTRODUCTION

1.1 The δ Scuti Stars

δ Scuti stars are variable stars that lie in the Cepheid instability strip, above the zero-age main sequence and below the RR Lyrae stars. These stars have periods that are less than 0.25 days, and the amplitudes of fluctuation are generally small. For many years a distinction was made between variables with amplitudes less tnan 0.3 magnitudes and those with amplitudes greater than 0.3 magnitudes. The former group was referred to as the δ Scuti stars, while the latter group was called the AI Velorum stars, the dwarf cepheids or the RRs stars. Unfortunately, both groups have been referred to in the past as dwarf cepheids, δ Scuti stars, or ultra-short-period variables, resulting in a very confused nomenclature. The problem was well summarized by Breger (1979), who points out that the distinction between the two groups is unrealistic and should be dropped. He suggests that all these stars be referred to as δ Scuti stars, and that practice will be followed here.

Almost all δ Scuti stars have amplitudes of 0.05 magnitudes or less, so that they are very difficult to identify and study. By 1956 only five δ Scuti stars were known. By 1973 more than 70 δ Scuti stars had been discovered, and the number now stands at approximately 250. Surveys indicate that about one-third of all stars in this

region of the HR diagram are δ Scuti stars. For several years it was suggested that the large-amplitude δ Scuti stars (then called AI Velorum stars) were below the Population I zero-age main sequence, and these stars were in a late evolutionary phase. It now seems that the true nature of all δ Scuti stars can be explained very simply: these stars are Population I A or F stars of approximately two solar masses, undergoing normal evolution on the main sequence or in the post-main-sequence shell hydrogen burning phase (Petersen 1975).

The best recent review of these stars is that by Breger (1979), which summarizes the main difficulties and discoveries in this field, and gives a large (but not comprehensive) catalogue of δ Scuti stars with their relevent properties. An earlier review article by Baglin et al. (1973) is now somewhat dated, but it gives an excellent discussion of the correct methods to be used for obtaining good photometric results for these stars, as well as a comprehensive list of all δ Scuti stars known at that time. Seeds and Yanchak (1972) produced an annotated catalogue and bibliography for δ Scuti stars, and it is still useful for finding references to the early literature and for its list of stars that are suspected to be δ Scuti variables. A recent review of the theoretical aspects of these stars was given by Petersen (1975), who summarized the information that stellar models have given us and the possible observational tests that could be performed to verify which models

most closely match the known δ Scuti stars.

Recent observations of stable periodicities in white dwarf stars (Nather 1978) have shown that the Cepheid instability strip extends from the classical Ceheids, past the δ Scuti stars and the main sequence and well into the white dwarf region of the HR diagram. The variability of these stars is due to pulsation, caused by instabilities in the He II and H ionization zones. Unlike the Cepheid variables however, many δ Scuti stars do not seem to have stable periodicities. Some observers have argued that many δ Scuti stars do not show strictly periodic behaviour (Breger 1979) and that any periods assigned to the stars are valid only in a statistical sense. Others, however (Fitch 1975), have insisted that these stars would show easily-explained periodic behaviour if only more strings of data were obtained. The problem is complicated by the very poor signal-to-noise ratios that are common in such data. Although it now seems that at least some δ Scuti stars are not strictly periodic, the question has not been fully resolved. Petersen (1975) has listed some of the many explanations that have been offered to explain this quasi-periodic behaviour. The most probable explanation is based on the fact that the time scale of convection in these stars is of the same order as the period of pulsation, so that a strong coupling between pulsation and convection can create non-linear atmospheric effects. Many of these stars are spectroscopic binaries, and for these stars it has been

suggested that tidal modulation or magnetic coupling with the companion star is responsible for the non-periodic light curves. Much more observational and theoretical work will be needed to resolve this problem completely.

One reason that so much effort has been spent trying to understand the observed periodicities is that these periods are potentially a very powerful tool in understanding the composition and structure of these stars. Many δ Scuti stars pulsate simultaneously at two periods, and the ratio of these two periods provides a dimensionless number, free from any dependence on the distance scale or interstellar absorption. Theory predicts that if the two periods observed are the fundamental radial mode and its first overtone, the period ratio will be approximately 0.76 . Unfortunately, the period ratio turns out to be rather insensitive to the particular stellar model used. If the mass of the model star is changed by a factor of two, or if the chemical composition is changed from extreme Population I to Population II, the period ratios change by only a few percent. A number of very accurately-determined period ratios will be necessary before the most accurate stellar models can be selected. Many authors have found values of the mean stellar density ρ for δ Scuti stars from the models, and calculated the pulsation constant $Q = P\sqrt{\rho}$ for the various periods P (in days) that have been observed. For pulsating stars, the values of Q for each mode of pulsation is independent of mass. Unfortunately, the values of Q

(Q_0 = 0.0333, Q_1 = 0.0252 etc.) are too closely spaced to provide unambiguous information about the modes of pulsation or the masses of δ Scuti stars.

1.2 Previous Work on AI, WZ and XX Sculptoris

The three δ Scuti stars investigated in this thesis are AI, WZ and XX Sculptoris; the positions and other designations of these stars and the nearby comparison stars used in this thesis are listed in Table 1-1. The four comparison stars were chosen because they were the brightest early-type stars near the three variables, and for convenience they will be referred to as "#1", "#2", "#3" and "#4" throughout this thesis. There were several reasons for investigating these three variables. Most importantly, they were known to be δ Scuti stars, but had not been adequately investigated to determine their periods or period ratios. Because they passed almost overhead at local midnight at the telescope during the observing run, they could be observed at low airmass throughout the night, giving the long strings of high-quality data that are necessary if periods are to be determined accurately. Lastly, all three variables were so close together in the sky that separate comparison stars were not necessary for each variable. It has occasionally happened that an observer has recorded the magnitudes of a variable and one nearby comparison star, only to find during the analysis that the comparison star was also a variable

TABLE 1-1

PROGRAM AND COMPARISON STARS

Star Name	HR Number	HD Number	α (1900)	δ (1900)	α (1979.0)	δ (1979.0)
AI Scl	359	7312	$1^h\ 08^m.2$	$-38^\circ\ 23'$	$1^h\ 11^m.8$	$-37^\circ\ 58'$
WZ Scl	431	9065	$1^h\ 24^m.2$	$-34^\circ\ 17'$	$1^h\ 27^m.8$	$-33^\circ\ 53'$
XX Scl	——	9133	$1^h\ 24^m.9$	$-33^\circ\ 50'$	$1^h\ 28^m.5$	$-33^\circ\ 26'$
#1	——	9093	$1^h\ 24^m.4$	$-33^\circ\ 52'$	$1^h\ 28^m.0$	$-33^\circ\ 28'$
#2	——	9027	$1^h\ 23^m.8$	$-33^\circ\ 32'$	$1^h\ 27^m.4$	$-33^\circ\ 08'$
#3	——	8833	$1^h\ 21^m.9$	$-33^\circ\ 04'$	$1^h\ 25^m.5$	$-32^\circ\ 40'$
#4	——	7269	$1^h\ 07^m.8$	$-38^\circ\ 47'$	$1^h\ 11^m.4$	$-38^\circ\ 22'$

and that the fluctuations of the individual stars were irretrievable. It was decided for this study that two comparison stars would be observed each night, so that this problem would almost certainly be avoided. There was only one night when just one comparison star was used, and on a few nights a third or fourth comparison star was occasionally measured also. All four stars were constant to the limits of observational accuracy.

The star AI Sculptoris has a curious observational history. The Third Supplement to the General Catalogue of Variable Stars (Kukarkin et al. 1976) lists this star as "δ Sct?", and gives V_{max} = 5.93, V_{min} = 5.98 and a period of 0.05 days (= 70 minutes). The reference given for this information is "Eggen, Aut. 1974 (preprint)", but a literature search of Eggen's publications on δ Scuti stars up to 1979 has not revealed this information. AI Scl is mentioned in one paper by Eggen (1976) where the following data are given:

$$V = 5.91$$
$$b-y = 0.176$$
$$m_1 = 0.190$$
$$c_1 = 0.809$$
$$\beta = 2.781$$
$$M_V = 2.3 \quad ,$$

and it is mentioned that forty spectrograms of the star had been taken, showing this to be a spectroscopic binary with a mean radial velocity of +8 km./sec. No mention of the amplitude or period of either the magnitude or the radial

velocity is given, however. The only source Eggen gives for these measures is Stokes (1972), but this paper, which gives four-colour and Hβ photometry of 511 bright southern early-type stars, does not mention AI Scl. The Catalogue of Bright Stars (Hoffleit 1964) lists this star's radial velocity of +8 km./sec. as variable, which is not surprising for a δ Scuti star. It does not state that it is a spectroscopic binary, however, and none of the three review articles mentioned in the first section of this thesis list AI Scl as a δ Scuti star. Thus the status of this star is quite unclear. Presumably Stokes measured this star but for some reason omitted it from his 1972 paper, but references to the binary nature and variability of this star were not found.

The situation for WZ Scl is much clearer. The review paper by Breger (1979) gives the following information for WZ Scl;

$$
\begin{aligned}
b-y &= 0.217 \\
(b-y)_o &= 0.199 \\
m_1 &= 0.144 \\
\beta &= 2.722 \\
c_1 &= 0.764 \\
M_v &= 1.55 \quad ,
\end{aligned}
$$

but does not give a reference for this information. The only information on the star's variability is from Demers

(1969), who observed it on three occasions in 1968 and 1969. The longest run of observations he obtained was on June 29, 1969 from 7:30 to 11:00 U.T. The data shown in his paper suggest variability, and from them he derives a period of 130 ± 4 minutes and an amplitude of 0.03 magnitudes. The observations on the other two dates were evidently not good enough to indicate values for the period or amplitude.

Demers is also the only source of information on the variability of XX Scl, as he had originally used it as a comparison star for WZ Scl. The light curve for XX Scl from 7:30 to 11:00 U.T. is given in Demers' paper and was used to derive a period of 66 ± 1 minutes and an amplitude of 0.035 magnitudes. He comments that this is a large amplitude for such a short-period star, and that only two other δ Scuti stars (HR 812 and HR 8494) have shorter periods. The comparison star used in his work was star #1 (HD 9093) and he found it to be constant in brightness.

The purpose of the present study is to obtain light curves of these stars, and analyze them as accurately as possible to find the periods, period ratios and amplitudes.

CHAPTER TWO

PHOTOELECTRIC PHOTOMETRY

2.1 Photoelectric Equipment

To obtain the data for this thesis, twenty-one nights of observing time were scheduled on the University of Toronto's 24-inch f/15 Cassegrain telescope at Las Campanas, Chile. This telescope is located at a latitude of $-29^{\circ}\ 00'\ 13''$, a longitude of $+70^{\circ}\ 42'.1$ and an altitude of 2282 meters. Originally it had been planned that uvby observations would be obtained, as most investigations of δ Scuti stars use intermediate-band photometry, but these filters were not available at the time of the observing run. Instead, UBV observations were obtained using an EMI9658R photomultiplier (extended S-20 photocathode), cooled with crushed dry ice that was placed in the photometer in the late afternoon and again at midnight.

Initially, a UBV photoelectric photometer with a 1P21 photomultiplier was used, but once observing was begun it became clear that the readings obtained were wildly unstable. The next five nights were spent tracking down and repairing faults in the system. After five nights, it was concluded that one source of instabilities was the photomultiplier itself. For the remainder of the observing session, the backup photometer with an EMI9658R photomultiplier was used.

Although this photometer was usable, it gave erratic readings on occasion, and it was found towards the end of

the observing run that erratic readings could be caused by simply touching the controls for the right ascension and declination. Evidently a shielding problem existed somewhere between the photomultiplier and the pulse amplifier. Erratic readings occasionally occurred even when no equipment was being operated, and on the night of October 23 such readings occurred continuously for several minutes with no apparent cause. These occurrences were infrequent enough that useful results could be obtained, but it does indicate that individual readings that seem peculiar should not be trusted.

Previous users of this photometer encountered serious light leaks. To prevent this, the sides of the photometer were wrapped with black felt cloth. The main source of unwanted light was from the lamp above the photometer printer, a few feet away from the photometer. On October 25 it was decided that a test should be made of the changes in readings when the photometer was exposed to stray light. At $04^h\ 51^m$ U.T., ten readings of dark sky were taken, which averaged 534 photoelectrons every ten seconds. When the lamp above the photometer printer was turned up to full intensity and pointed toward the photometer the average of ten readings was 562 photons every ten seconds, and when the light was turned off the average of ten readings was 533 photons every ten seconds. As readings on the program and comparison stars were never below 100,000 photons every ten seconds, it was concluded that the effects of any remaining

light leakage were insignificant.

A more important source of uncertainty in the measurements was round-off error. A single ten-second observation was printed out as a four-digit number, the last digit being an exponent. Thus, a reading of 2345 should be interpreted as 2.34×10^5 photons detected in a ten-second interval. While the first three digits could range between 100 to 999, it so happened that in this program of differential photometry the digits always fell between 100 and 300. A reading of 100 has an uncertainty of ±0.5 counts, and this leads to a magnitude uncertainty of 0.0054 . Similarly, a reading of 300 has an uncertainty of ±0.5 counts, leading to a magnitude uncertainty of 0.0018, and it was concluded that the average read-out uncertainty was about 0.0036 magnitudes. Because three readings were obtained instead of just one, the readout uncertainty was reduced by a factor of $\sqrt{3}$, to 0.0021 magnitudes. As this error applies to both the program stars and the comparison stars in differential photometry, this figure must be increased by a factor of $\sqrt{2}$, to 0.003 magnitudes.

Another source of uncertainty is shot noise, due to the random arrival of photons. If N photons arrive on the average during a certain interval, the expected fluctuation of the measured number of photons is $\sqrt{N}$. Thus the uncertainty in a measured magnitude is given by $-2.5 (\log N - \log (N + \sqrt{N}))$. Table 2-1 tabulates an estimate of the uncertainties in magnitudes caused by shot noise for the stars that were used in differential photometry,

Table 2-1

Estimates of uncertainties caused by shot noise, σ , in observations of the δ Scuti stars and their comparison stars. N gives the total number of counts in three ten-second integrations and σ gives the calculated uncertainty in magnitudes caused by shot noise.

TABLE 2-1

STAR	N	σ
AI	8.1×10^6	.0004
Comparison star for AI	4.5×10^5	.0016
WZ	4.5×10^6	.0005
Comparison star for WZ	4.2×10^5	.0017
XX	5.5×10^5	.0015
Comparison star for XX	4.2×10^5	.0017

assuming typical values of N. The uncertainty in a program star was taken to be the square root of the sum of the squares of the uncertainties for the program star and its comparison star. The resulting total uncertainties in the program stars due to shot noise is:

AI Scl: ±0.0016

WZ Scl: ±0.0018

XX Scl: ±0.0023 .

Because of round-off error and shot noise, a typical observation will have an estimated uncertainty of 0.0035 magnitudes. Other sources of error that may increase this lower limit are instabilities in the extinction coefficients, instabilities in the high-voltage supply, interference caused by inadequate signal shielding, and inexact centering of the star in the photometer aperture. Although the size of these extra errors is difficult to estimate, they are probably smaller than the shot noise and round-off errors mentioned above. This conclusion is supported by the light curves of the comparison stars shown in Figures 2-12 to 2-21, which show approximately this amount of scatter. It will also be shown in Section 5.2 that this is also the approximate amount of residual scatter in the light curves of WZ and XX Scl.

2.2 Reduction of All-Sky Photometry

2.2.1 General

On the night of October 24, UBV observations of the program and comparison stars were obtained using "all-sky" photometry (i.e. non-differential photometry). The values of V, B-V and U-B for the comparison and extinction stars were taken from Iriarte et al. (1965). A typical observation of one star in one colour consisted of three ten-second integrations on the stars, and two ten-second integrations on an adjacent region of sky. These two sets of numbers were averaged and the second subtracted from the first. A magnitude was then derived using the formula:
20 - 2.5 log(average star reading - average sky reading).
The number 20 was arbitrarily chosen. The sidereal time used is that of the second star reading in the blue filter. Airmass, X, was calculated using the relation:

$$X^{-1} = \sin(\phi)\sin(\delta) + \cos(\phi)\cos(\delta)\cos(HA),$$

where HA is the sidereal time minus the right ascension of the star, δ is the declination of the star and ϕ is the latitude of the telescope. For these observations,
$\phi = -29^{\circ}\ 00'\ 13''$.

2.2.2 Extinction Measurements

The v, b-v and u-b values (lower case denotes values untransformed to a standard system) for a star change with airmass according to the formulae:

$v_o = v - k_v X$,

$(u-b)_o = (u-b) - k_{ub} X$ and

$(b-v)_o = (b-v) - k_{bv} X$, where $k_{bv} = k'_{bv} + k''_{bv}(b-v)$.

v_o , $(u-b)_o$ and $(b-v)_o$ are the instrumental magnitude and colours corrected for extinction, and k_v, k_{ub}, k'_{bv} and k''_{bv} are the extinction coefficients. To obtain k_v, the v magnitudes of the extinction stars were plotted against airmass (shown in Figure 2-1) and were fitted by linear least squares to obtain a value of k_v for each star. The weighted average of these values was taken to be the overall value of k_v and was entered in Table 2-2. The values of (u-b) were similarly plotted against X in Figure 2-2 and used to derive a value of k_{ub} entered in Table 2-2. The value of k_{ub} for HR 718 was peculiar, but there seemed no reason not to include it. The point not used for HR 8858 (shown with a square symbol) was obtained during a short interval when erratic counts were suspected.

The b-v values for each extinction star were plotted against airmass to obtain k_{bv} and $(b-v)_o$ as shown in Figure 2-3. As $k_{bv} = k'_{bv} + k''_{bv}(b-v)_o$, the values of k_{bv} were plotted versus $(b-v)_o$ as shown in Figure 2-4 and the resulting least-squares fit on the weighted points gave the values for k'_{bv} and k''_{bv} entered in Table 2-2. For the observations of transformation, extinction and program and comparison stars, the values of v_o , $(b-v)_o$ and $(u-b)_o$ were calculated and entered in Tables 2-3, 2-4 and 2-5 respectively.

Figure 2-1

The v magnitudes of the extinction stars plotted versus airmass for October 24, 1978. The magnitude scale for HR 8841 is given on the right-hand side of the graph.

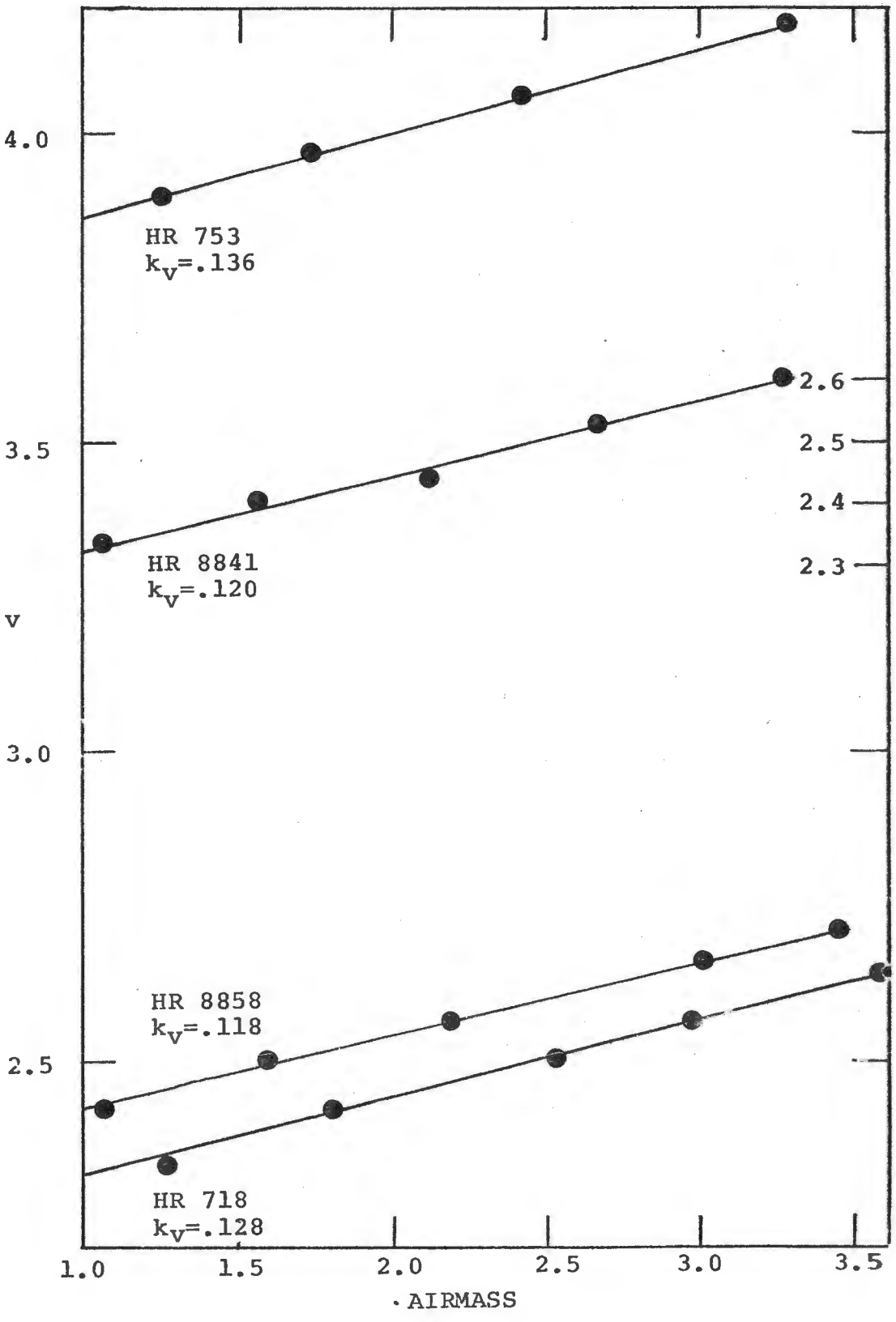
4.0
3.5
3.0
2.5
V
HR 753
k_V=.136
HR 8841
k_V=.120
HR 8858
k_V=.118
HR 718
k_V=.128
2.6
2.5
2.4
2.3
1.0
1.5
2.0
2.5
3.0
3.5
AIRMASS

Table 2-2

Extinction and transformation coefficients derived from October 24 data.

TABLE 2-2

Coefficient	Value
k_v	0.125 ± .007
k_{ub}	0.20 ± .03
k'_{bv}	0.137 ± .003
k''_{bv}	-0.016 ± .002
ε	-0.057 ± .02
ζ_v	2.17 ± .02
μ	1.06 ± .02
ζ_{bv}	-1.05 ± .02
ψ	1.22 ± .02
ζ_{ub}	-1.34 ± .02

Figure 2-2

The u-b colours of the extinction stars plotted versus airmass. The square indicates a data point for HR 8858 that was not used in the analysis.

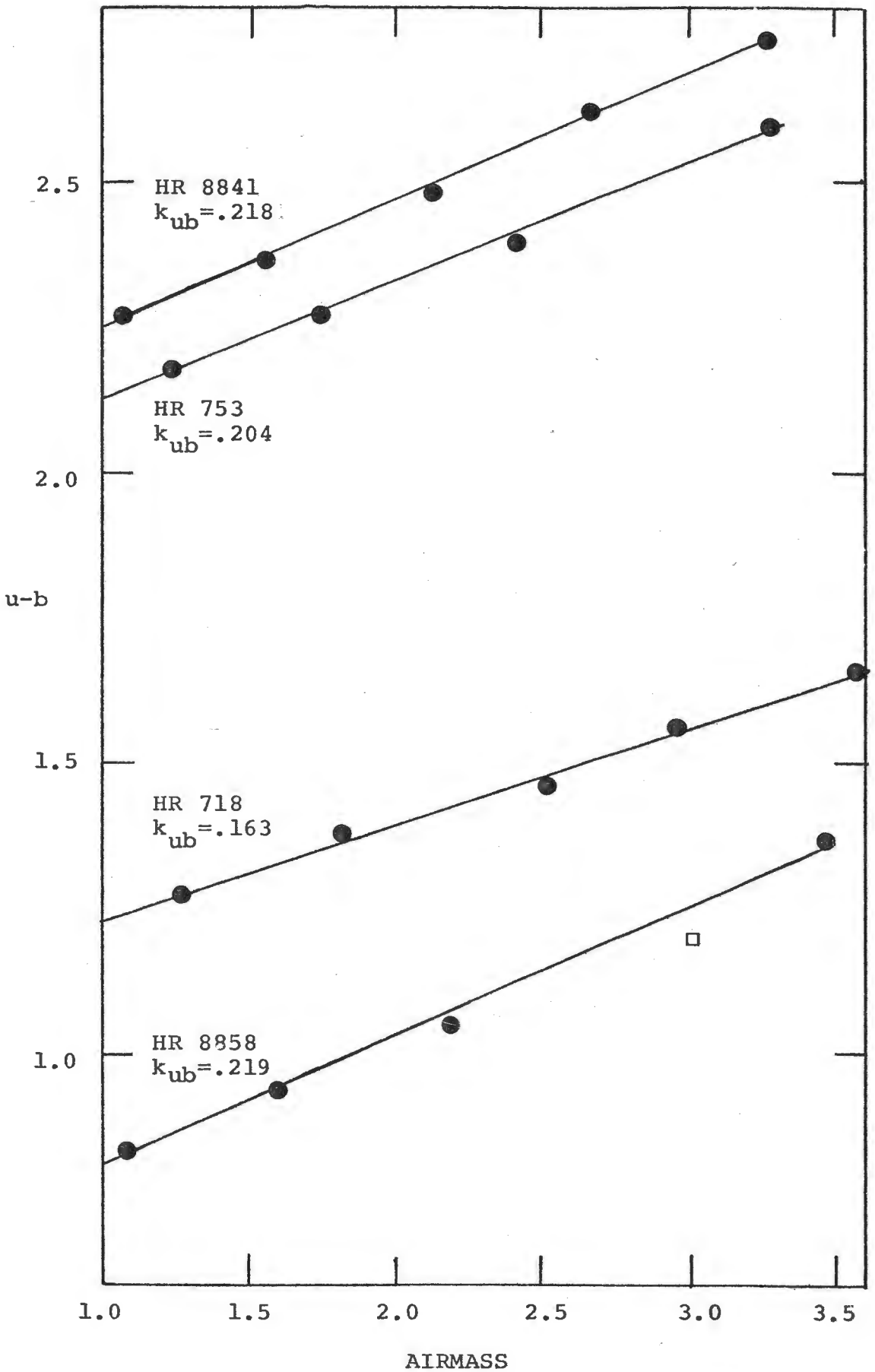
HR 8841
k_{ub}=.218
HR 753
k_{ub}=.204
HR 718
k_{ub}=.163
HR 8858
k_{ub}=.219
2.5
2.0
1.5
1.0
u-b
1.0
1.5
2.0
2.5
3.0
3.5
AIRMASS

Figure 2-3

The b-v colours of the extinction stars plotted versus airmass.

Figure 2-4

A diagram of the k_{bv} and $(b-v)_o$ values taken from Figure 2-3.

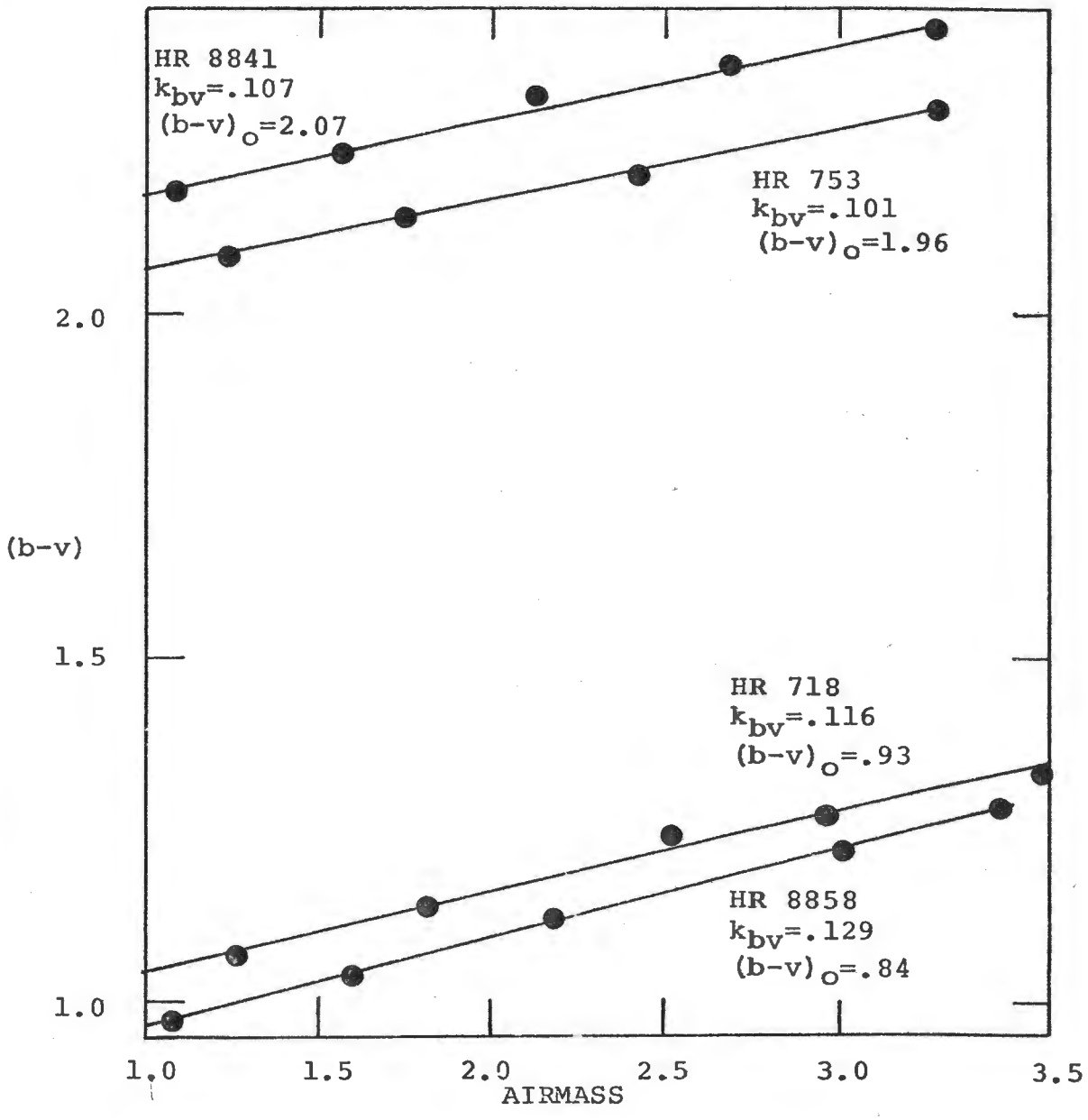
HR 8841
k_{bv}=.107
$(b-v)_o$=2.07
HR 753
k_{bv}=.101
$(b-v)_o$=1.96
HR 718
k_{bv}=.116
$(b-v)_o$=.93
HR 8858
k_{bv}=.129
$(b-v)_o$=.84
(b-v)
2.0
1.5
1.0
1.0
1.5
2.0
2.5
3.0
3.5
AIRMASS

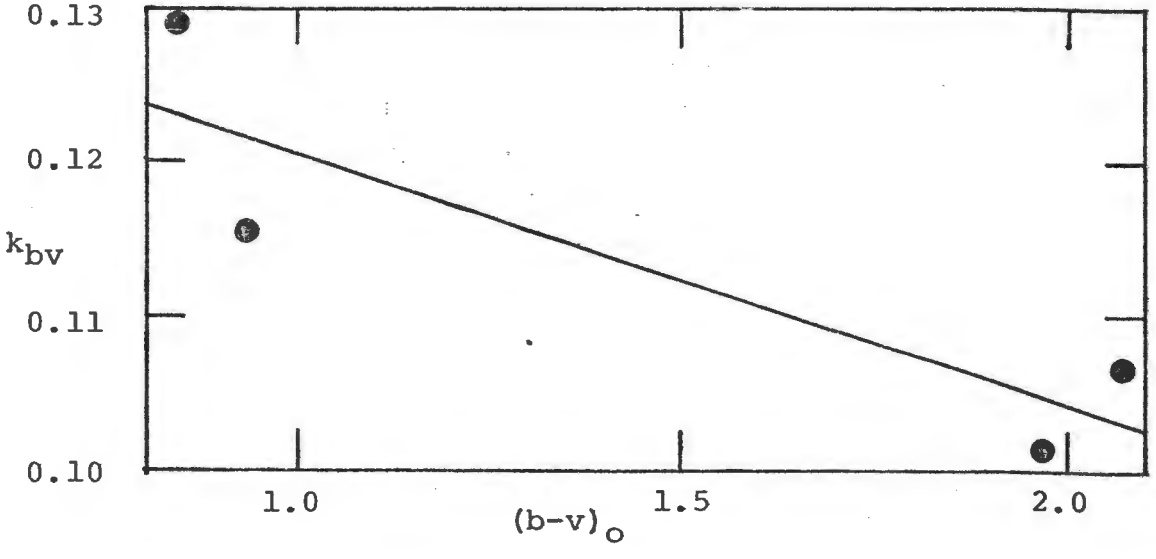
0.13
0.12
0.11
0.10
k_{bv}
1.0
1.5
2.0
$(b-v)_o$

TABLE 2-3

TRANSFORMATION STARS

HR	SIDEREAL TIME	AIRMASS	v	b-v	u-b	v_o	$(b-v)_o$	$(u-b)_o$	V	ΔV
8060	22:54.5	1.121	2.860	1.281	1.437	2.720	1.149	1.213	4.822	-.018
8278	22:59.5	1.080	1.786	1.353	1.481	1.651	———	1.265	———	———
8418	23:04.6	1.067	2.311	1.026	1.089	2.178	0.695	0.876	4.294	.044
8573	23:09.6	1.068	2.829	1.069	1.259	2.696	0.939	1.045	4.810	-.010
8628	23:15.6	1.010	2.207	0.991	0.979	2.081	0.867	0.777	4.199	.039
612	04:39.5	1.204	2.700	0.982	0.930	2.550	0.834	0.689	4.670	-.020
708	04:44.5	1.243	2.899	1.112	1.287	2.744	0.961	1.038	4.856	-.034
740	04:49.5	1.216	2.785	1.555	1.333	2.633	1.417	1.090	4.719	-.021
811	04:54.5	1.205	2.293	1.002	0.962	2.142	0.854	0.721	4.260	.010
818	04:58.5	1.183	2.517	1.573	1.352	2.369	1.439	1.115	4.454	-.006
1173	05:03.5	1.053	2.269	1.493	1.314	2.137	1.372	1.103	4.226	-.004
1213	05:11.6	1.052	2.623	1.002	0.926	2.492	0.873	0.716	4.609	-.031
1240	05:15.6	1.050	2.646	0.999	0.977	2.515	0.870	0.767	4.632	-.028
1298	05:21.6	1.130	2.122	1.383	1.418	1.981	———	1.192	———	———
1520	05:26.6	1.128	2.089	0.967	0.826	1.948	0.828	0.600	4.068	.048
1560	05:31.6	1.106	2.427	1.340	1.435	2.289	1.210	1.214	4.387	-.003
1617	05:36.6	1.090	2.791	0.965	0.729	2.655	0.831	0.511	4.775	-.015
1621	05:41.6	1.026	2.888	1.066	1.204	2.760	0.941	0.999	4.873	-.037
1679	05:47.7	1.080	2.290	0.936	0.586	2.155	0.802	0.370	4.276	.006
1696	05:52.7	1.062	2.486	1.006	0.992	2.353	0.876	0.780	4.470	.040
1705	05:57.7	1.059	2.390	1.014	0.983	2.258	0.884	0.771	4.375	.015
1789	06:03.7	1.183	2.939	0.970	0.596	2.791	0.824	0.359	4.911	-.039
1861	06:08.7	1.141	3.332	0.983	0.582	3.189	0.842	0.354	5.308	-.042
1934	06:25.8	1.221	2.585	1.050	0.695	2.432	0.901	0.451	4.548	-.042

TABLE 2-4

EXTINCTION STARS

HR	SIDEREAL TIME	AIRMASS	v	b-v	u-b	v_o	$(b-v)_o$	$(u-b)_o$	V	ΔV
718	22:02.4	3.580	2.647	1.336	1.654	2.200	0.898	0.938		
753	22:13.4	3.284	4.171	2.294	2.596	3.761	1.949	1.939		
718	22:19.4	2.967	2.564	1.272	1.564	2.193	0.910	0.971		
718	22:37.5	2.525	2.506	1.245	1.467	2.190	0.938	0.962		
753	22:46.5	2.414	4.057	2.206	2.397	3.755	1.953	1.914		
718	23:32.6	1.798	2.420	1.139	1.378	2.195	0.920	1.018		
753	23:41.7	1.740	3.968	2.140	2.271	3.751	1.957	1.923		
718	02:45.2	1.263	2.348	1.069	1.273	2.190	0.915	1.020	4.305	0.025
753	02:50.2	1.236	3.891	2.086	2.178	3.737	———	———		
8841	23:21.6	1.063	2.339	2.178	2.271	2.206	———	———		
8858	23:25.6	1.063	2.427	0.975	0.844	2.294	0.844	0.631	4.411	0.011
8841	02:32.1	1.562	2.403	2.232	2.370	2.208	2.071	2.058		
8858	02:38.1	1.589	2.500	1.036	0.940	2.301	0.840	0.622		
8841	03:26.3	2.122	2.440	2.315	2.487	2.175	2.097	2.063		
8858	03:32.3	2.181	2.563	1.122	1.053	2.290	0.854	0.617		
8841	03:54.4	2.672	2.527	2.360	2.621	2.193	2.085	2.087		
8858	04:08.4	3.011	2.661	1.220	1.195	2.285	0.849	0.593		
8841	04:13.4	3.267	2.608	2.409	2.747	2.200	2.072	2.094		
8858	04:20.4	3.465	2.714	1.284	1.366	2.281	0.858	0.673		

TABLE 2-5

PROGRAM AND COMPARISON STARS

STAR	SIDEREAL TIME	AIRMASS	v	b-v	u-b	v_o	$(b-v)_o$	$(u-b)_o$
WZ	23:49.7	1.074	4.553	1.434	1.360	4.419	1.310	1.145
WZ	00:05.7	1.052	4.562	1.428	1.359	4.431	1.306	1.149
WZ	00:18.8	1.038	4.567	1.428	1.354	4.437	1.308	1.146
WZ	00:37.8	1.021	4.570	1.430	1.350	4.442	1.312	1.146
WZ	00:54.9	1.011	4.565	1.426	1.346	4.439	1.309	1.144
WZ	01:12.9	1.005	4.553	1.423	1.343	4.427	1.307	1.142
WZ	01:37.0	1.004	4.539	1.418	1.350	4.414	1.302	1.149
WZ	01:51.0	1.007	4.543	1.419	1.350	4.417	1.303	1.149
WZ	02:04.1	1.013	4.539	1.425	1.351	4.412	1.308	1.148
WZ	02:17.1	1.021	4.546	1.429	1.347	4.418	1.311	1.143
XX	23:55.7	1.066	6.879	1.360	1.436	6.746	1.236	1.223
XX	00:09.7	1.048	6.873	1.356	1.434	6.742	1.234	1.224
XX	00:22.8	1.034	6.879	1.357	1.403	6.750	1.236	———
XX	00:41.8	1.018	6.798	1.429	1.429	———	———	1.225
XX	00:59.9	1.009	6.862	1.344	1.438	6.736	1.226	1.236
XX	01:17.9	1.004	6.858	1.347	1.432	6.733	1.230	1.231
XX	01:42.0	1.004	6.871	1.353	1.432	6.746	1.236	1.231
XX	01:55.0	1.008	6.863	1.348	1.434	6.737	1.230	1.232
XX	02:08.1	1.014	6.854	1.356	1.422	6.727	1.238	1.219
XX	02:21.1	1.023	6.860	1.354	1.432	6.732	1.235	1.227

TABLE 2-5 cont.

STAR	SIDEREAL TIME	AIRMASS	v	b-v	u-b	v_o	$(b-v)_o$	$(u-b)_o$
AI	00:00.7	1.047	3.938	1.339	1.413	3.807	1.277	1.204
AI	00:13.7	1.035	3.934	1.398	1.409	3.805	1.278	1.202
AI	00:32.8	1.023	3.922	1.391	1.409	3.794	1.272	1.204
AI	00:50.9	1.015	3.923	1.394	1.406	3.796	1.276	1.203
AI	01:03.9	1.013	3.924	1.393	1.406	3.797	1.275	1.203
AI	01:21.9	1.013	3.916	1.389	1.406	3.789	1.271	1.203
AI	01:46.0	1.020	3.912	1.396	1.411	3.785	1.278	1.207
AI	01:59.0	1.028	3.919	1.397	1.414	3.791	1.278	1.208
AI	02:13.1	1.038	3.926	1.400	1.406	3.796	1.280	1.198
AI	02:26.1	1.051	3.920	1.401	1.408	3.789	1.279	1.198
#1	00:27.8	1.029	7.165	2.152	1.990	7.036	2.046	1.784
#1	00:45.8	1.016	7.164	2.153	1.956	7.037	2.048	1.753
#2	03:07.2	1.076	7.285	1.283	1.443	7.151	1.156	1.228
#2	03:16.2	1.091	7.283	1.262	1.473	7.147	1.133	1.255
#3	04:29.4	1.293	7.366	1.761	1.447	7.204	1.618	1.188
#3	04:33.5	1.309	7.370	1.755	1.482	7.206	1.610	1.220
#4	01:08.9	1.014	7.066	1.592	1.327	6.939	1.478	1.124
#4	01:25.9	1.015	7.063	1.592	1.317	6.936	1.478	1.114

2.2.3 Transformation to Standard UBV System

For all stars the values of V, B-V and U-B are calculated from the values of v_o , $(b-v)_o$ and $(u-b)_o$ using the formulae:

$$V = v_o + \varepsilon(b-v)_o + \zeta_v$$

$$(B-V) = \mu(b-v)_o + \zeta_{bv}$$

$$(U-B) = \psi(u-b)_o + \zeta_{ub} \quad .$$

The observations of the transformation stars and the extinction stars at low airmass were plotted in Figures 2-5, 2-6 and 2-7 and fitted using linear least squares. This gave the values for the transformation coefficients given in Table 2-2.

For all stars, values of V were obtained using the formula $V = v_o + \varepsilon(b-v)_o + \zeta_v$ and listed in Tables 2-3, 2-4 and 2-6. For the transformation stars and the two extinction star observations that were taken at small airmass, values of ΔV in the sense of V(Johnson)- V(observed) were calculated and entered in Tables 2-3 and 2-4. The observations of the extinction stars at large airmass were not used for estimating the residuals, because the large airmass made their values of V(observed) somewhat less certain than the values for the transformation stars. The plot of ΔV versus sidereal time as given in Figure 2-8 did not show any systematic trends, so the calculated values of V could be accepted without further corrections. Table 2-6 shows the non-differential

Figure 2-5

$V-V_o$ versus $(b-v)_o$ for the transformation stars.

Figure 2-6

B-V versus $(b-v)_o$ for the transformation stars. The squares indicate data points that appeared suspicious and were not used in the analysis.

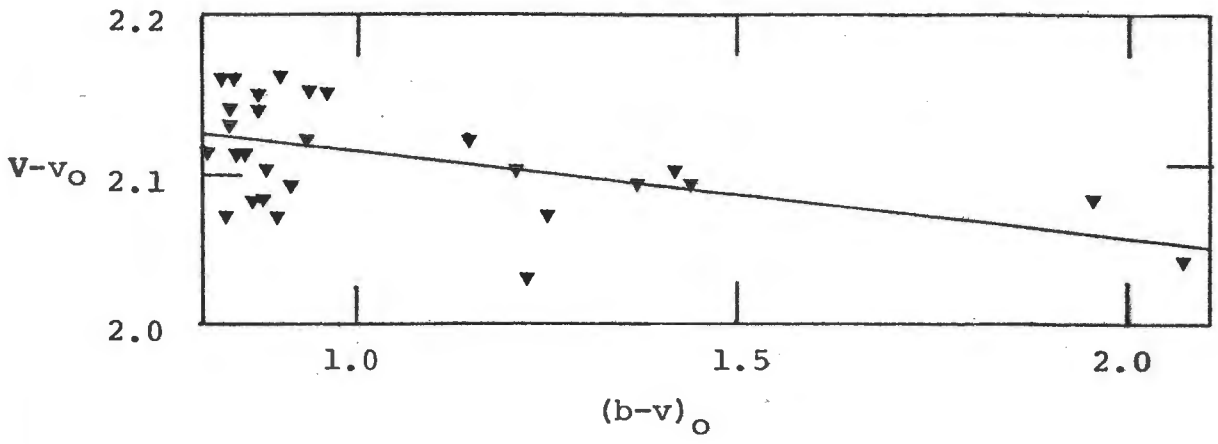
2.2
2.1
2.0
V-V$_o$
1.0
1.5
2.0
(b-v)$_o$

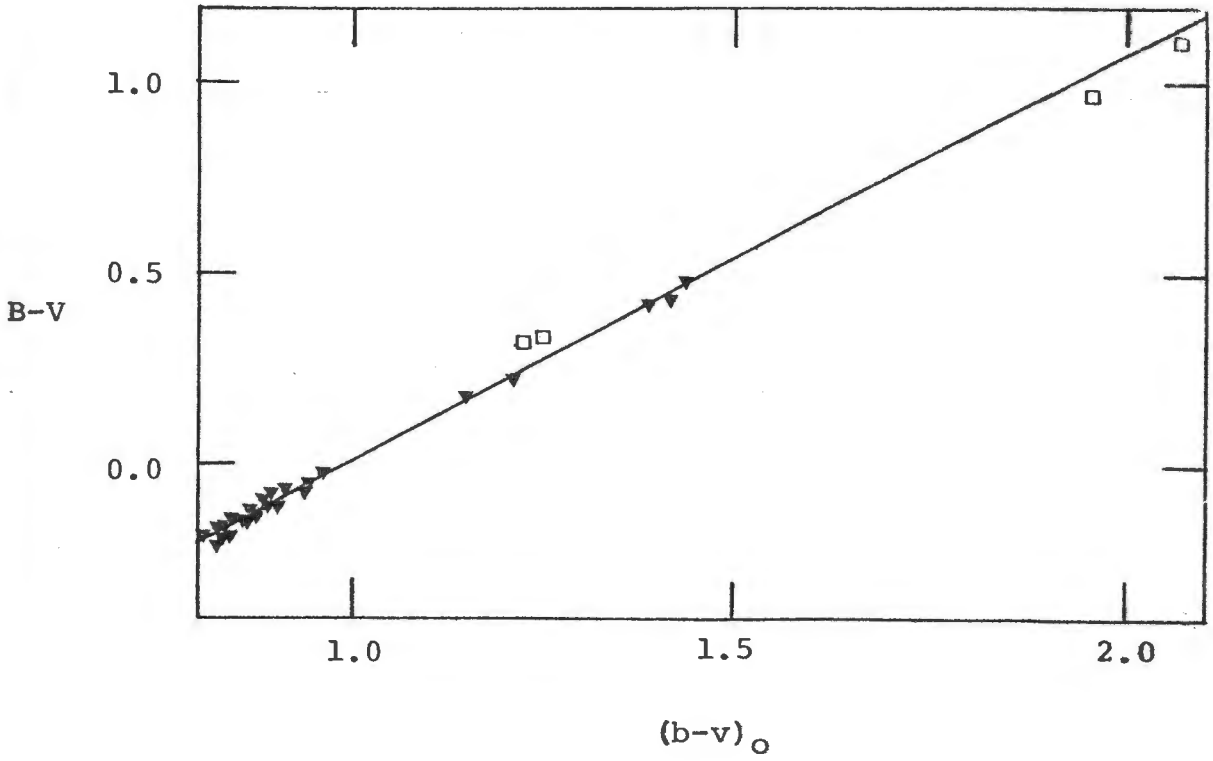
1.0
0.5
0.0
B-V
1.0
1.5
2.0
(b-v)$_o$

Figure 2-7

U-B versus $(u-b)_o$ for the transformation stars. The squares indicate data points that were not used in the final analysis.

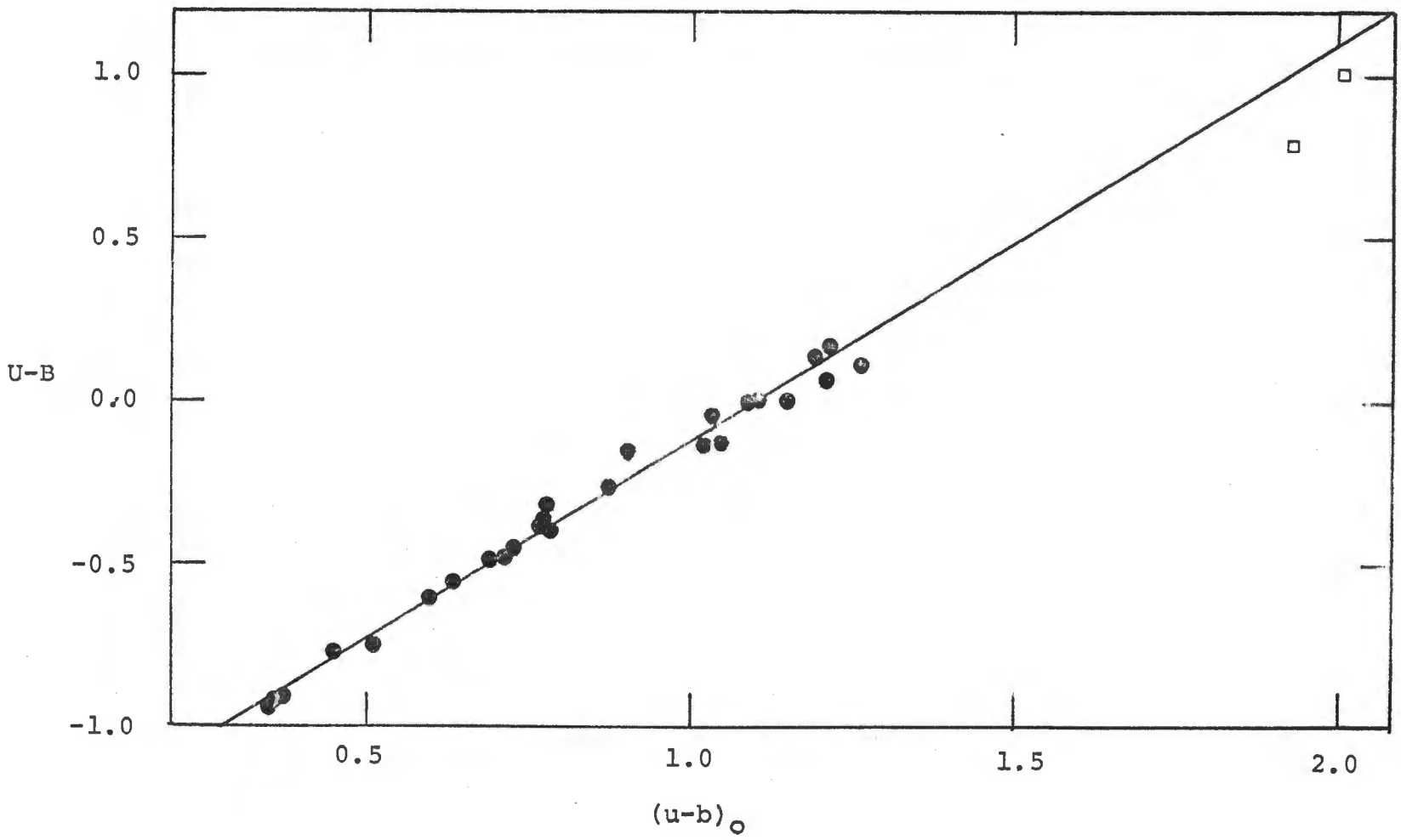
1.0
0.5
0.0
-0.5
-1.0
U-B
0.5
1.0
1.5
2.0
(u-b)o

Figure 2-8

The residuals of V versus time. No trends are evident in these residuals.

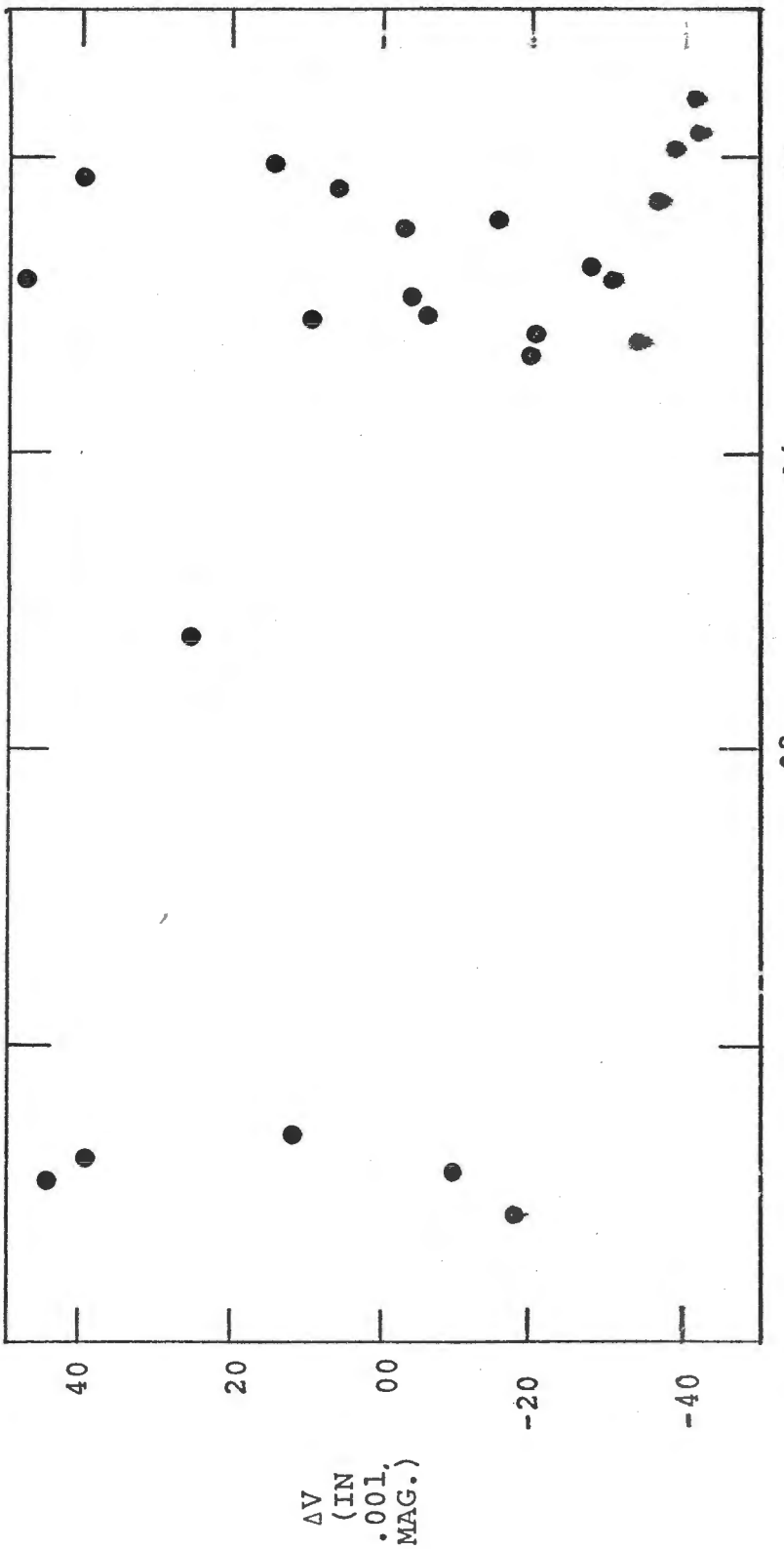
40
20
00
-20
-40
ΔV
(IN
.001
MAG.)
22
00
02
04
06
SIDEREAL TIME

TABLE 2-6

VARIABLE AND COMPARISON STARS

STAR	SIDEREAL TIME	V_{obs}	$(B-V)_{obs}$	$(U-B)_{obs}$
WZ	23:49.7	6.511	.343	.053
WZ	00:05.7	6.524	.339	.058
WZ	00:18.8	6.530	.341	.055
WZ	00:37.8	6.534	.345	.055
WZ	00:54.9	6.532	.342	.052
WZ	01:12.9	6.520	.340	.050
WZ	01:37.0	6.507	.334	.058
WZ	01:51.0	6.510	.335	.058
WZ	02:04.1	6.505	.341	.057
WZ	02:17.1	6.510	.344	.051
XX	23:55.7	8.843	.264	.148
XX	00:09.7	8.839	.262	.149
XX	00:22.8	8.847	.264	———
XX	00:41.8	———	———	.151
XX	00:59.9	8.833	.253	.164
XX	01:17.9	8.830	.258	.158
XX	01:42.0	8.843	.264	.158
XX	01:55.2	8.834	.258	.159
XX	02:08.1	8.824	.266	.143
XX	02:21.1	8.829	.263	.153
AI	00:00.7	5.901	.308	.125
AI	00:13.7	5.899	.309	.123
AI	00:32.8	5.889	.302	.125
AI	00:50.9	5.890	.307	.124
AI	01:03.9	5.891	.306	.124
AI	01:21.9	5.884	.301	.124
AI	01:46.0	5.879	.309	.129
AI	01:59.0	5.885	.309	.130
AI	02:13.1	5.890	.311	.118
AI	02:26.1	5.883	.310	.118
#1	00:27.8	9.087	1.126	.830
#1	00:45.8	9.087	1.128	.793
#2	03:07.2	9.252	.179	.154
#2	03:16.2	9.250	.155	.187
#3	04:29.4	9.279	.671	.106
#3	04:33.5	9.281	.662	.145
#4	01:08.9	9.022	.522	.028
#4	01:25.9	9.019	.522	.016

magnitudes and colours for the variable and comparison stars observed on October 24. Table 2-7 shows the differences in B-V and U-B between the tabulated values and the values found on this night. From the residuals given in Tables 2-3, 2-4 and 2-7, one obtains the following standard deviations: $\Delta V = 0.029$, $\Delta(B-V) = 0.017$, $\Delta(U-B) = 0.031$.

2.2.4 Results for AI, WZ and XX Sct

The results in Table 2-6 were used to make Figures 2-9, 2-10 and 2-11. From these colour-colour and colour-magnitude diagrams it is clear that because these were non-differential observations, any regular fluctuations were much smaller that the noise. A simple average of the results in Table 2-6 gives the final result of this night of photometry, the average colours and magnitudes of the program and comparison stars, as given in Table 2-8. Although the remainder of this thesis will use magnitude differences and not magnitudes, the results can be easily converted, using the values in Table 2-8.

TABLE 2-7

TRANSFORMATION STARS

HR	$(B-V)_{obs}$	$\Delta(B-V)$	$(U-B)_{obs}$	$\Delta(U-B)$
8060	.172	-.008	.136	.076
8278	———	———	.199	-.011
8418	-.099	-.029	-.274	-.004
8573	-.052	.008	-.068	.052
8628	-.129	-.009	-.394	-.072
612	-.164	-.004	-.501	-.011
708	-.028	-.008	-.077	-.037
740	.457	.017	-.014	-.014
811	-.142	-.002	-.462	-.012
818	.480	.000	.017	.017
1173	.409	-.011	.002	.002
1213	-.122	.008	-.468	.012
1240	-.125	.015	-.406	-.016
1298	———	———	.109	-.031
1520	-.170	-.010	-.609	-.009
1560	.236	.006	.137	-.033
1617	-.167	.023	-.718	.032
1621	-.050	.000	-.124	.026
1679	-.198	-.008	-.889	.021
1696	-.119	-.029	-.391	.009
1705	-.110	-.020	-.401	-.031
1789	-.174	.036	-.902	.018
1861	-.155	.035	-.909	.021
1934	-.092	.018	-.791	-.021
718	-.077	-.017	-.099	.031
8858	-.153	-.013	-.572	-.022

Figures 2-9, 2-10 and 2-11

The light curve, colour-magnitude and colour-colour diagrams for AI,WZ and XX Scl respectively on the night of October 24.

FIGURE 2-9: AI SCL

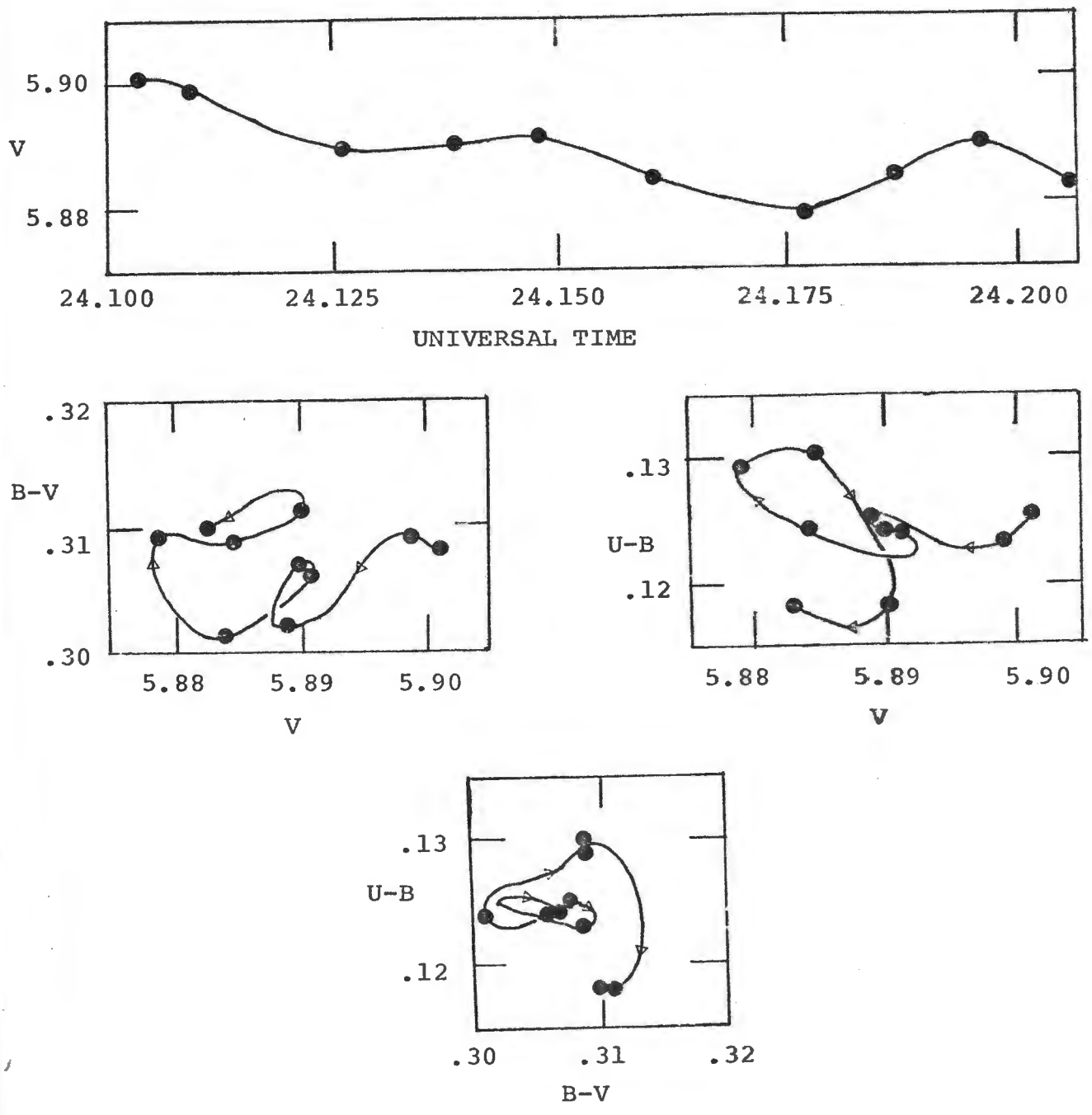

FIGURE 2-10: WZ SCL

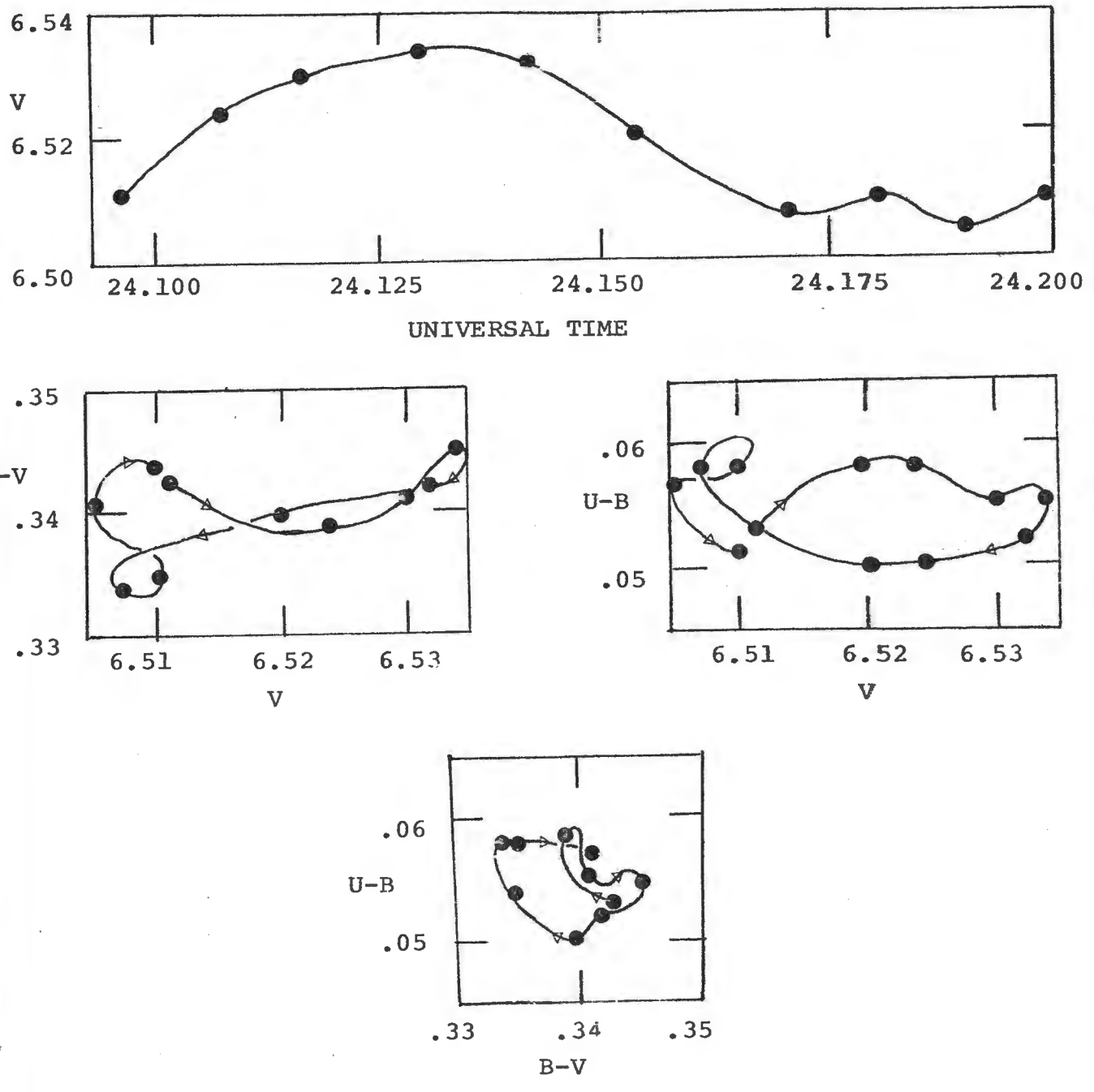

FIGURE 2-11: XX SCL

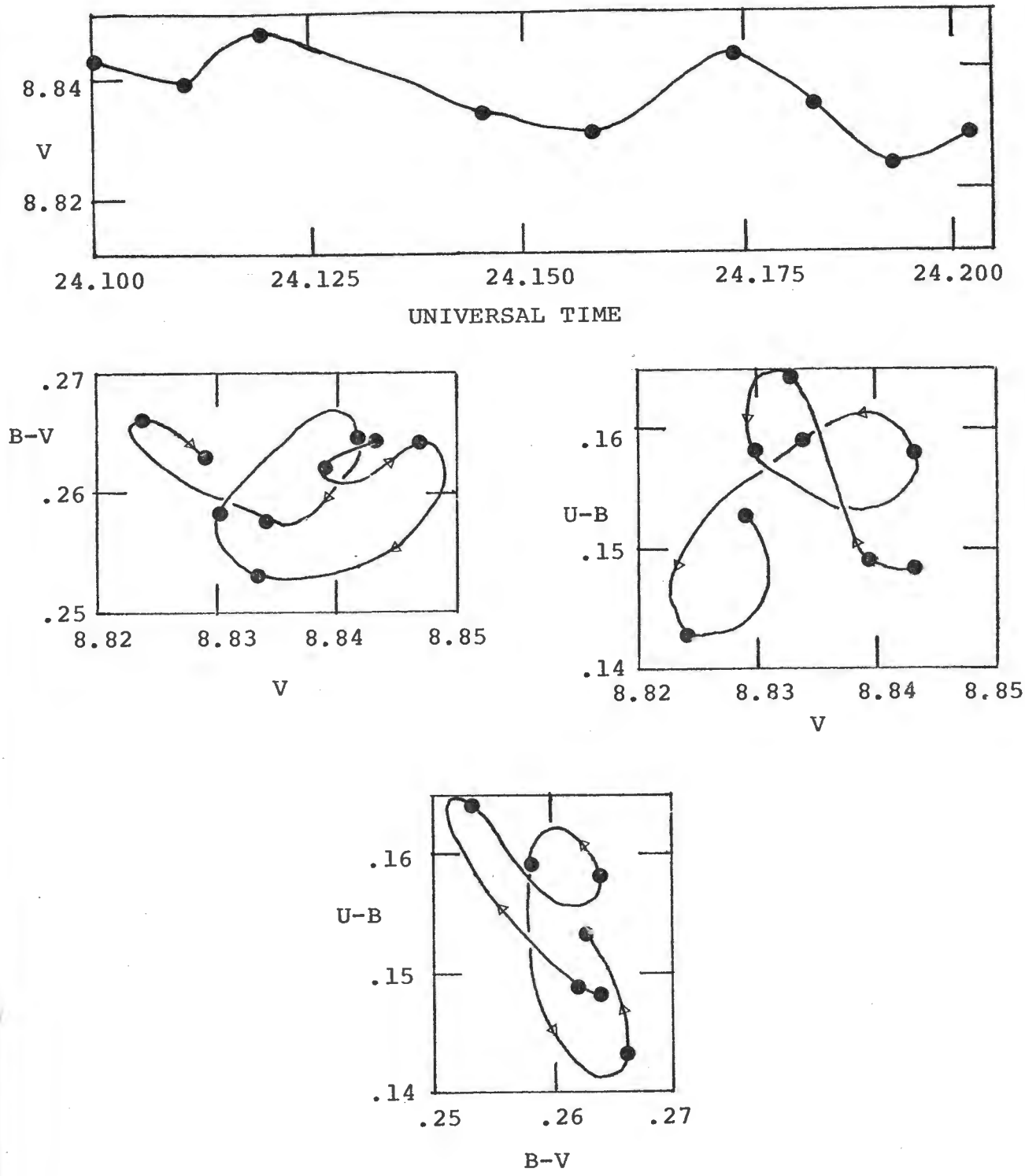

Table 2-8

The averaged magnitudes and colours of the variables and comparison stars found on the night of October 24. The standard deviations for these magnitudes are:

$$V = 0.03$$

$$B-V = 0.02$$

$$U-B = 0.03$$

TABLE 2-8

STAR	<V >	<B-V >	<U-B >
AI	5.89	0.31	0.12
WZ	6.52	0.34	0.06
XX	8.84	0.26	0.15
#1	9.09	1.13	0.81
#2	9.25	0.17	0.17
#3	9.28	0.67	0.13
#4	9.02	0.52	0.02

2.3 Reduction of Differential Photometry

Differential photometry of the three variable stars was obtained on ten nights, using the V filter and an 18" aperture in the photometer. A typical measurement consisted of three ten-second integrations on the star, and two ten-second integrations on an adjacent region of the sky. Occasionally the star would drift out of the aperture or spurious counts would appear, so that one of the readings would be unusable. When that occurred, the averages of the other readings were utilized. The Universal Time for each measurement was taken to be the time of the second of the three star readings, which was printed out to the nearest minute. The clock was checked against the WWV short-wave time signals three times during the observing run; it was never more than a few seconds off.

To analyze these data the observations were punched onto computer cards and read into permanent files. The three star readings and the two sky readings were averaged and converted to magnitudes. Corresponding airmass, Universal Time, and sidereal time data were also made available for data reduction. To convert to the Julian Date from the dates based on Universal Time used in this thesis, add 2443781.5 . Note that the time used in this thesis has not been converted to heliocentric time, and this correction must be made if these observations are linked to observations taken at some other time. Visual extinction coefficients for each night were determined by a least-squares fit to

magnitude versus airmass data for star #1, the only comparison star observed every night. The resulting values for the visual extinction coefficient are shown in Table 2.9, along with other data relating to observing conditions. The visual extinction coefficient for the night of October 24 was taken from the results of the previous section. A zero-point correction of 2.07 magnitudes was added to the instrumental magnitudes to force the weighted average to equal 9.09, as found in Section 2.2.4 . The large standard deviation in Table 2-9 for the night of October 23 was not due to random fluctuations, but was instead due to a slow increase in the sky's transparency over the course of the night, from $k_v = .15$ to $k_v = .11$. In differential photometry, such an increase does not have a significant effect on the final results although the random fluctuations will likely be slightly larger, compared to nights of lower and more constant extinction.

Using the nightly values for the extinction, a third set of data files was created. In each data file, each observation contained the name of the star, the Universal Time in fractions of a day, and the instrumental magnitude corrected to zero airmass. These results were then plotted on a Tektronix Model 4662 x-y digital plotter, and examined. On the basis of this examination several discordant data points were discarded. An examination of the light curves of the four comparison stars indicated that if they were oscillating at all, the amplitudes of oscillation were much

TABLE 2-9

OBSERVING CONDITIONS

Date (October)	Extinction Coefficient	V for Star #1	Standard Deviation for Star #1	Temperature (Centigrade)	Wind (mph)	Humidity (per cent)	Seeing (")
14	.122	9.10	.012	10°	NONE	30	1-3
15	.148	9.08	.008	11°	NONE	35	1-2
16	.144	9.09	.006	12°	NONE	38	1-2
22	.125	9.08	.009	14°	10-30	35	1-3
23	.132	9.10	.021	15°	15-35	20	2-7
24	.125	9.09	---	13°	NONE	30	1-2
25	.166	9.07	.004	14°	0-5	30	1-2
26	.146	9.09	.003	15°	NONE	20	2-3
27	.123	9.10	.010	15°	0-10	20	1-3
28	.114	9.11	.007	14°	NONE	30	2-3
29	.125	9.10	.007	14°	0-15	25	2-3

smaller than the amplitudes of the three variable stars.

The final operation that was needed to bring the data files into usable form for period-searching was to subtract the magnitudes of the comparison stars from those of the variable stars. This was necessary to correct for minor fluctuations in the atmosphere or in the response of the photometer. It was decided that star #1 would be used as the comparison star for both WZ and XX Sculptoris, as all three stars were close together in the sky, and that star #4 would be used as the comparison star for AI Sculptoris. Star #2 and star #3 had been observed on only three nights as a check on the stability of the other comparison stars, and trying to use them would have been an unadvisable complication. The comparison stars were, of course, observed at slightly different times than the program stars. For each observation of a program star, the one immediately previous and the one immediately following comparison star observations were linearly interpolated to give a comparison star magnitude. At the end-points of the data, the nearest two points were extrapolated to provide the comparison star magnitude. A more complicated fitting routine, such as a quadratic fit was considered, but this was deemed unnecessary, because the comparison star observations were spaced closely enough to accurately follow any reasonable fluctuations. Each observation now consisted of the variable star's name, the Universal Time in fractions of a day, and the difference between the magnitude of the variable and the interpolated

magnitude of the comparison star. For convenience in handling the data, these files were then arranged so that the nightly observations of each variable star were in separate files. In addition, a data file for each variable was created that contained all the observations of that variable. It is these data files that were used in the period-searching techniques given in Chapters Four and Five. The contents of these data files are given in Appendices 7.1, 7.2 and 7.3 and are shown in Figures 2-12 to 2-21. The lines drawn through the data points will be explained in Section 5.2 .

Because some period-searching techniques require equally-spaced data, an extra set of nightly data files was created. In each new data file, the observations were placed at intervals of .004 days (=5.76 minutes) with the time span of the new data file completely within the span of the old file. For example, if the observation times of the first and the last data points in an old data file were at 0.009 and 0.362, the first and last observation times in the new data file would be 0.012 and 0.360 . The new data files were created by a computer program that would linearly interpolate between the observations given in the old data files. The justification for using linear interpolation is the same as that given in the previous paragraph.

On several nights, a break occurred in the data while the dry ice was replaced in the photometer. Because a linear interpolation across such a break would not give a true

Figures 12 to 21

Data points obtained on the photometric nights between October 9 and 29,1978. The x axis gives the Universal Time in fractions of a day. The y axis has been arbitrarily shifted, and does not represent the differential magnitude of any star. The size of the tic marks represent error bars of ±.005 magnitudes, approximately the typical error found for the data points. For the stars WZ and XX Scl, the curves drawn are given by the formulae;

$$f(t) = -2.5623 + .0057 \sin(95.554t + 1.8) + .0078 \sin(65.485t + 4.0)$$, and

$$f(t) = -.2445 + .0088 \sin(128.50t + 0.0) + .0075 \sin(122.36t + 1.3)$$

respectively, as explained in Section 5.2 . For the other stars, the data points are connected with straight lines. The horizontal lines through the data points represents the average magnitude of the star for that night.

FIGURE 2-12

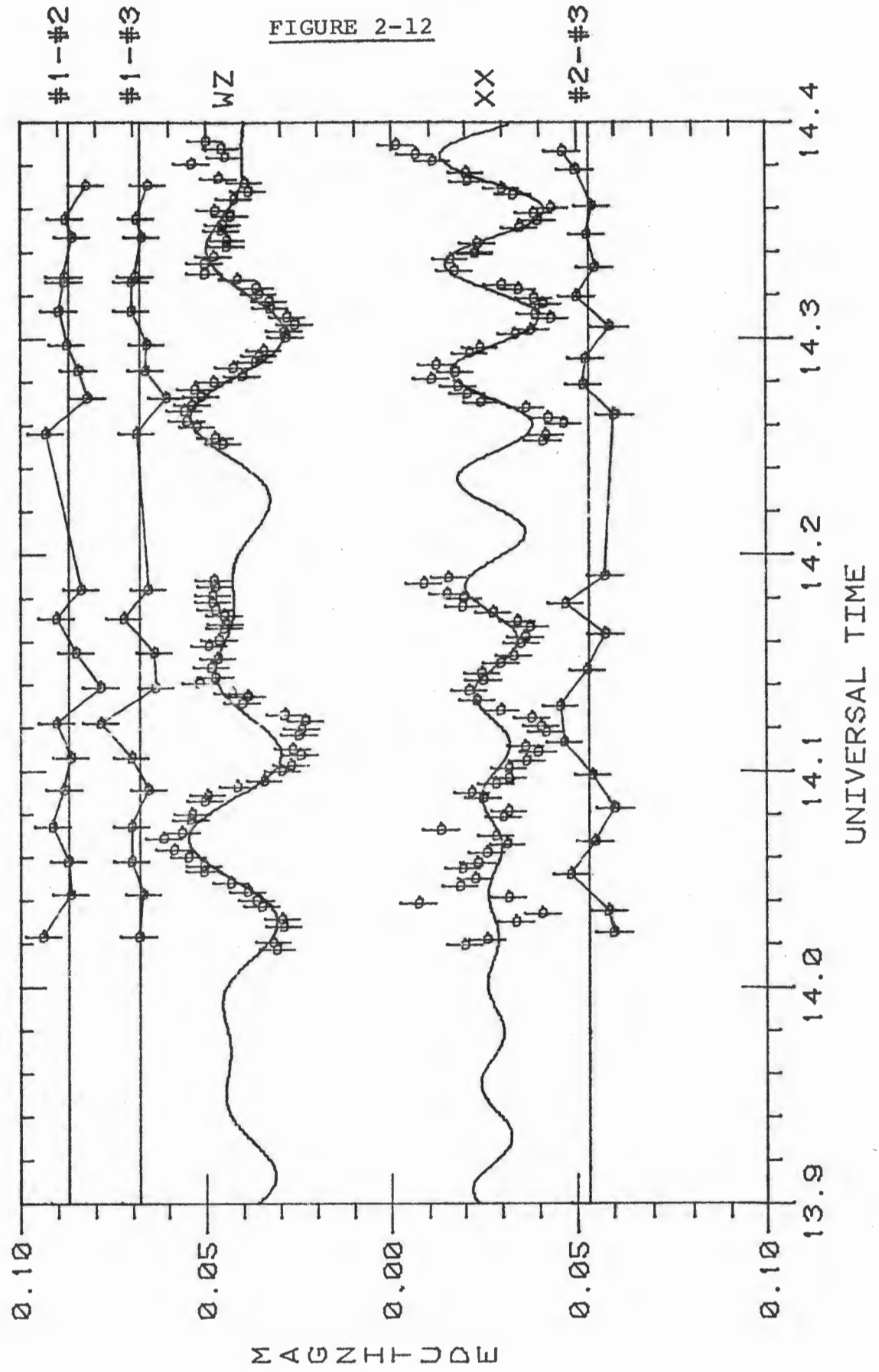
#1-#2
#1-#3
WZ
XX
#2-#3
0.10
0.05
0.00
0.05
0.10
MAGNETIC
13.9
14.0
14.1
14.2
14.3
14.4
UNIVERSAL TIME

FIGURE 2-13

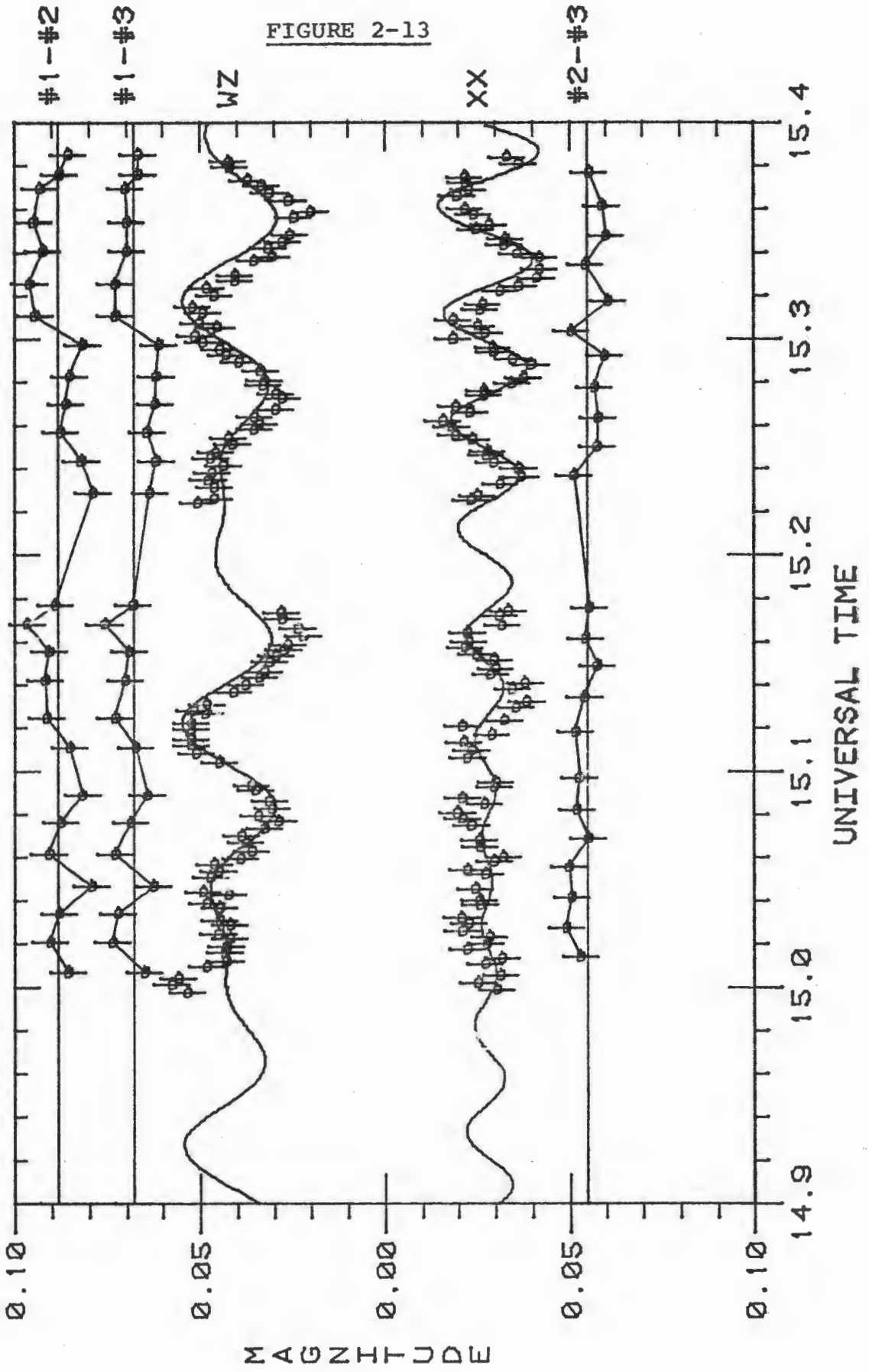
#1-#2
#1-#3
WZ
XX
#2-#3
0.10
0.05
0.00
0.05
0.10
14.9
15.0
15.1
15.2
15.3
15.4
UNIVERSAL TIME
MAGNITUDE

FIGURE 2-14

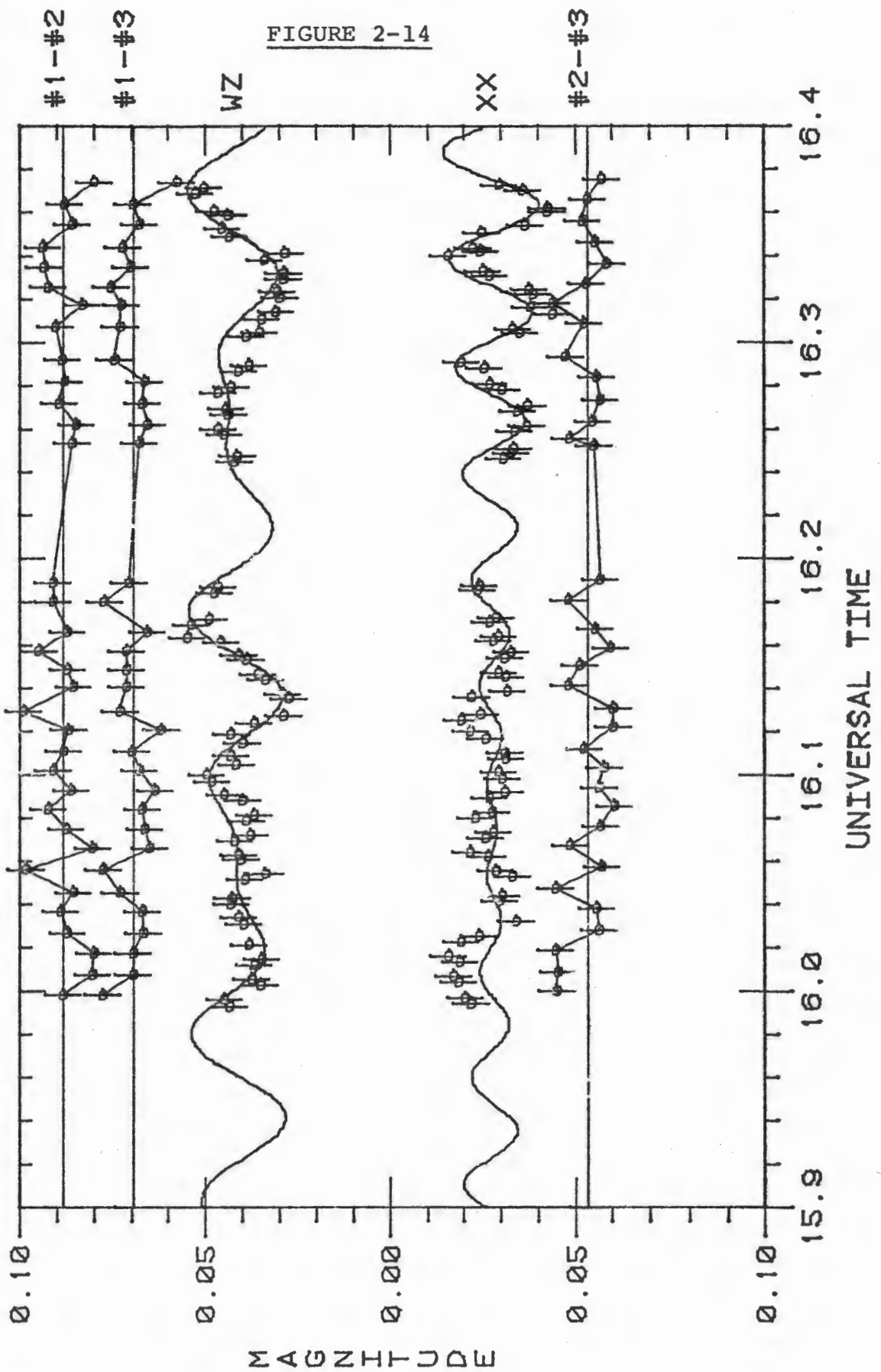
#1-#2
#1-#3
WZ
XX
#2-#3
16.4
16.3
16.2
16.1
16.0
15.9
UNIVERSAL TIME
0.10
0.05
0.00
0.05
0.10
MAGNITUDE

FIGURE 2-15

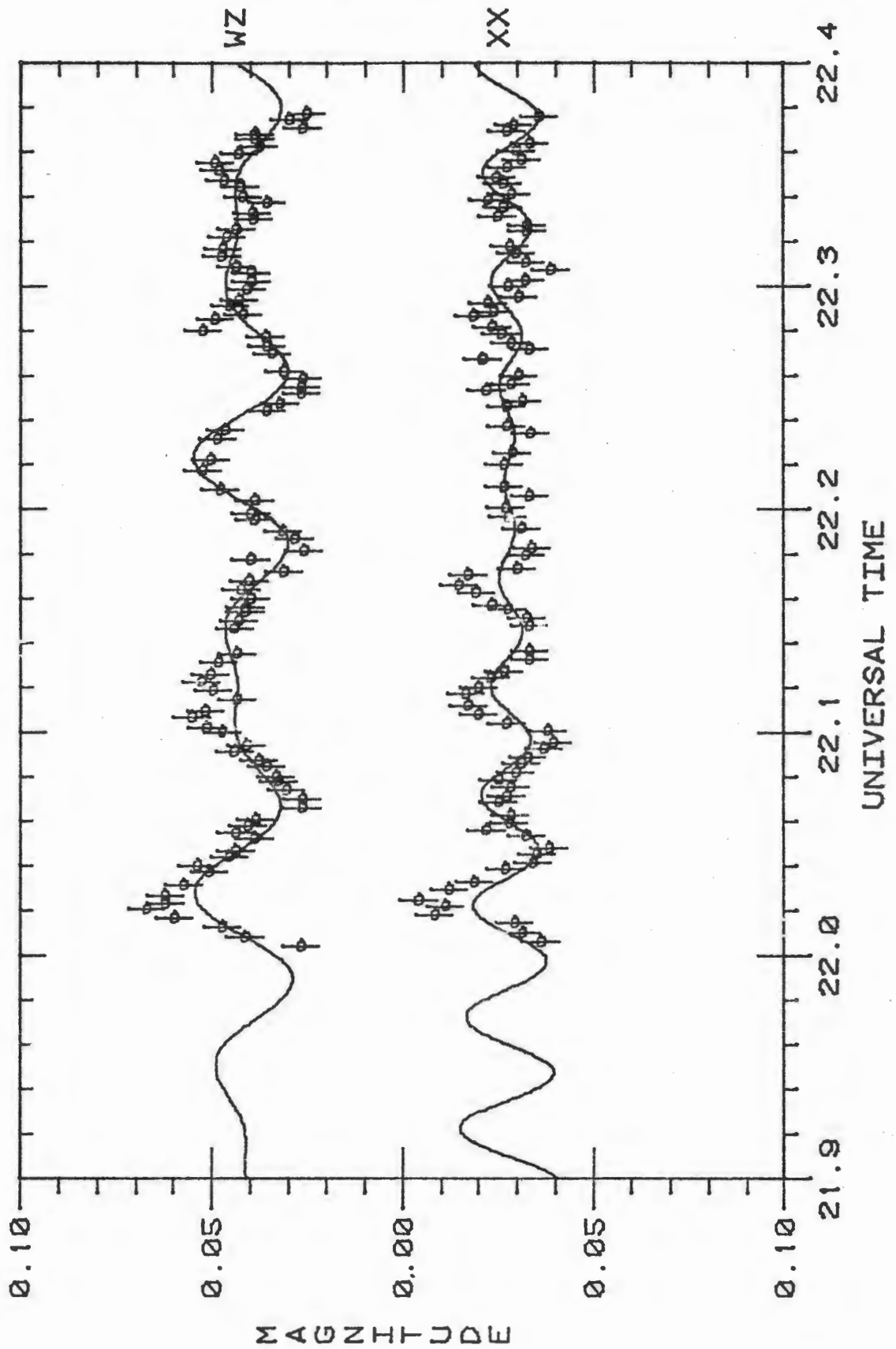
WZ
XX
0.10
0.05
0.00
0.05
0.10
MAGNITUDE
21.9
22.0
22.1
22.2
22.3
22.4
UNIVERSAL TIME

FIGURE 2-16

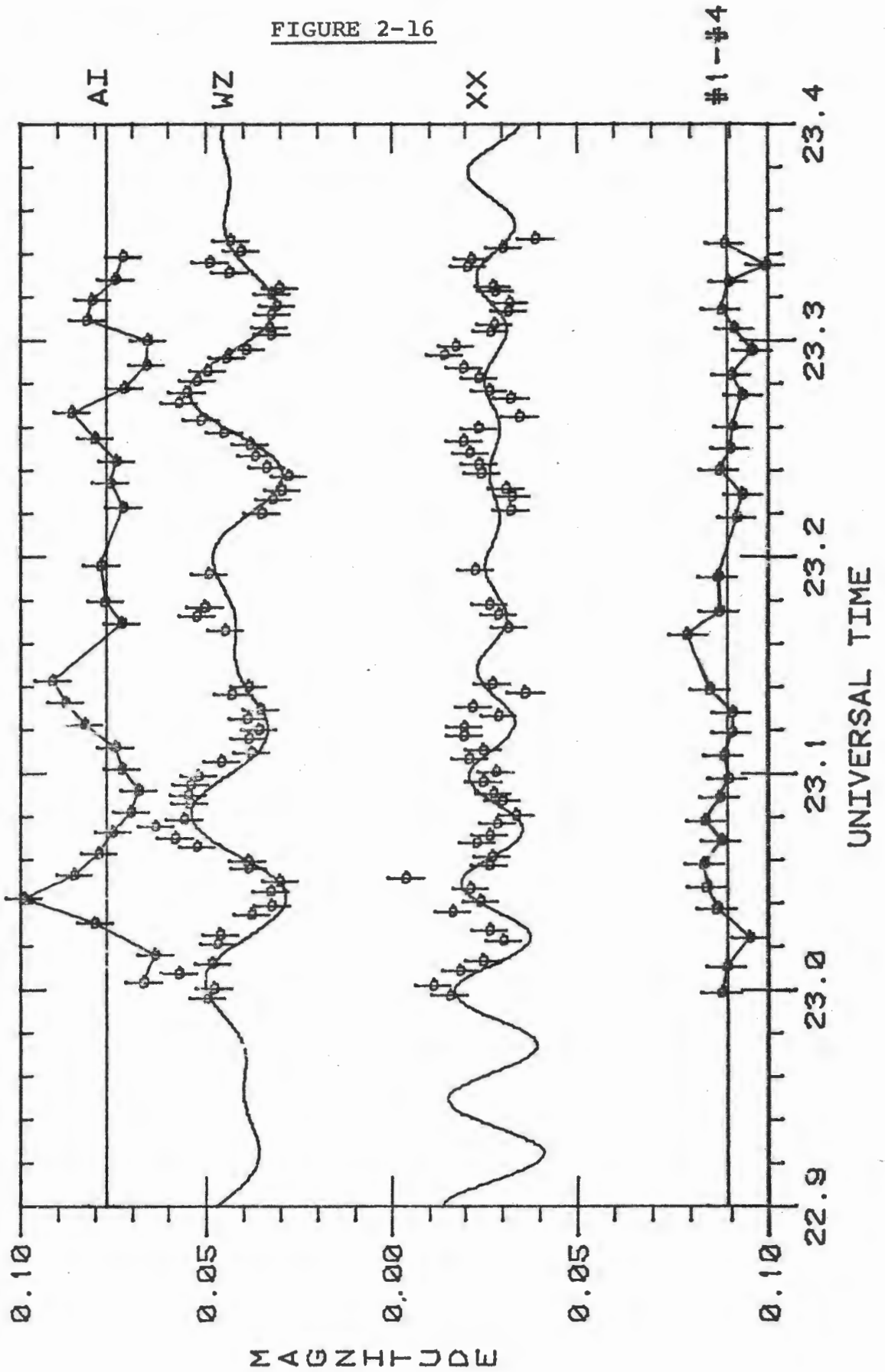
AI
WZ
XX
#1-#4
0.10
0.05
0.00
0.05
0.10
MAGNETIC
22.9
23.0
23.1
23.2
23.3
23.4
UNIVERSAL TIME

FIGURE 2-17

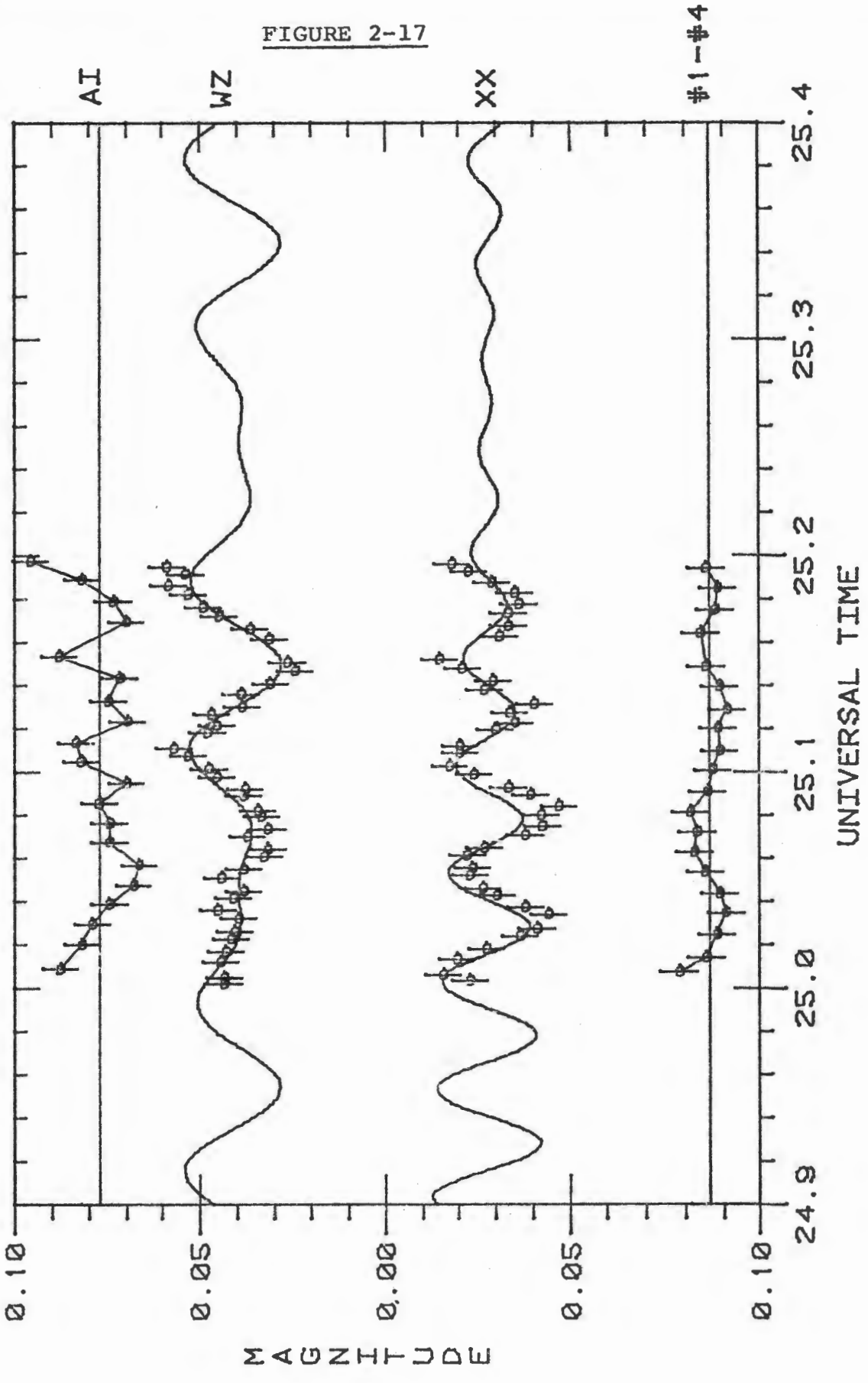
AI
WZ
XX
#1-#4
0.10
0.05
0.00
0.05
0.10
MAGNITUDE
24.9
25.0
25.1
25.2
25.3
25.4
UNIVERSAL TIME

FIGURE 2-18

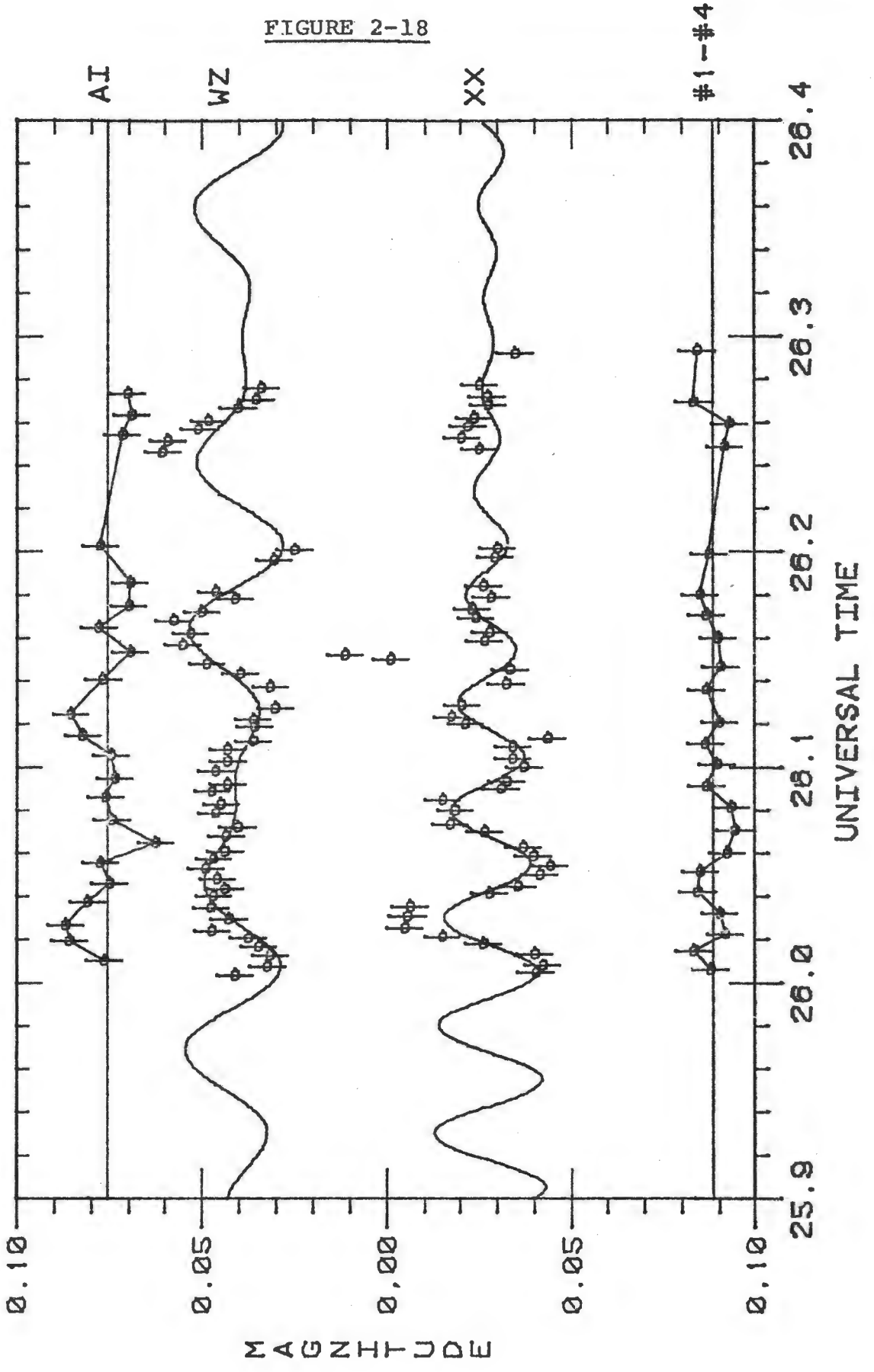
AI
WZ
XX
#1-#4
0.10
0.05
0.00
0.05
0.10
MAGNITUDE
25.9
26.0
26.1
26.2
26.3
26.4
UNIVERSAL TIME

FIGURE 2-19

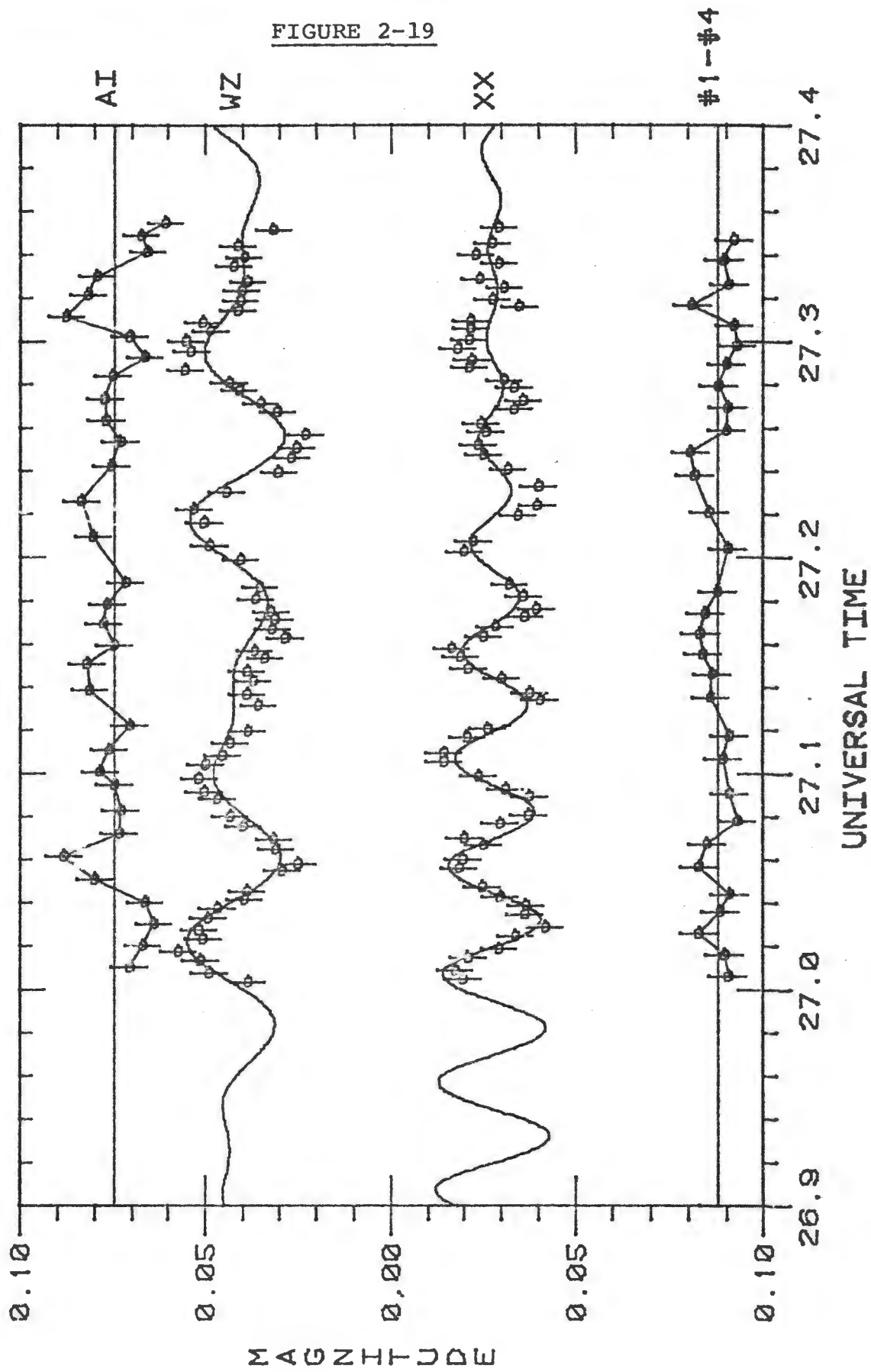
AI
WZ
XX
#1-#4
0.10
0.05
0.00
0.05
0.10
MAGNETIC
26.9
27.0
27.1
27.2
27.3
27.4
UNIVERSAL TIME

FIGURE 2-20

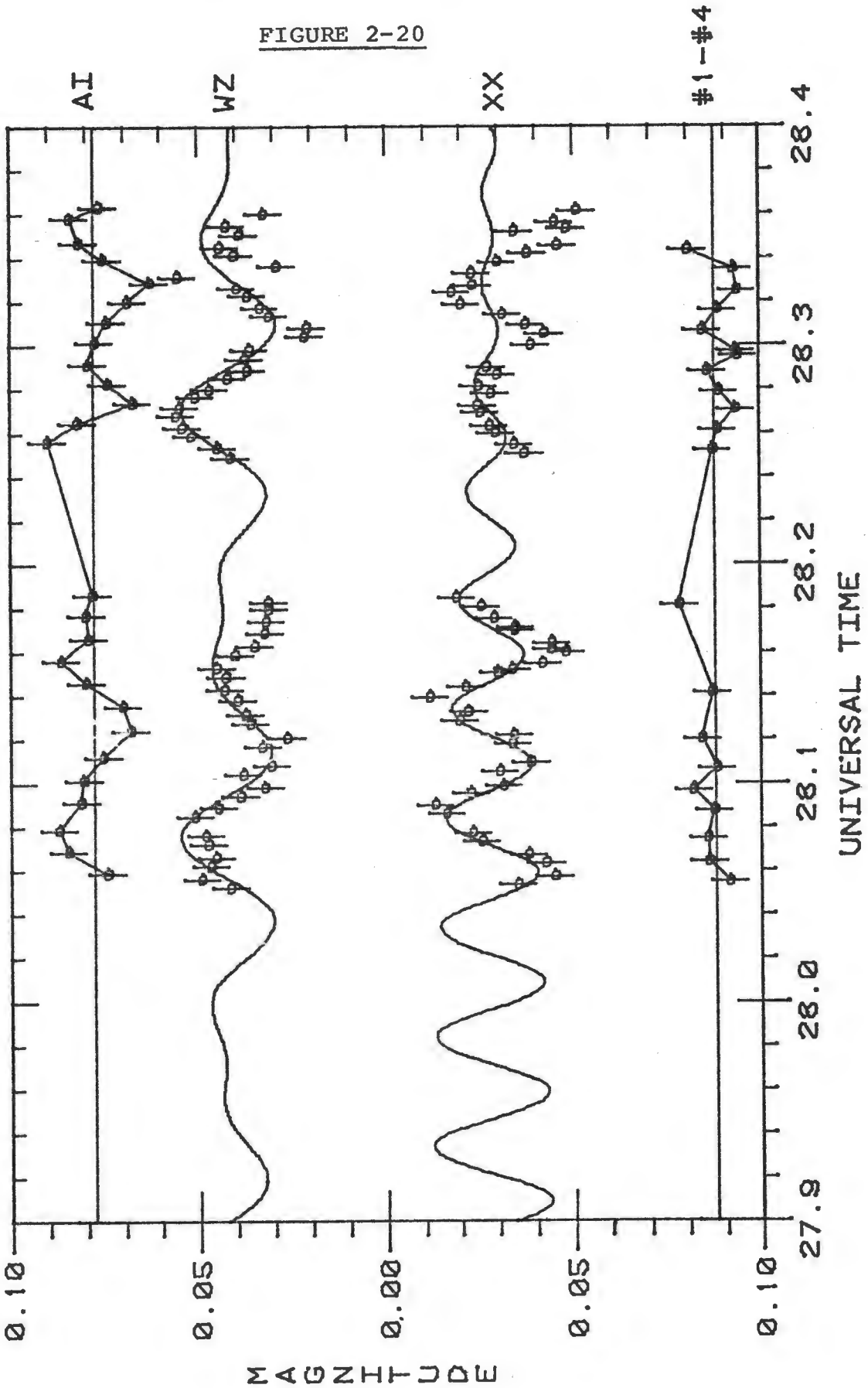
AI
WZ
XX
#1-#4
0.10
0.05
0.00
0.05
0.10
MAGNITUDE
27.9
28.0
28.1
28.2
28.3
28.4
UNIVERSAL TIME

FIGURE 2-21

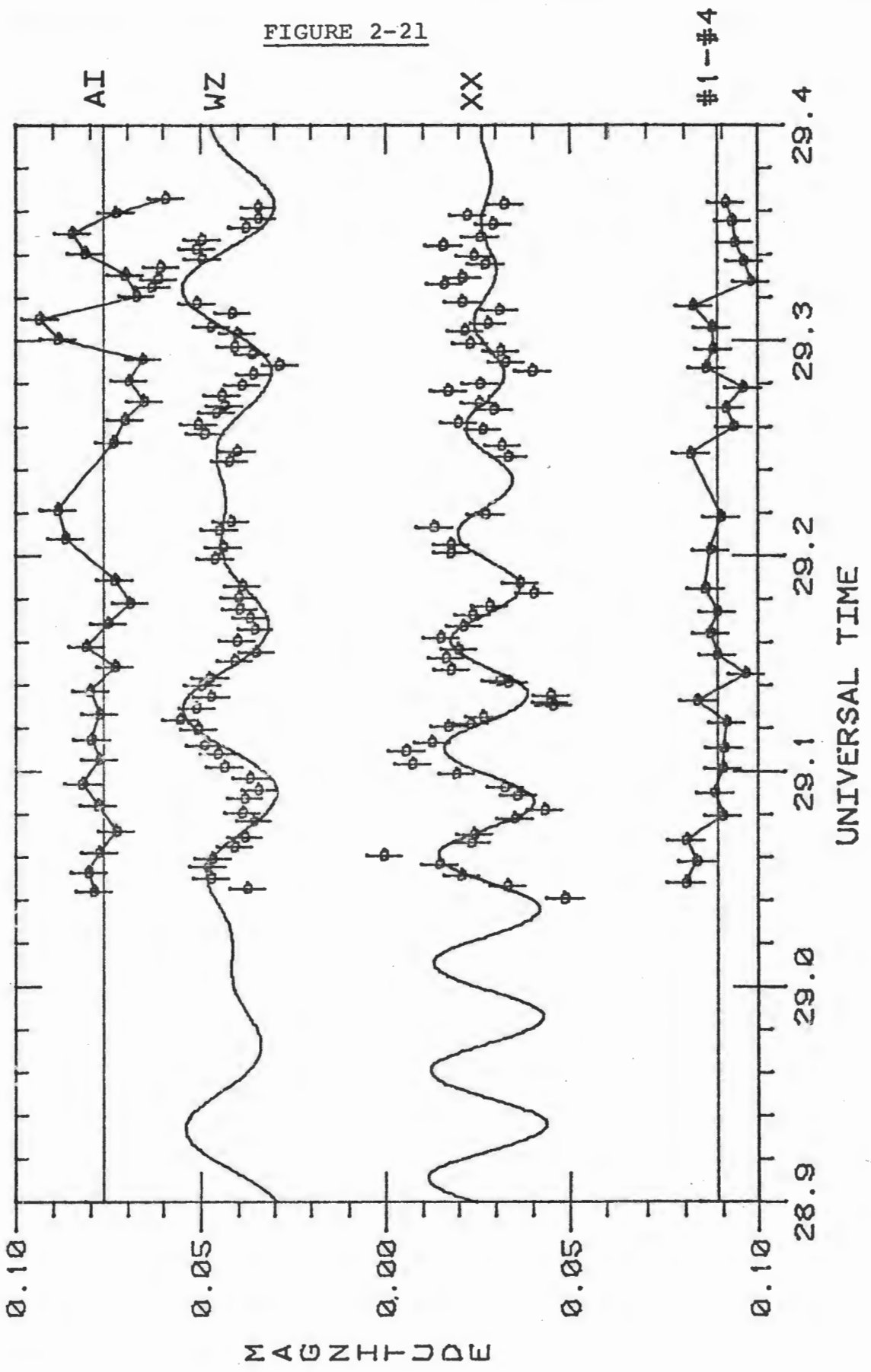
AI
WZ
XX
#1-#4
0.10
0.05
0.00
0.05
0.10
MAGNITUDE
28.9
29.0
29.1
29.2
29.3
29.4
UNIVERSAL TIME

picture for the light curves of the stars, a curve was drawn free-hand through the graph following the star's expected light curves, and the resulting magnitudes were substituted into the new data files. To check that this did not influence the results, a few data files with and without these substituted magnitudes were searched for periods using the Jurkevich method. As the resulting two sets of periodograms were very similar in appearance, it was concluded that the hand-drawn interpolation did not distort the results.

All the necessary data files were then available to search the data for periodicities.

CHAPTER THREE

AN OVERVIEW OF PERIOD-SEARCHING

3.1 Basic Period-Searching Methods

A basic aspect of data analysis is the search for periodicities in data, and many methods have been devised to carry this out. Unfortunately, no single method is generally agreed upon as the best, and for this thesis two methods were used to search for periods. In addition, a non-linear least-squares solution was used to refine the periods and amplitudes that were found using the previous methods.

Figure 3-1 shows a set of data points that follow a sine curve given by the formula $y = A \sin(2\pi x/P)$, where A is the half-amplitude of the curve and P is the period. For each data point (x_i, y_i) the phase ϕ_i may be calculated using the formula $\phi_i = \mathrm{mod}((x_i - x_o)/P)$, where mod is a function that yields the fractional part of its argument, and x_o is the average of the x_i values. For example, mod(17.673) = .673 . A graph of (ϕ_i, y_i) is called a phase diagram, and Figure 3-2a shows an idealized phase diagram for the data in Figure 3-1. Figure 3-2b represents a phase diagram for these data using an incorrect value for the period, causing the data points to scatter randomly along the ϕ axis. The differing mathematical properties between these two figures are used by many period-searching methods. The presence of the horizontal and vertical lines in these two figures will be explained in the next section.

Figure 3-1

Artificial light curve given by $f(x) = A \sin(2\pi x/P)$, where P = 100 minutes.

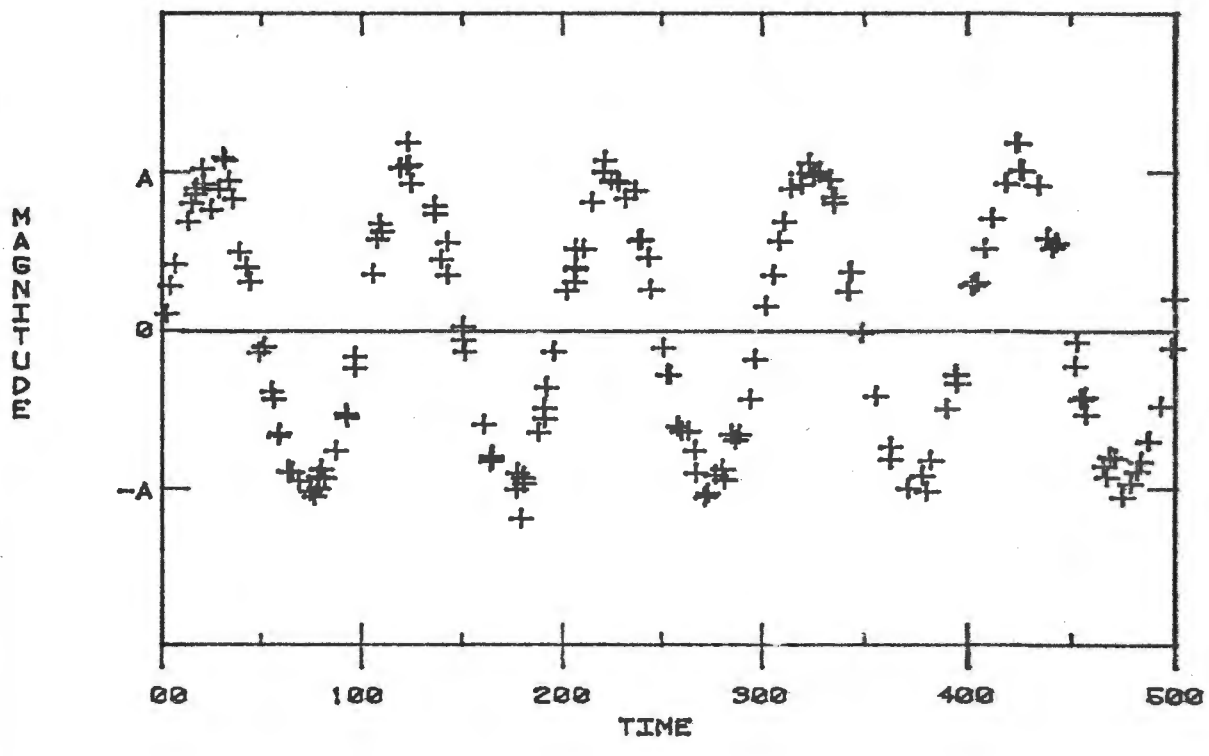
MAGNITUDE
A
0
-A
00
100
200
300
400
500
TIME

Figure 3-2a

Phase diagram for P = 100 minutes, using the data given in Figure 3-1. This diagram is divided vertically into three 'bins', and the three horizontal lines labelled $\bar{y}_1$, $\bar{y}_2$ and $\bar{y}_3$ are the average values of y_i for the data points in each bin.

Figure 3-2b

The same as in Figure 3-2a, but for an incorrect value of the period.

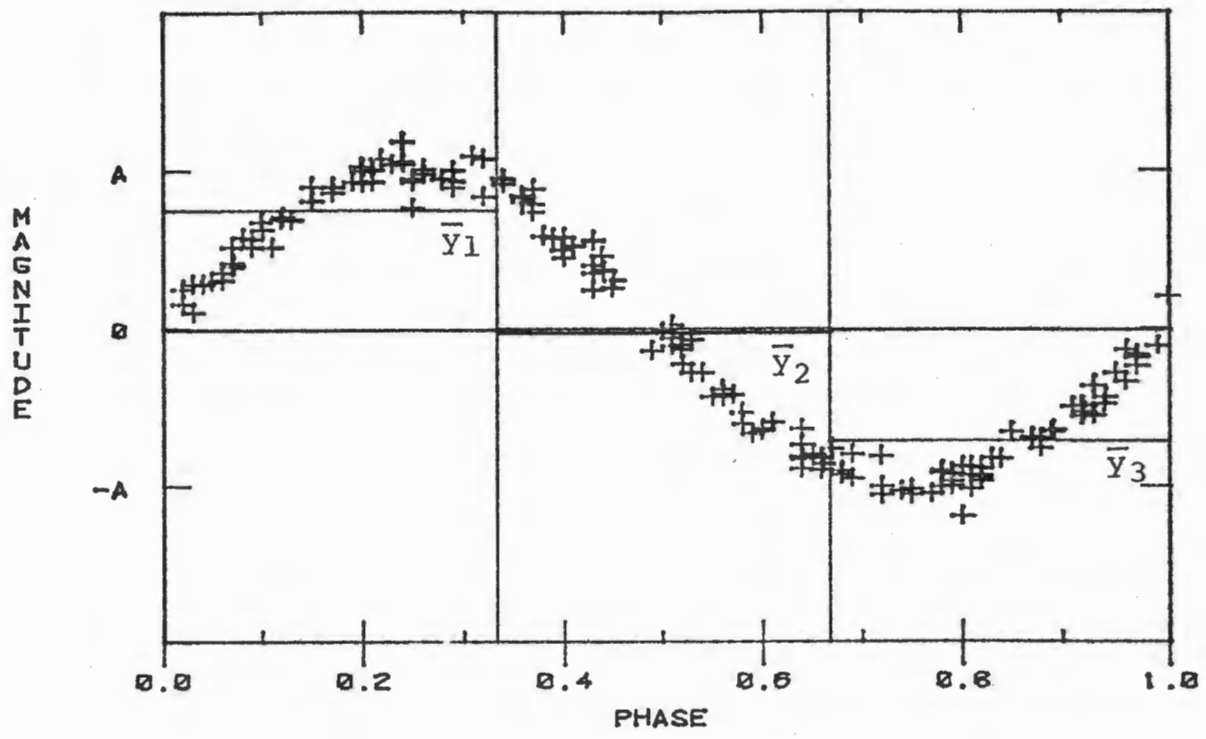
MAGNITUDE
A
0
-A
$\bar{y}_1$
$\bar{y}_2$
$\bar{y}_3$
0.0
0.2
0.4
0.6
0.8
1.0
PHASE

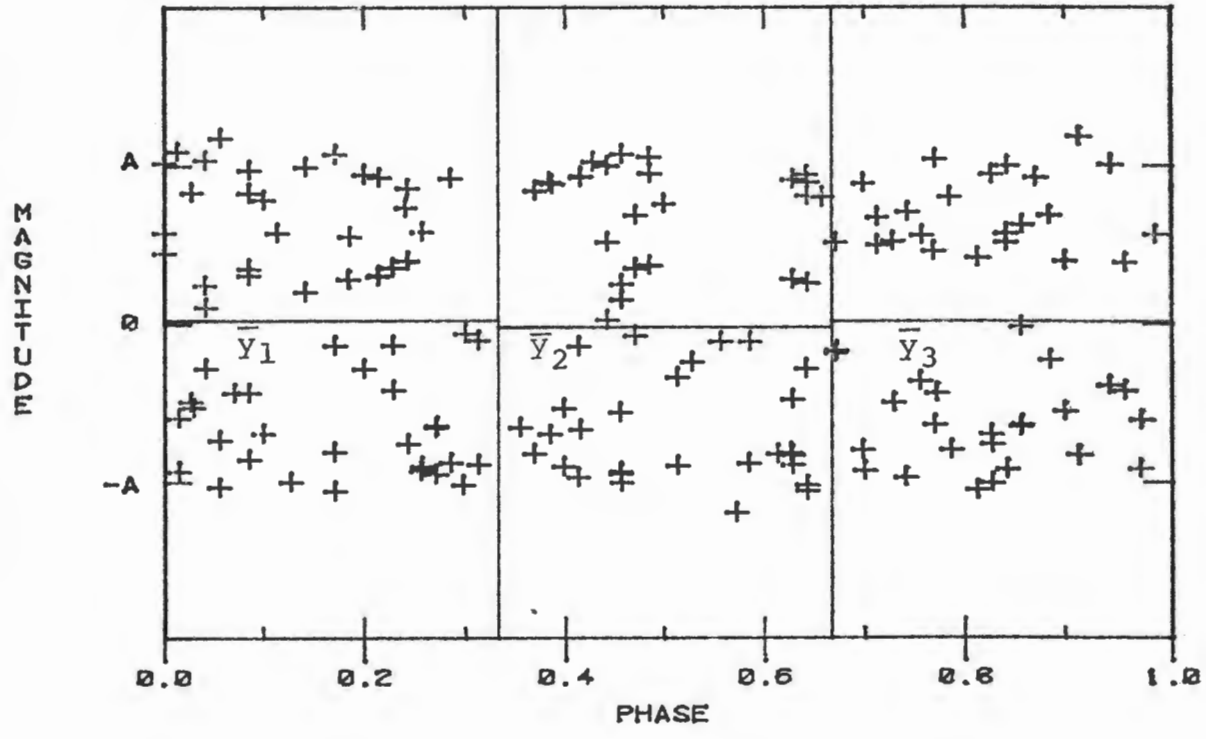
MAGNITUDE
A
0
-A
$\bar{y}_1$
$\bar{y}_2$
$\bar{y}_3$
0.0
0.2
0.4
0.6
0.8
1.0
PHASE

A period-searching method generally investigates a number of trial periods, and to each trial period assigns an index I(P). A graph of I(P) versus P is called a periodogram, and a typical example is shown in Figure 3-3. If a period P is present in the data, a peak in the value of I(P) appears. The trial periods must not be spaced so far apart that the peak is missed, but computer time will be wasted if the trial periods are spaced too closely together. Note that in Figure 3-3 the peak drops rapidly from P to a very small value at $P + \delta P$. To find the value of δP, assume the data are evenly distributed over a time span L. The number of cycles present will be $N = L/P$. It is not too difficult to see that if a slightly different period is chosen so that only N-1 cycles occur across a time span L, then all the data points that ought to fall on a given phase will instead be distributed uniformly across the phase diagram; this will clearly cause the very small value of the index seen at $P + \delta P$. Therefore we have the two equations $L=NP$ and $L = (N-1)(P+\delta P)$, and solving for δP gives $\delta P = P^2/(L-P) \approx P^2/L$ when $L \gg P$. For this thesis it was decided to space the trial periods at intervals of $P^2/6L$ to avoid missing the top of the peak.

One difficulty common to most period-searching methods is aliasing, which is the presence of several false peaks due to some peculiarity in the spacing of the data points along the x-axis. The most common and most serious alias occurs when the data are clustered at nightly intervals, with no data points obtained during the daytime. Suppose that two

Figure 3-3

A periodogram of data similar to that given in Figure 3-1, using the Jurkevich method.

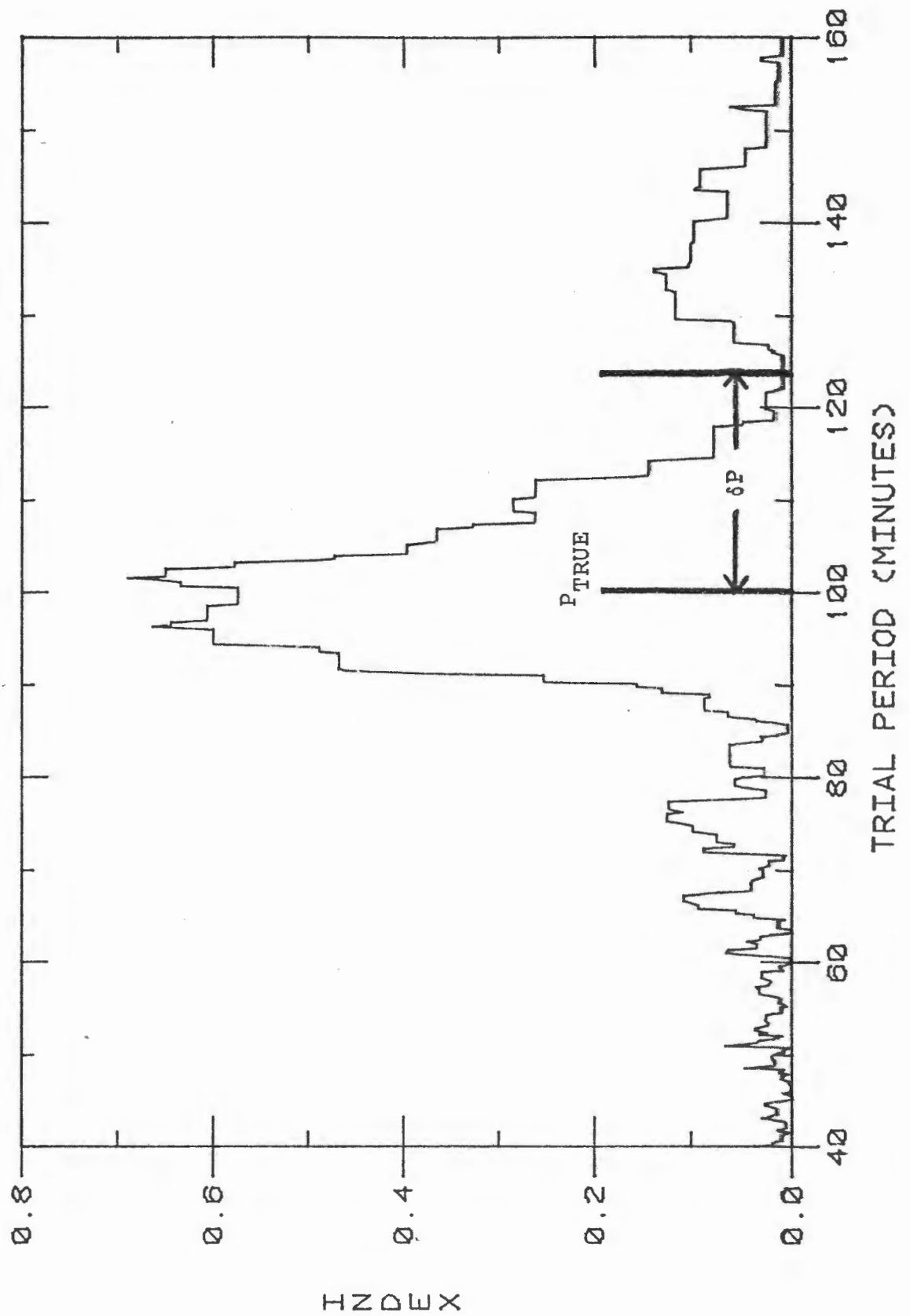
0.8
0.6
0.4
0.2
0.0
INDEX
40
60
80
100
120
140
160
TRIAL PERIOD (MINUTES)
P_{TRUE}
δP

sets of data with period P are separated by a time span L, so that the number of cycles is N = L/P. Aliasing arises because a period P + δP that creates only N-1 cycles will fit the observations on the two nights almost as well as the period P. This leads to the same two equations L = NP and L = (N-1)(P+δP) that were found for the width of the periodogram peaks, so that $\delta P = P^2/L$ is the spacing to be expected between the true peaks and the aliased peaks in a periodogram. Peaks will also occur at distances of $2\delta P$, $3\delta P$ .... from the true peak corresponding to N-2, N-3 .... number of cycles, but these peaks will have progressively smaller indices because they do not fit the nightly data as well. The problem of aliasing can only be overcome by obtaining high-quality data or by obtaining enough data to overcome the noise, and thereby distinguish between N or N-1 elapsed daytime cycles.

If two nearly equal frequencies f_1 and f_2 are present in the data, the resulting curves will have a frequency $(f_1 + f_2)/2$ with variable amplitude as shown in Figure 3-4. The variable amplitude is caused by the two frequencies alternately cancelling and re-enforcing, a phenomenon referred to as beating, and the frequency of the envelope, $f_1 - f_2$, is called the beat frequency. In terms of periods, the curve will have a period $2P_1P_2/(P_1 + P_2)$ and a beat period of $P_1P_2/(P_2 - P_1)$.

Figure 3-4

Two sine curves of nearly equal frequency, and the modulated curve that results when the first two curves are added together. B is the beat period.

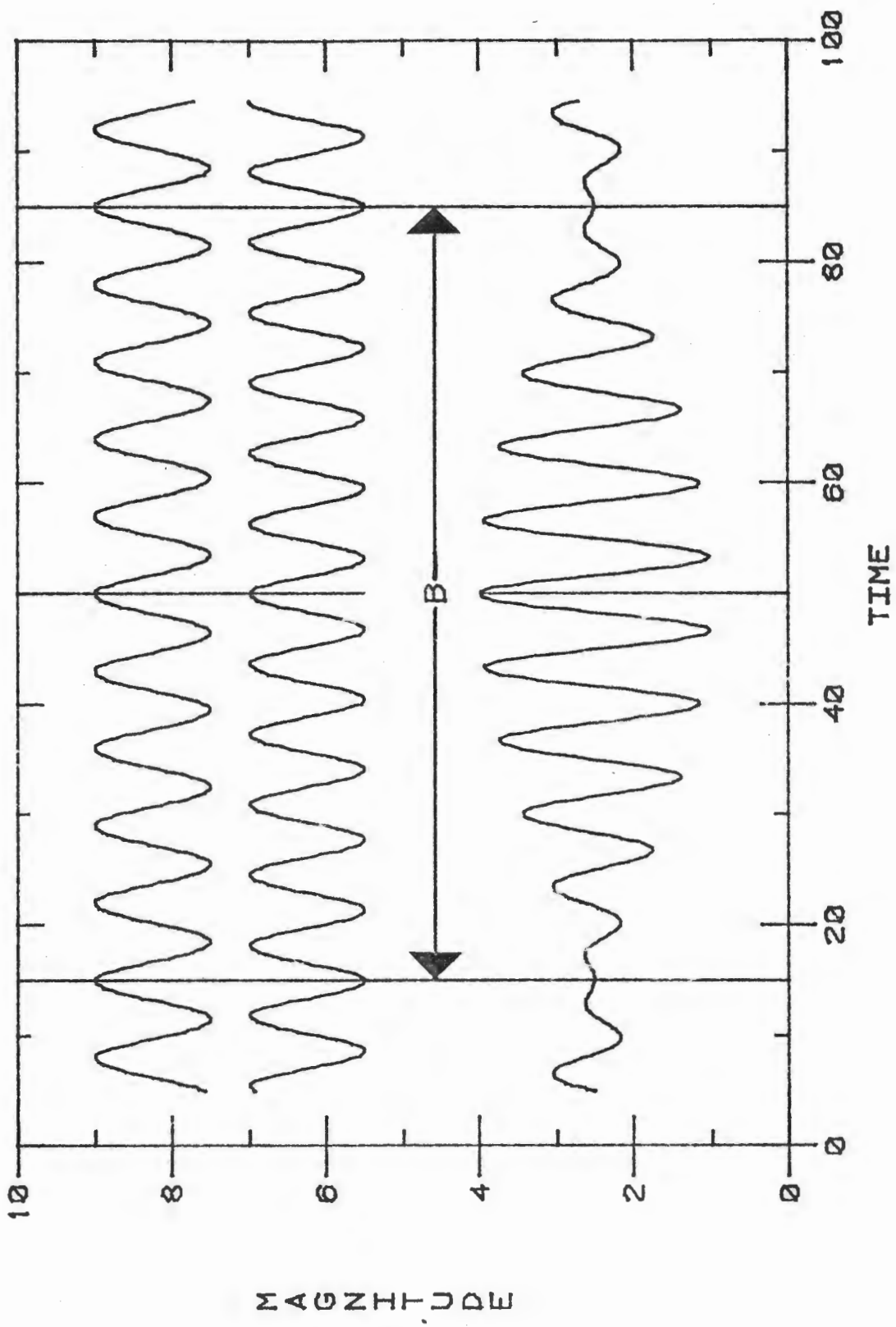
MAGNITUDE
10
8
6
4
2
0
0
20
40
60
80
100
TIME
B

3.2 The Jurkevich Method

The Jurkevich period-searching method as outlined by Jurkevich (1971) will be used extensively in this thesis. To illustrate this method, suppose that N data points of the form (x_i, y_i) are to be searched for periodicities. The x_i values need not be evenly spaced, and the periodic behaviour need not be sinusoidal. The procedures described in the previous section are used to find a suitable set of trial periods to be investigated. For each trial period a phase diagram is constructed and the x-axis divided into k intervals, commonly called 'bins'. For each bin, the y values of all the data points are averaged and are called $\bar{y}_i$ where i runs from 1 to k. Suppose there are m_i data points in each bin and let V represent the variance of the N values of y_i. Then for each trial period P, the Jurkevich method assigns and index I given by $I = V^2 - \sum_{i=1}^{k} m_i \bar{y}_i^2$. For computational convenience it is assumed that the N values of y_i have been averaged to zero. Figure 3-3 illustrates what a graph of $\sum_{i=1}^{k} m_i \bar{y}_i^2$ will look like. When $P \neq P_{TRUE}$, the data points will scatter randomly in a phase diagram and the values of $\bar{y}_i$ will be close to zero, as in Figure 3-2b. When $P = P_{TRUE}$ as in Figure 3-2a, the values of $\bar{y}_i$ will not all be close to zero, and so $\sum_{i=1}^{k} m_i \bar{y}_i^2$ will not be close to zero.

It is not immediately obvious what value should be used for k, the number of bins. Jurkevich comments in his paper that k=3 is the minimum value that should be used, but gives no guidance towards finding the optimum value. From

previous experience the author of this thesis has found that for small values of N (between 20 and 80) the most pronounced peaks occur when k=3. This is not surprising because a large value of k implies that occasionally the data points will be unevenly distributed among the bins, creating greater fluctuation in the values of I(P). Figures 3-5a and 3-5b show the same periodogram but with k=3 and k=9 respectively. It is clear that for large values of N (in this case N = 650) the value of k is not important, although as k increases the noise does increase slightly. Thus it can be taken as a general rule that the optimum value for k is three, and this value is used in the following analyses.

Suppose that a set of data gives for period P a sinusoidal phase diagram like that shown in Figure 3-2. It would be very useful if the index I(P) could be used to find the half-amplitude A of this sine curve. The presence of another period or of noise will serve only to change this curve from a line to a wide band, but the values of $\bar{y}_1^2$, $\bar{y}_2^2$ and $\bar{y}_3^2$ should remain essentially unaltered. This argument assumes in effect that there are a large number of data points equally distributed among the three bins, but as long as N is large (N >80) this is a reasonable assumption. If the data points follow the functional dependence $y(x) = A \sin 2\pi(x - \phi)$, what will be the value of $\bar{y}_1^2 + \bar{y}_2^2 + \bar{y}_3^2$?

The value of $\bar{y}_1$ will be given by

$$\bar{y}_1 = 3A \int_0^{\sqrt{3}} \sin 2\pi(x - \phi)\,dx = (3A/4\pi)(3 \cos 2\pi\phi - \sqrt{3} \sin 2\pi\phi).$$

Similarly, $\bar{y}_2 = (3\sqrt{3}A/2\pi)(\sin 2\pi\phi)$ and

Figure 3-5a

Periodogram of the data obtained for XX Scl, using m=3.

Figure 3-5b

Same as in Figure 3-5a, but using m=9.

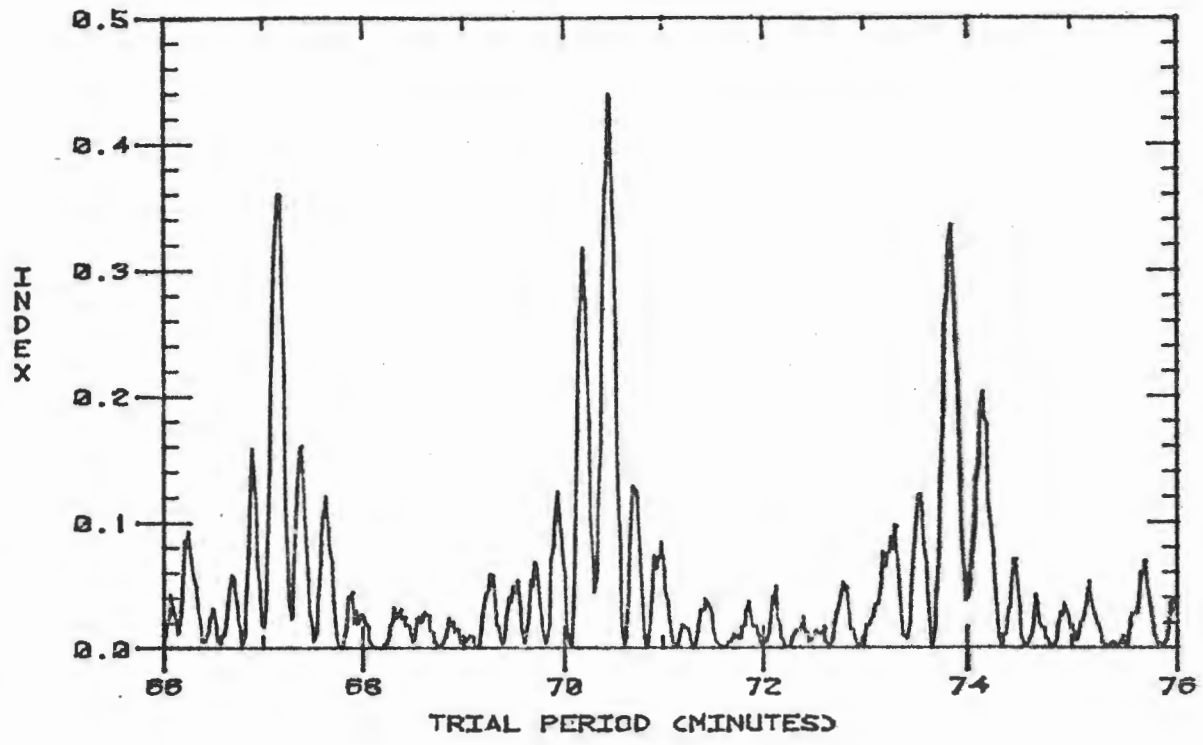
0.5
0.4
0.3
0.2
0.1
0.0
INDEX
66
68
70
72
74
76
TRIAL PERIOD (MINUTES)

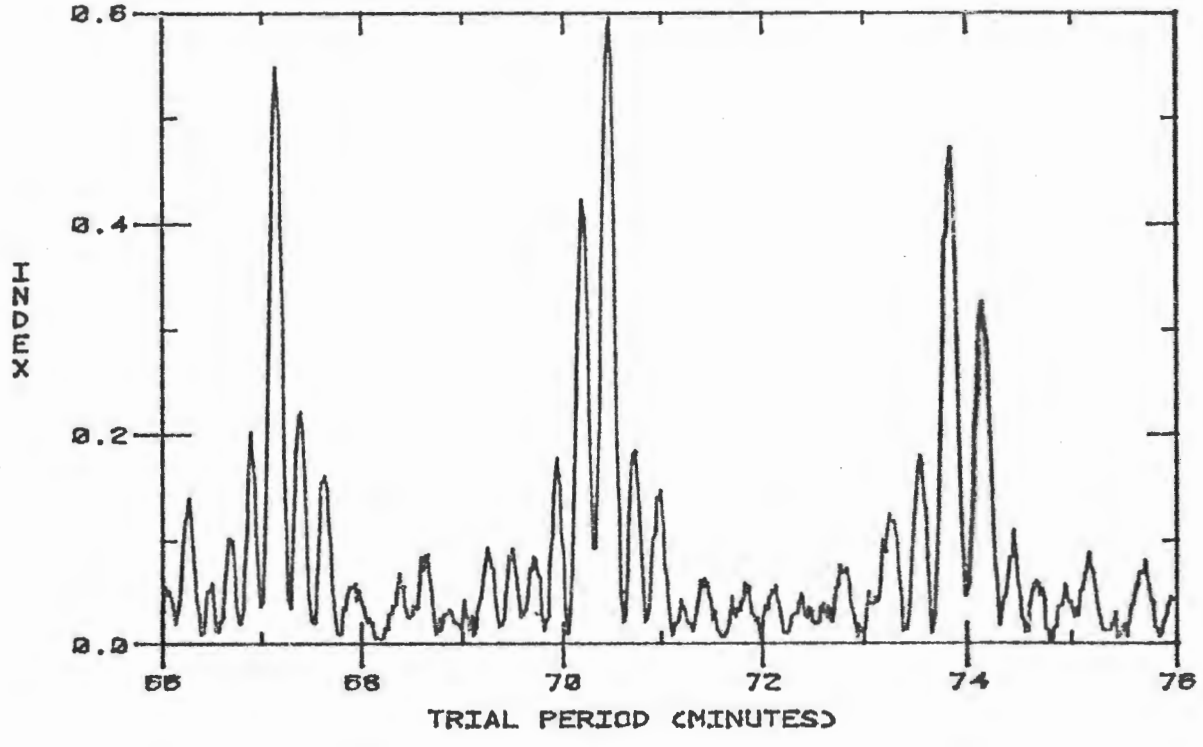
0.6
0.4
0.2
0.0
INDEX
66
68
70
72
74
76
TRIAL PERIOD (MINUTES)

$\bar{y}_3 = (3A/4\pi)(-3\cos 2\pi\phi - \sqrt{3}\sin 2\pi\phi)$.

Squaring these and adding gives $\bar{y}_1^2 + \bar{y}_2^2 + \bar{y}_3^2 = 81A^2/8\pi^2$,

and so $A^2 = (8\pi^2/81)(\bar{y}_1^2 + \bar{y}_2^2 + \bar{y}_3^2)$.

It is useful to know that such a simple relation exists and is independent of ϕ. Recall that Jurkevich originally defined the index to be $I(P) = V^2 - \sum_{i=1}^{k} m_i \bar{y}_i^2$. In future work, it appears more useful to set k = 3 and to use the new index $I(P) = (8\pi^2/27N) \sum_{i=1}^{k} m_i \bar{y}_i^2$, so that the value of I(P) gives the square of the half-amplitude A for the sine curve of period P that would be used to fit the data. In this thesis the index used was $(80000\pi^2/27N) \sum_{i=1}^{k} m_i \bar{y}_i^2$ $\approx (29243/N) \sum_{i=1}^{k} m_i \bar{y}_i^2$, so that the results are in hundredths of a magnitude. This is a more convenient measurement for the magnitude fluctuations found in δ Scuti stars.

3.3 The Jurkevich Method Applied to Artificial Data

To test how well this method could detect periods in noisy data, two sets of artificial data were created, according to the formulae:

$y(t) = .006 \sin(2\pi t/77) + .008 \sin(2\pi t/100) + \sigma(.005)$

$y(t) = .006 \sin(2\pi t/77) + .008 \sin(2\pi t/100) + \sigma(.010)$,

where $\sigma(x)$ represents Gaussian noise of standard deviation x, added to each data point. The time of observation t is in minutes, and the number and spacing of the artificial data are identical to those obtained for AI Scl.

Figure 3-6 shows the phase diagram for P = 77 minutes

Figure 3-6a

Phase diagram for P = 77 minutes, for data generated from $y(t) = .006 \sin(2\pi t/77) + .008 \sin(2\pi t/100) + \sigma(.005)$.

Figure 3-6b

Phase diagram for P = 77 minutes, for data generated from $y(t) = .006 \sin(2\pi t/77) + .008 \sin(2\pi t/100) + \sigma(.010)$.

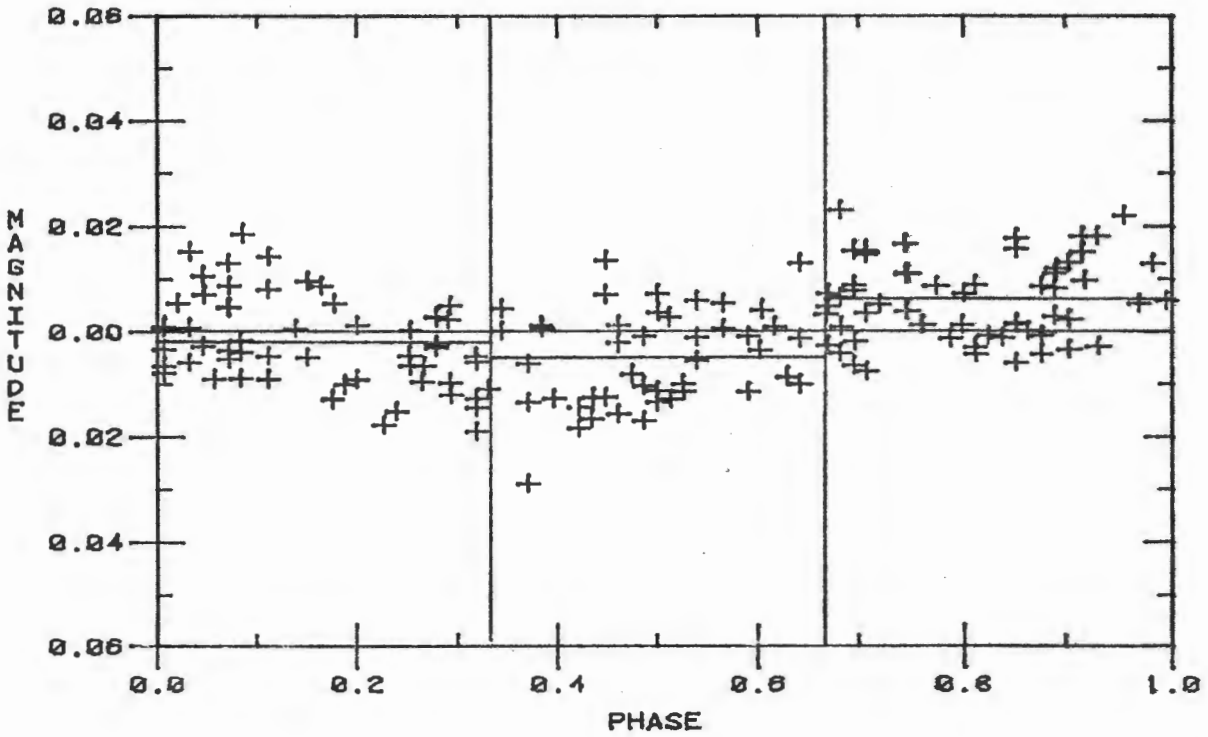
0.08
0.04
0.02
0.00
0.02
0.04
0.06
MAGNITUDE
0.0
0.2
0.4
0.6
0.8
1.0
PHASE

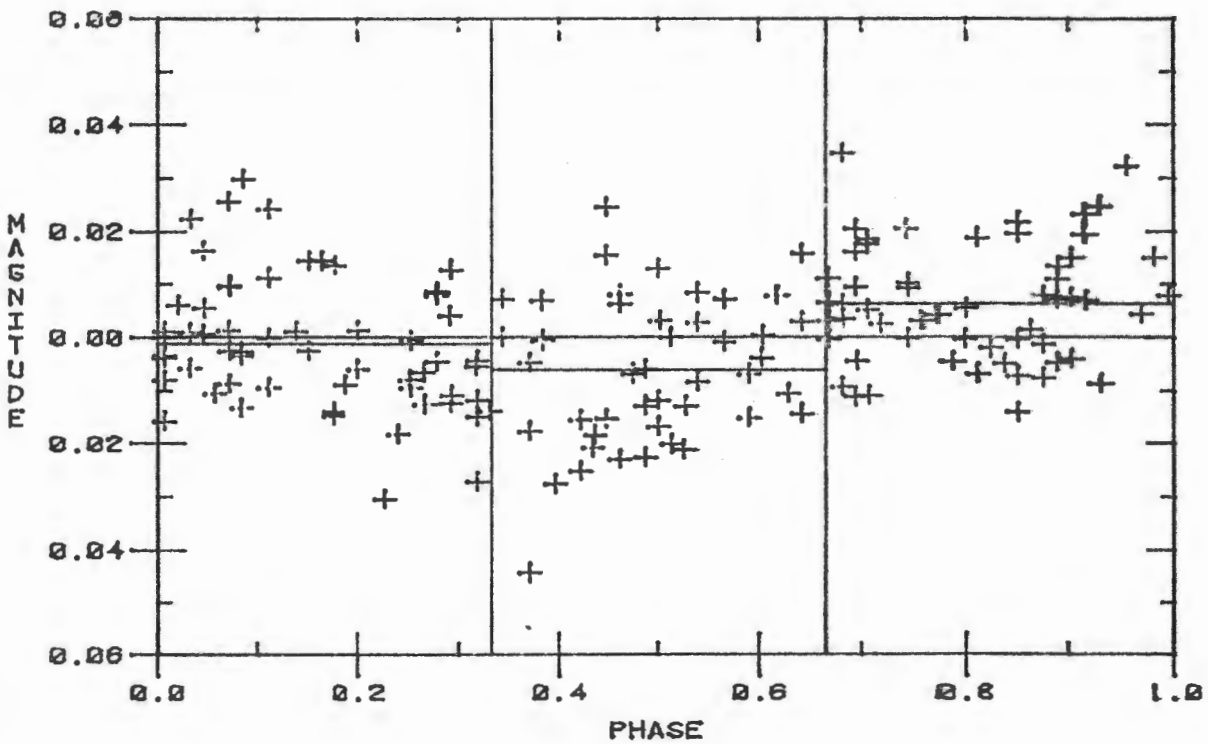
0.08
0.04
0.02
0.00
0.02
0.04
0.06
MAGNITUDE
0.0
0.2
0.4
0.6
0.8
1.0
PHASE

for both data sets, and Figures 3-7 and 3-8 show their Jurkevich periodograms. The periodograms in Figures 3-7 and 3-8 show both periods remarkably well, considering the amount of noise present. The periods and amplitudes used in these sets of data are typical of those found in periodic δ Scuti stars, and in Section 5.2 it will be shown that the noise level for the observations obtained for this thesis was approximately σ(.005). Figure 3-8 clearly shows the period at 77 minutes of half-amplitude 0.006, despite the noise level of approximately σ(.018) due to the Gaussian noise component of σ(.010) and the presence of the period at 100 minutes with half-amplitude 0.008 . The half-amplitude detected in this case is three times smaller than the noise, and as the noise level in the data is approximately σ(.005), one would therefore expect to detect any periodicities in the real data down to at least a half-amplitude of 0.0017 magnitudes. Of course, if more than one period is present or if the oscillation in the data is not strictly periodic, this lower limit would have to be increased.

In all periodograms several smaller peaks to the sides of the true peaks are found. From Figures 3-7 and 3-8, the two peaks beside the peak at 77 minutes were found to be at 73.35 and 81.22 minutes (measured on expanded-scale periodograms), and the peaks beside the peak at 100 minutes were found to be at 93.44 and 107.43 minutes. Using the formula for aliasing given in Section 3.1, the time-spans L that would give rise to such aliasing were calculated to

Figure 3-7

Jurkevich periodogram of data generated from:

$y(t) = .006 \sin(2\pi t/77) + .008 \sin(2\pi t/100) + \sigma(.005)$.

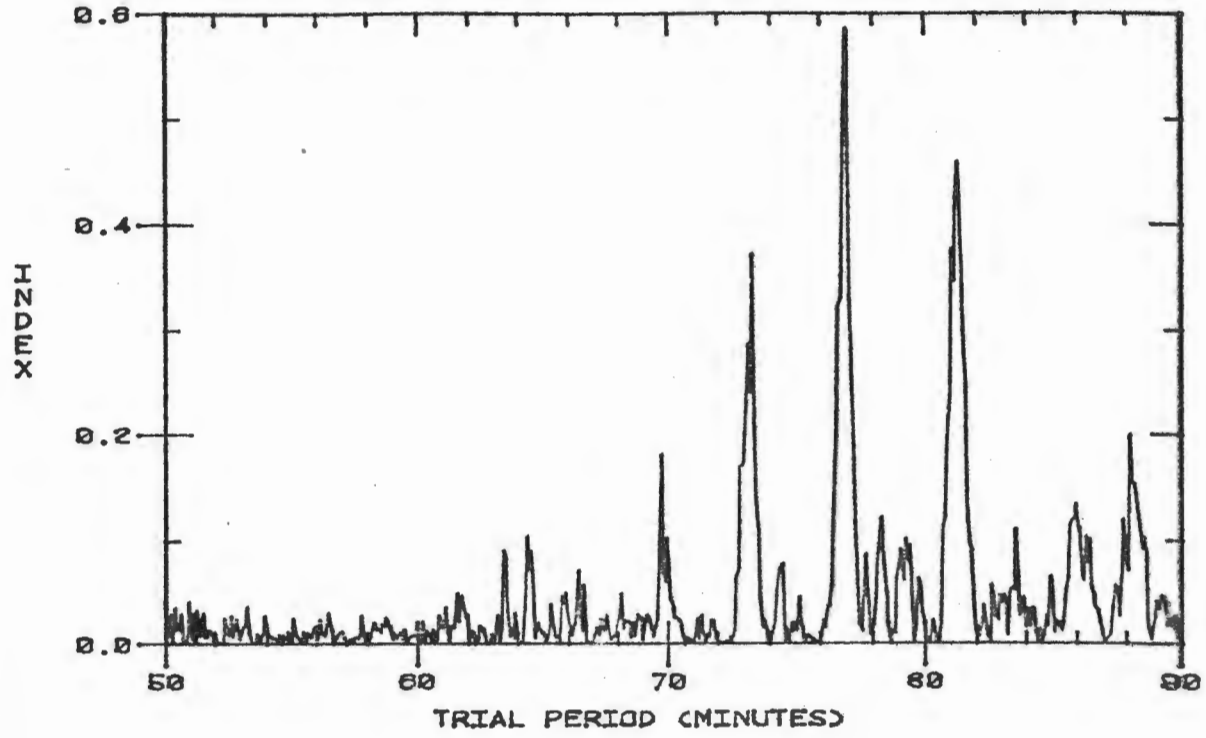
0.8
0.4
0.2
0.0
INDEX
50
60
70
80
90
TRIAL PERIOD (MINUTES)

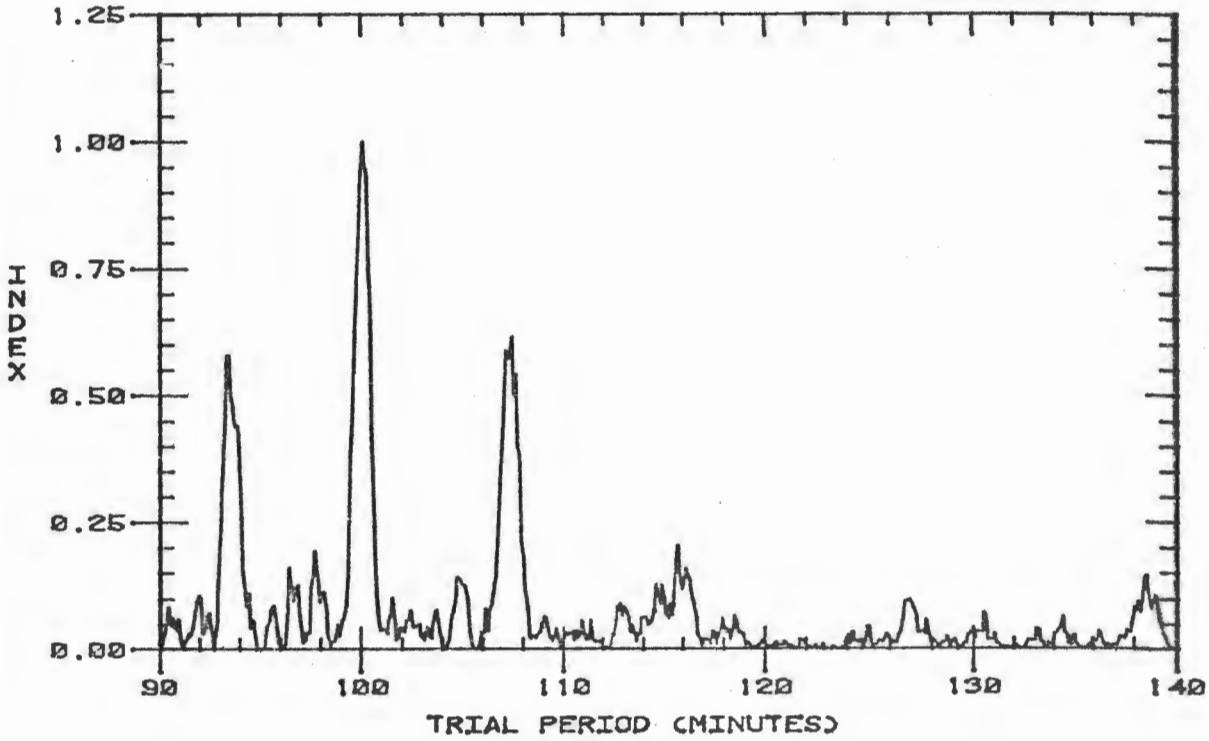
1.25
1.00
0.75
0.50
0.25
0.00
INDEX
90
100
110
120
130
140
TRIAL PERIOD (MINUTES)

Figure 3-8

Jurkevich periodogram of data generated from:

$y(t) = .006 \sin(2\pi t/77) + .008 \sin(2\pi t/100) + \sigma(.010)$.

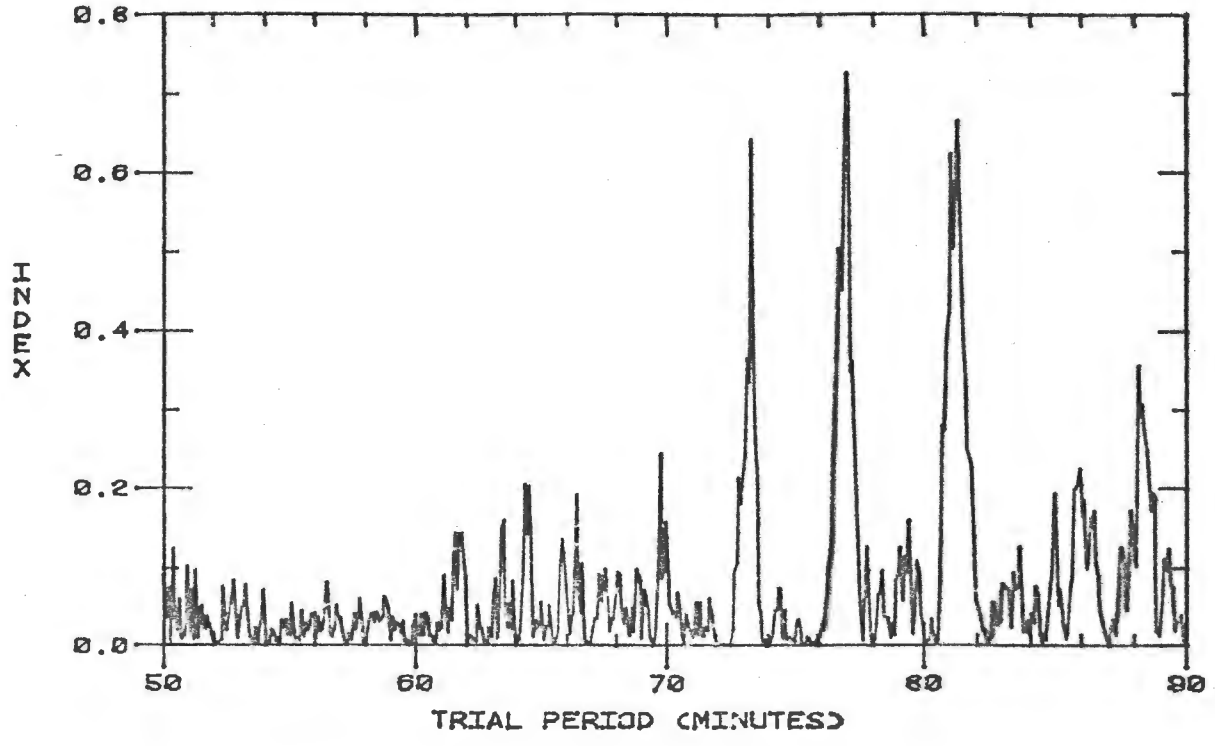
0.6
0.6
0.4
0.2
0.0
XEDNH
50
60
70
80
90
TRIAL PERIOD (MINUTES)

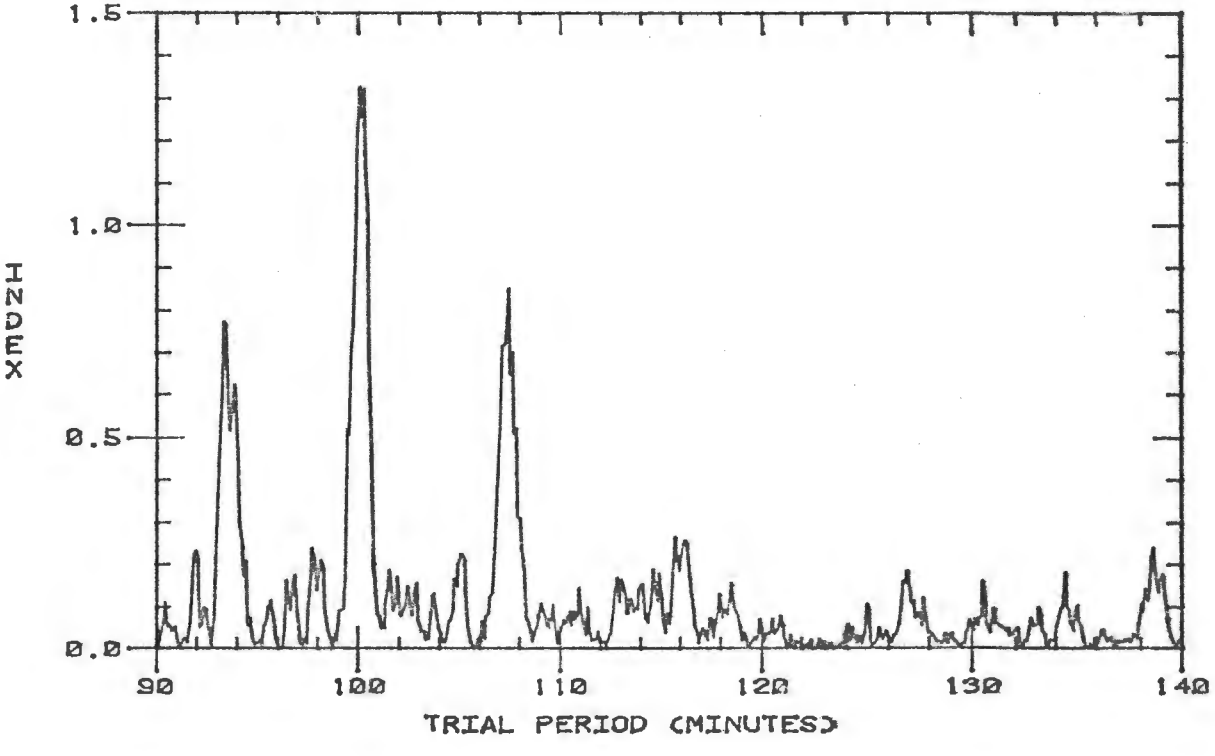
1.5
1.0
0.5
0.0
XEDNH
90
100
110
120
130
140
TRIAL PERIOD (MINUTES)

be 1547, 1482, 1424 and 1446 minutes for the four peaks. It is clear that these peaks are caused by aliasing due to the spacing of one day (1440 minutes) between the nights of observation, and that such peaks may be expected when the real data are analyzed. Figure 3-9 shows the peak at 77 minutes on an expanded-scale periodogram for the second set of data, and it may be seen that despite the great amount of noise present, the Jurkevich method was able to give a very good estimation of the true period.

3.4 The Maximum Entropy Method Applied to Artificial Data

The maximum entropy method of spectral analysis is an adaptation of the standard Fourier method that has been in use for many years. If a function g(t) is composed of N sinusoids of frequency f_i, then its Fourier transform $G(f) = \int_{-\infty}^{+\infty} g(t)\exp(\sqrt{-1}ft)dt$ will be a series of Dirac delta functions, $G(f) = \delta_1(f-f_1) + \delta_2(f-f_2) + ... + \delta_N(f-f_N)$, which will indicate the correct frequencies. Unfortunately, this method assumes that a function g(t) is known for $-\infty<t>+\infty$. In practice, g(t) is known for only a few intervals of time, or for only a finite number of points. Deeming (1975, 1976) has published a short computer program that generates the Fourier transform for a discrete number of unequally-spaced points, but this method suffers from severe aliasing problems because of the lack of data over

Figure 3-9

Expanded-scale Jurkevich periodogram of data generated from: $y(t) = .006 \sin(2\pi t/77) + .008 \sin(2\pi t/100) + \sigma(.010)$. The vertical line at P = 77 minutes indicates one of the two periods present in the data.

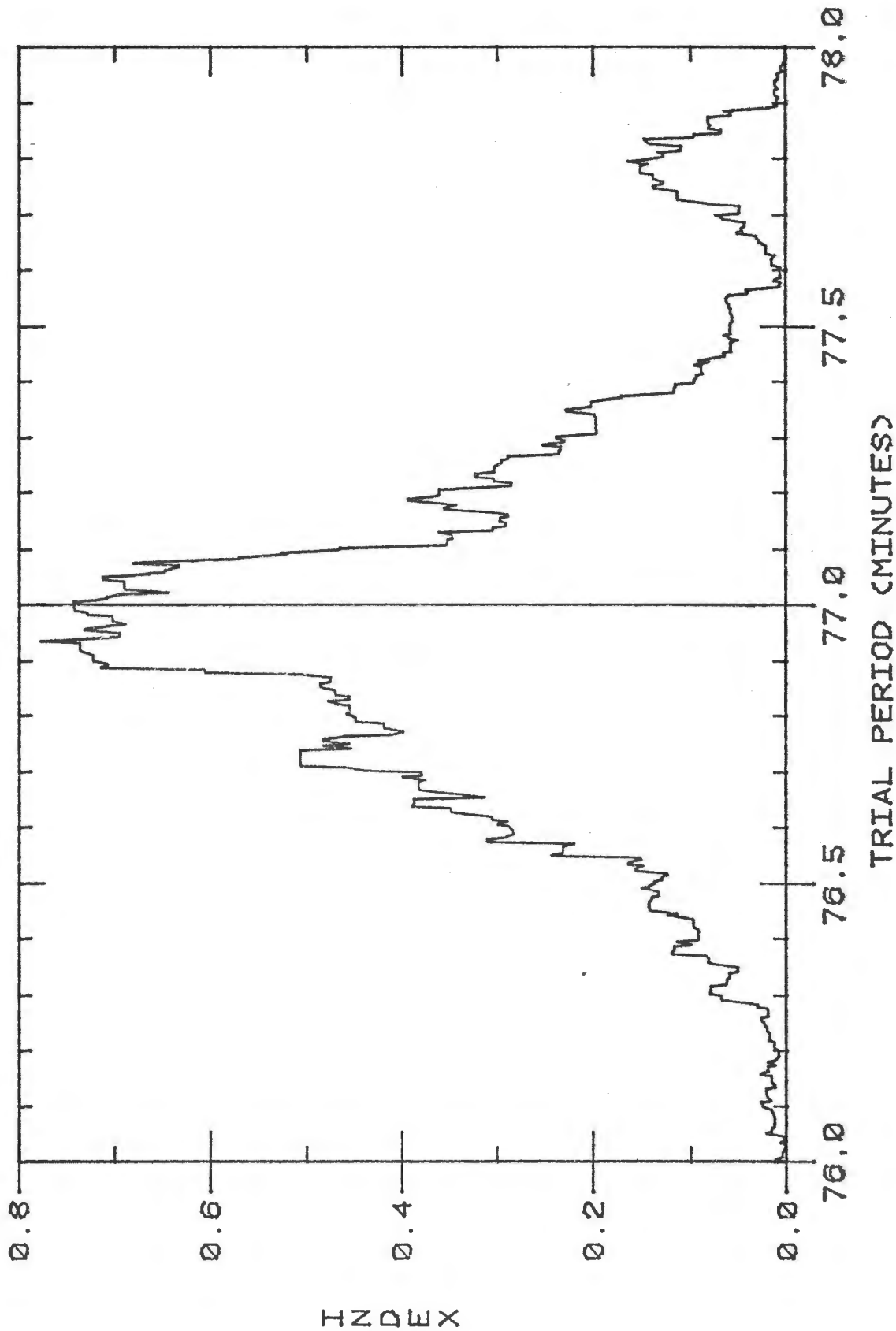
INDEX
0.0
0.2
0.4
0.6
0.8
76.0
76.5
77.0
77.5
78.0
TRIAL PERIOD (MINUTES)

the entire time range. Gray and Desikachary (1973) present a technique that generates the Fourier transforms of a function known at only a few intervals, and predicts how the aliasing will appear. The best Fourier technique would be one that is maximally noncommittal about the behaviour of g(t) outside the regions where g(t) has been measured. As entropy is a measure of the lack of information about a system, such a method would be called a maximum entropy method, and the computational details of just such a method have been given by Anderson (1974), based on the well-known algorithm first published by Burg (1967). The computer program used in this study was supplied by Dr. J.R. Percy; the principles of the computation will not be reviewed here. See Percy (1977) for a brief review of the method and experiments with artificial data, produced to resemble some short-period variable stars.

One severe difficulty with this particular maximum entropy program that greatly limits its usefulness to astronomers is that it can only be used on equally-spaced data. The observations taken during one night can be interpolated to produce equally-spaced data points, but these sets of nightly data cannot be linked together in this program and searched for periods using this method. Anderson (1978) has suggested a method for linking nights together, but this approach has not yet appeared in the astronomical literature. To test the maximum entropy method, the artificial data generated using $\sigma(.005)$ in the previous section were broken into

nightly sets of data, and linearly interpolated to produce equally spaced observations. Figure 3-10 is a typical periodogram based on the artificial data generated for the night of October 23. The solid line is a period-search of moderate resolution, and the broken line is a period-search of higher resolution. The units along the y axis are arbitrary, and may have different scales for the two curves. Nightly periodograms were constructed for all six nights and the locations of the peaks measured and placed in Table 3-1. The periods generally occurred around 77 and 100 minutes, and these two sets were averaged together to produce two mean periods for the entire set of data. It may be seen from Table 3-1 that the peaks at 77 and 100 minutes are located with an accuracy of about two percent. Percy (1977) has noted that even using data with low noise, the periods found are generally inaccurate by one or two percent. Swingler (1979a) has reported, however, that this error can be reduced by using a simple window function, so this may not be an obstacle in the use of this method. Percy (1975) finds that the light curve of the star CY Aquarii can be modelled by a sawtooth curve, and that a previous analysis of this light curve based on the maximum entropy method was incorrect, because a sawtooth function generates several false peaks in its periodogram. A bin-type period analysis like the Jurkevich method is relatively insensitive to asymmetric light curves, as demonstrated by Stellingwerf (1978). Swingler (1979b) has also found that the maximum entropy

Figure 3-10

Maximum entropy method periodogram generated by the function: $y(t) = .006 \sin(2\pi t/77) + .008 \sin(2\pi t/100) + \sigma(.005)$. The solid line is a periodogram of medium resolution, and the broken line is a periodogram of higher resolution. The 84 data points used in this periodogram were equally spaced over an interval of 478 minutes.

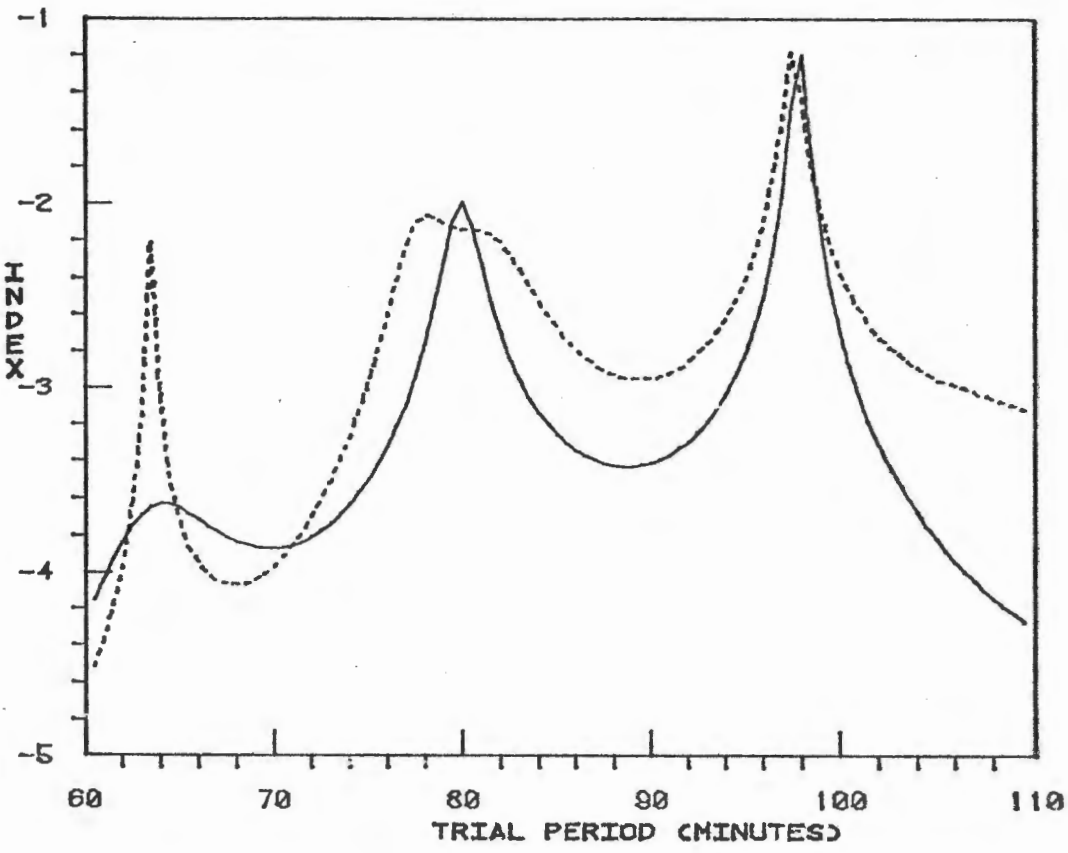
-1
-2
-3
-4
-5
HINDEX
60
70
80
90
100
110
TRIAL PERIOD (MINUTES)

TABLE 3-1

MAXIMUM ENTROPY METHOD RESULTS ON ARTIFICIAL DATA

Date of Observation (October)	Periods (minutes) (Moderate Resolution)	Periods (minutes) (High Resolution)
23	80,98	78,97
25	84	79,86
26	102	80,105
27	80	77,101
28	78,100	76,82,100
29	98	78,98
Average of All Nights	80.5, 99.5	79.5, 100.2

method should not be automatically regarded as superior to the much simpler discrete Fourier transform. In Section 5.1 it is shown that when the nightly maximum entropy periodograms are averaged together ('stacked'), they are very similar to the stacked Jurkevich periodograms. Both methods appear equally powerful when used on continuous, equally-spaced data, but the Jurkevich method is more appropriate for discontinuous data, where $L \gg P$.

CHAPTER FOUR

PERIOD-SEARCHING USING THE JURKEVICH METHOD

4.1 The Initial Search for Periods

To begin searching for periodicities in the data, a free-hand curve was drawn through the data points and the times of local maxima and minima were measured. The difference between a maximum and an adjacent minimum, when multiplied by two, gives a period for the oscillation of the star at that time. These periods were plotted against the time of observation, as shown in Figures 4-1, 4-2 and 4-3 for AI, WZ and XX Scl respectively. This is, of course, a poor method for finding periods in a star, because noise and personal bias will seriously alter the results. Also, if two periods are present, then the periods found by this method will be spread over a wide range around the true periods. This method does, however, indicate the approximate range that should be searched for periodicities, and after some consideration of the data in Figures 4-1, 4-2 and 4-3, it was decided that any periods present in all three stars must lie between 42 and 160 minutes.

A FORTRAN computer program was written to compute the Jurkevich index for 500 consectutive periods and plot the resulting periodogram using the Tektronix PLOT-10 subroutine package and digital x-y plotter. The periodogram results from the nightly data files were searched for peaks between 42 and 300 minutes, and the location of all signif-

Figure 4-1

Periods derived from the individual oscillations in the light curve of AI Scl.

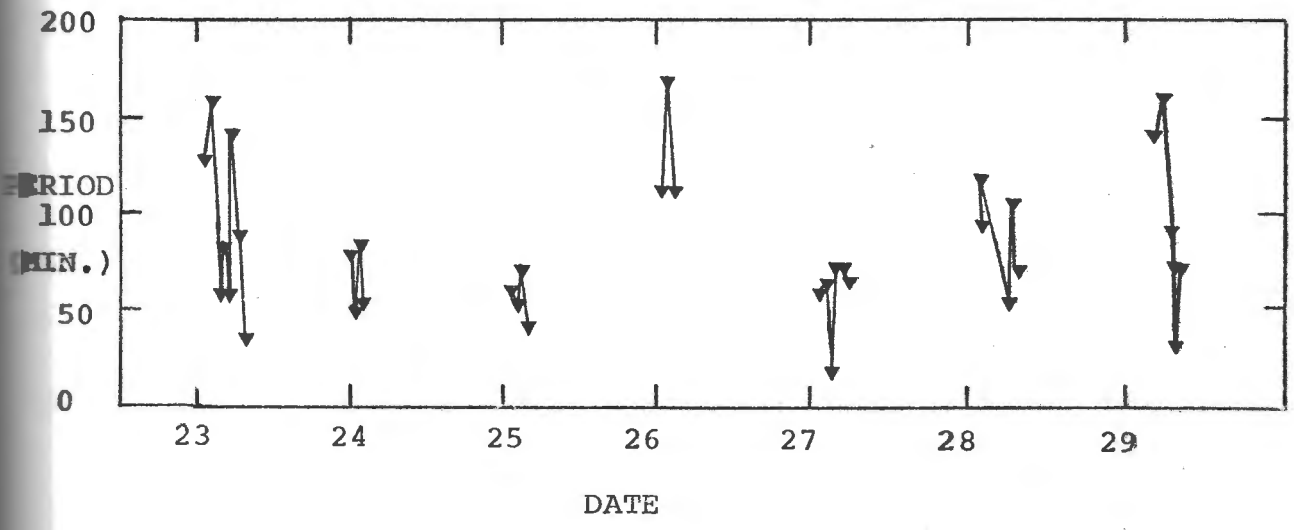
200
150
PERIOD
100
(MIN.)
50
0
23
24
25
26
27
28
29
DATE

Figure 4-2

Periods derived from the individual oscillations in the light curve of WZ Scl.

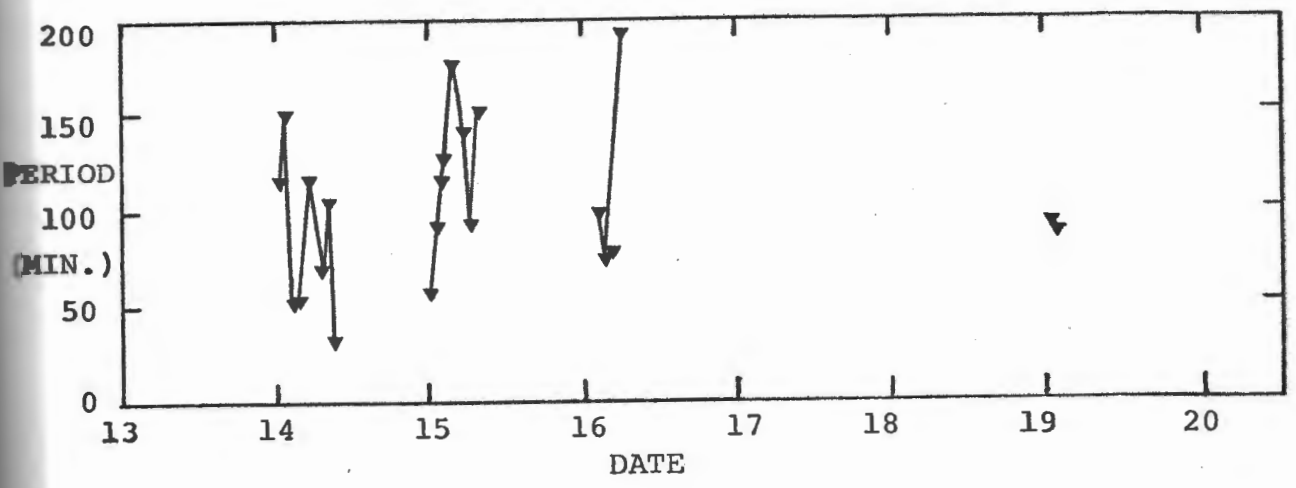
200
150
PERIOD
100
(MIN.)
50
0
13
14
15
16
17
18
19
20
DATE

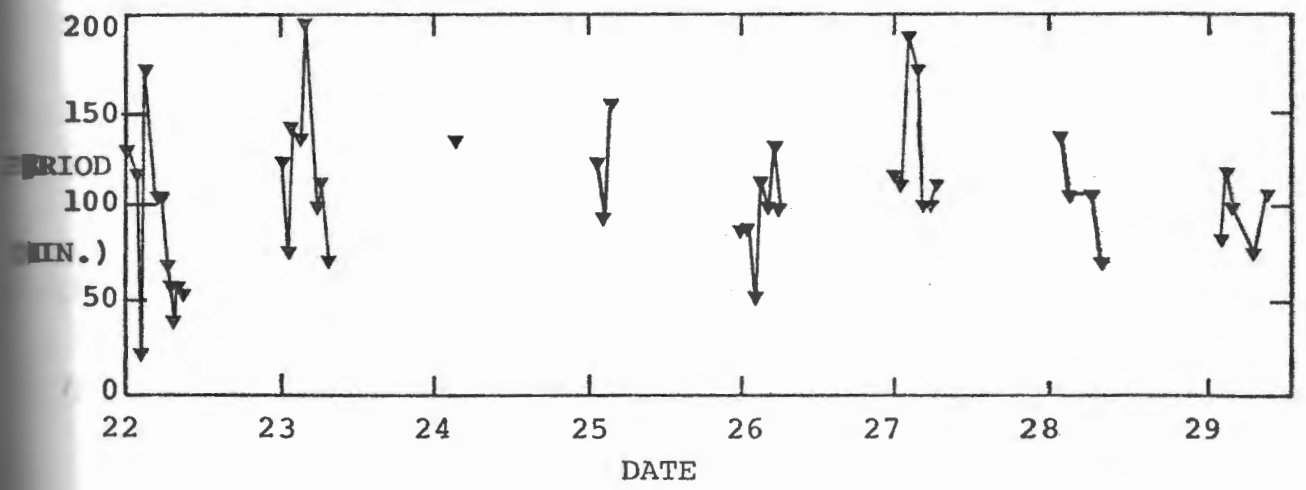
200
150
PERIOD
100
(MIN.)
50
0
22
23
24
25
26
27
28
29
DATE

Figure 4-3

Periods derived from the individual oscillations in the light curve of XX Scl.

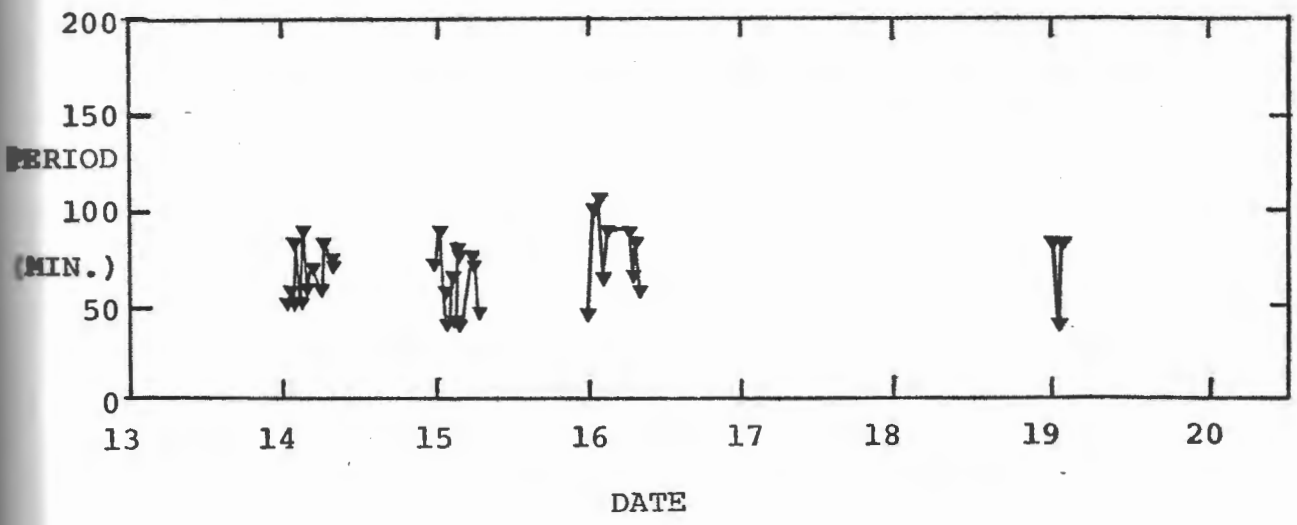
200
150
PERIOD
100
(MIN.)
50
0
13
14
15
16
17
18
19
20
DATE

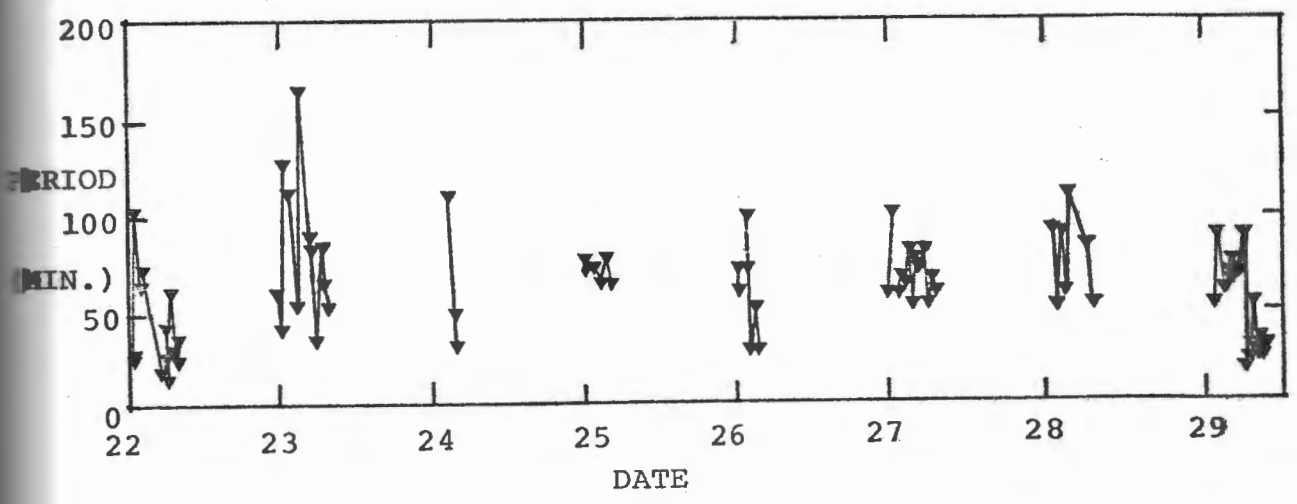
200
150
PERIOD
100
(MIN.)
50
0
22
23
24
25
26
27
28
29
DATE

icant peaks were entered in Table 4-1. As an extra precaution the data files were also searched for periods between 14 and 42 minutes, but no significant peaks were found. Figure 4-4 shows two typical examples of these nightly periodograms.

A more accurate way of finding the periods is to stack the nightly periodograms. Figures 4-5, 4-6 and 4-7 are the stacked periodograms obtained for AI, WZ and XX Scl respectively, and the periods that gave peaks in these figures are listed in Table 4-1. AI Scl shows several small peaks, but only the peaks at 64 and 134 minutes are large enough to have any significance. Both WZ and XX Scl show two large peaks, but for XX Scl the period for the second peak is almost exactly double the first peak, which means that the second peak is probably not real, but is instead an artifact of the method.

The great advantage of the Jurkevich method is that, unlike many other methods, the data do not have to be equally spaced, and so the Jurkevich method can be applied to the complete run of observations of a star and not just the nightly observations. When doing this, one must of course keep in mind that the period increment must not be made so large that peaks in the periodogram are missed. Such periodograms were constructed for all three stars, and the results are discussed below.

TABLE 4-1

PERIODS FROM JURKEVICH PERIODOGRAMS

Time of Observation	AI (minutes)	WZ (minutes)	XX (minutes)
14-15	———	97,135	72,145
15-16	———	93,137	70,100,134
16-17	———	95,146	78,96,148
22-23	———	94,134	65,127
23-24	63,79	96,135	70,87
25-26	61,68,136	114	68
26-27	137	97,127	96
27-28	66,76,126	98,142	70,139
28-29	69,80,136	94	68,88,137
29-30	64,76,130	101,150	76,158
All nights stacked	64,134	95,138	69,143
Complete run of data	62.068 64.800 123.337 134.387 148.661	94.68 138.2	67.1546 70.465 73.856

Figure 4-4

Two periodograms for XX Scl for the night of October 14.

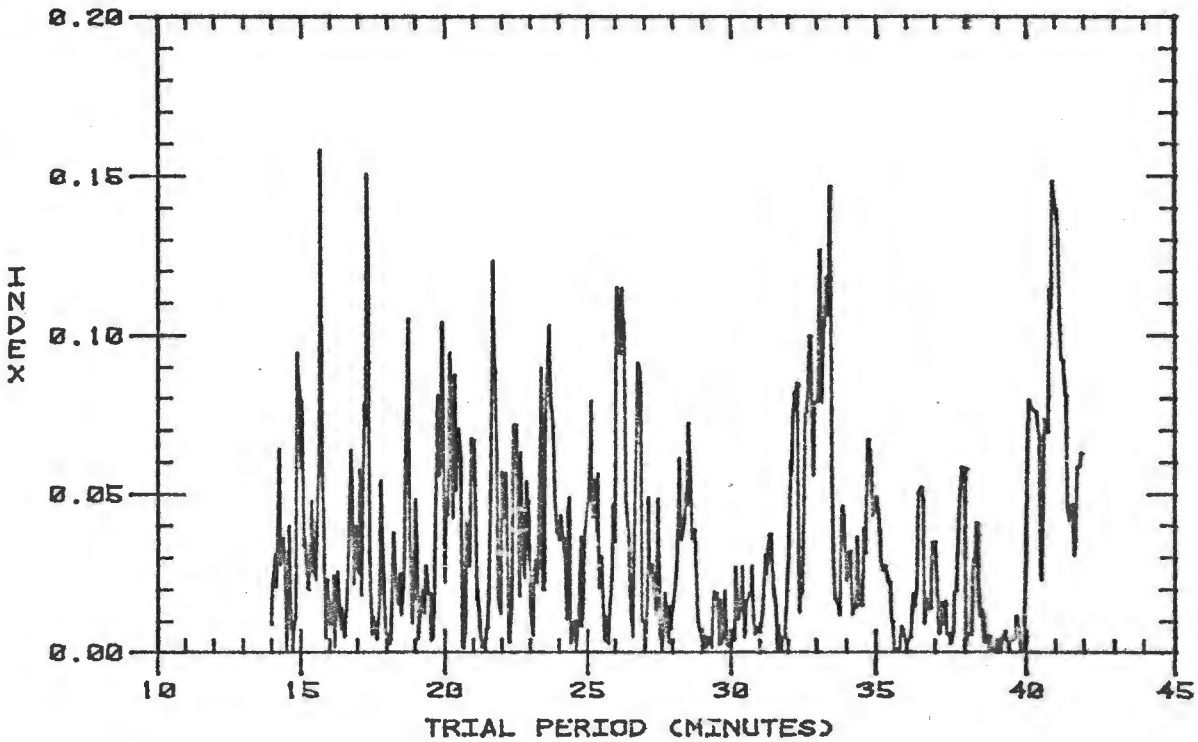
0.20
0.15
0.10
0.05
0.00
INDEX
10
15
20
25
30
35
40
45
TRIAL PERIOD (MINUTES)

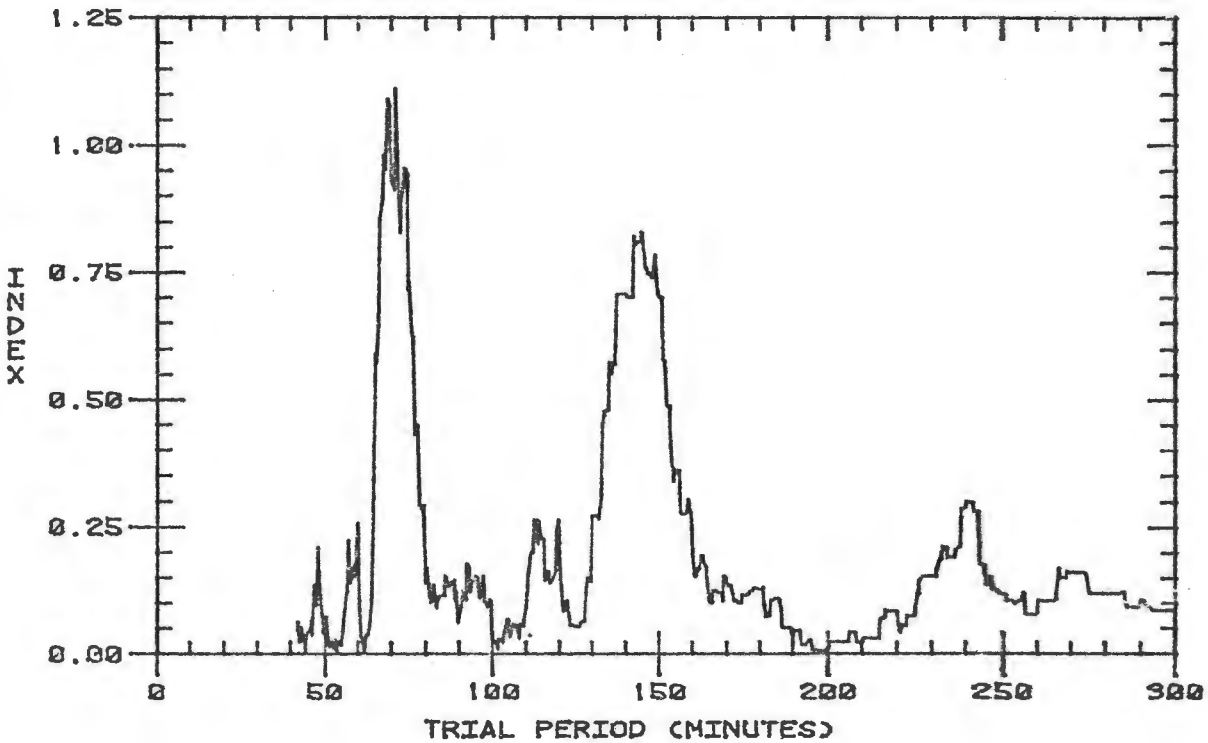
1.25
1.00
0.75
0.50
0.25
0.00
INDEX
0
50
100
150
200
250
300
TRIAL PERIOD (MINUTES)

Figure 4-5

The stacked periodogram of AI Scl.

Figure 4-6

The stacked periodogram for WZ Scl.

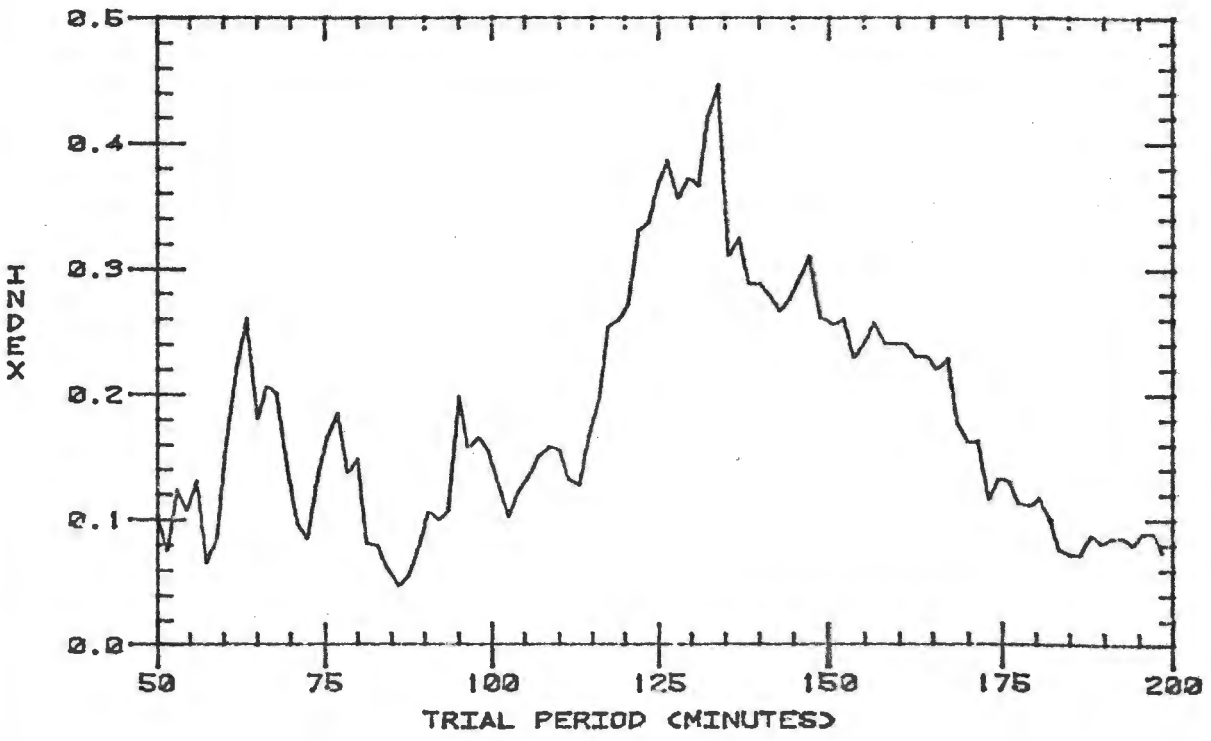
0.5
0.4
0.3
0.2
0.1
0.0
INDEX
50
75
100
125
150
175
200
TRIAL PERIOD (MINUTES)

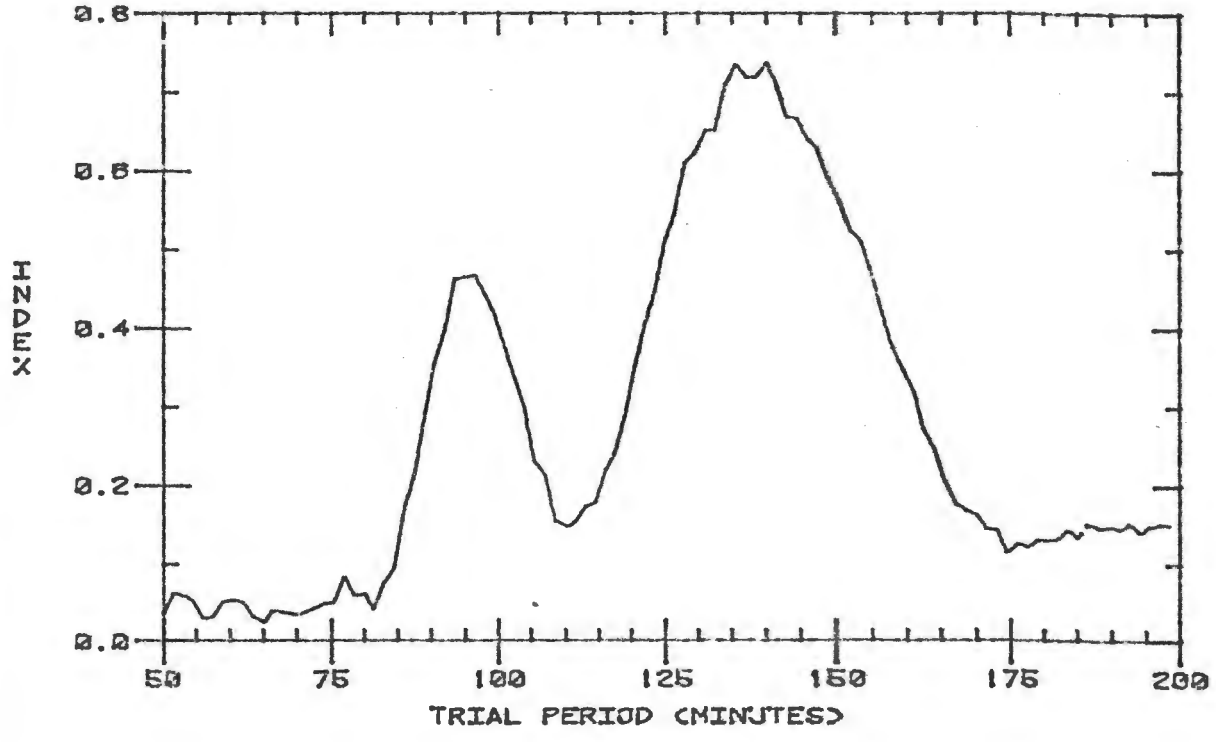
0.8
0.6
0.4
0.2
0.0
INDEX
50
75
100
125
150
175
200
TRIAL PERIOD (MINUTES)

Figure 4-7

The stacked periodogram of XX Scl.

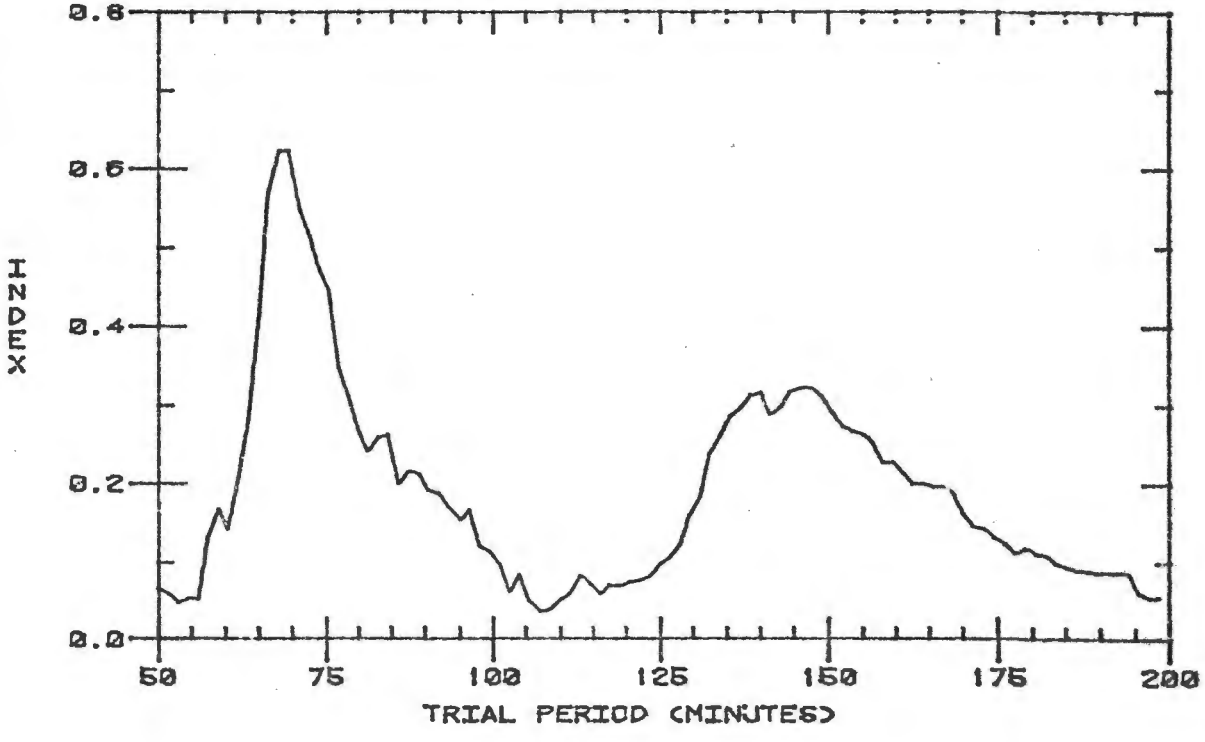
0.8
0.6
0.4
0.2
0.0
INDEX
50
75
100
125
150
175
200
TRIAL PERIOD (MINUTES)

4.2 AI Scl

A periodogram for the entire run of data on AI Scl is shown in Figure 4-8. Based on the stacked periodograms shown in Figure 4-5, one would expect to see Figure 4-8 dominated by two large peaks at 64 and 134 minutes. The periodogram is surprising however, as it does not show any significant peaks near 64 minutes and instead shows several peaks between 120 and 150 minutes. Figure 4-9 shows these two regions in more detail, and in both cases the great number of large peaks makes it unlikely that these are anything but noise. Nonetheless additional periodograms were constructed to obtain exact periods for the two highest peaks in Figure 4-9a and the three highest peaks in Figure 4-9b, and these periods were entered into Table 4-1.

The peak with the largest index was at 134.387 minutes, and Figure 4-10 shows the phase diagram that results from this period, as well as three horizontal lines showing the average magnitude in each bin. There is such a great deal of scatter in this diagram that it is difficult to say if a period is truly present. The phase diagrams for the other possible periods appeared to be a random scatter of points. These data suggest 134.387 minutes is the most likely periodicity, if any are present. Assuming this is indeed the major period in the data, the nightly light curves were re-plotted with a sine curve of this period drawn through the data points. Figure 4-11 shows such a plot for the night of October 29, when the star was fluctuating strongly.

Figure 4-8

A periodogram of AI Scl for all data points.

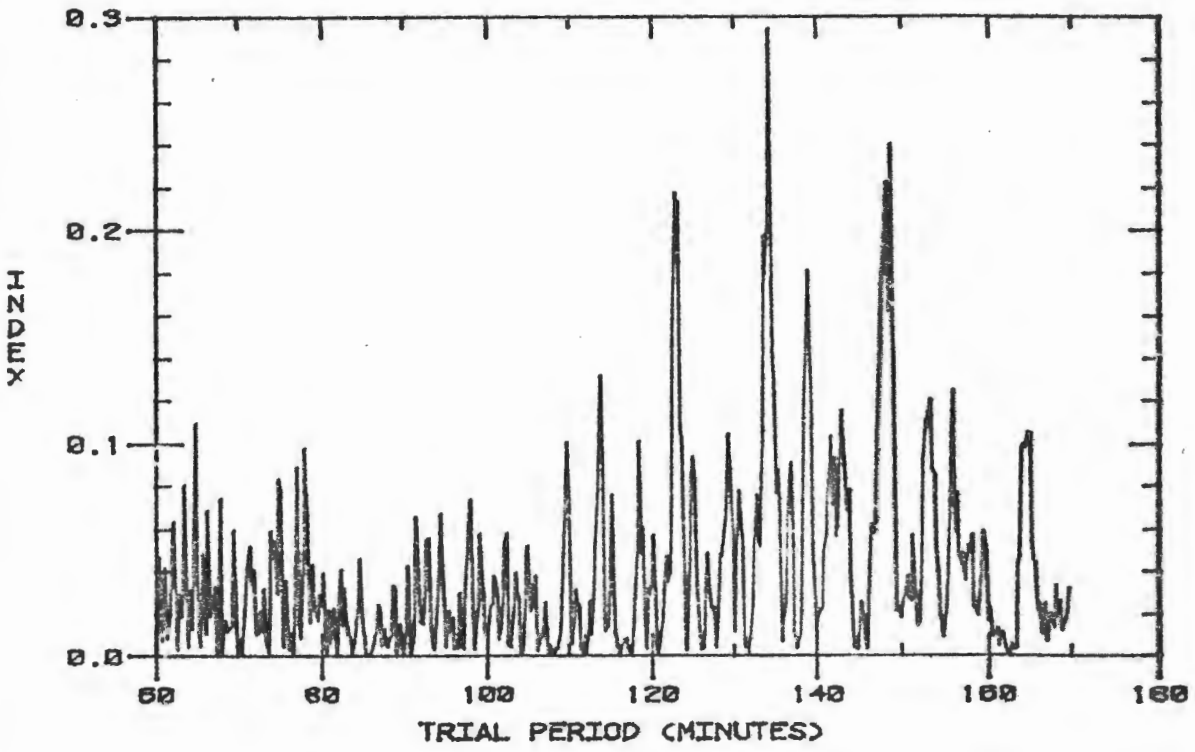
0.3
0.2
0.1
0.0
INDEX
60
80
100
120
140
160
180
TRIAL PERIOD (MINUTES)

Figure 4-9a

A high-resolution periodogram of AI Scl.

Figure 4-9b

A high-resolution periodogram of AI Scl.

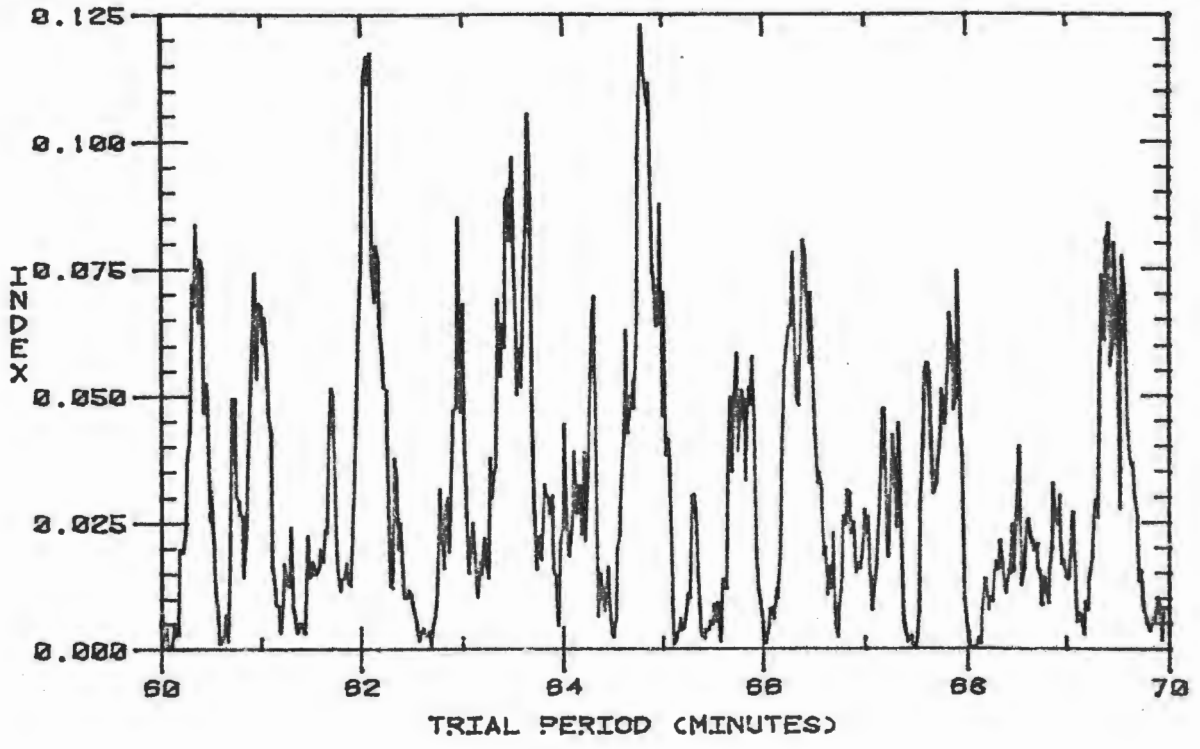
0.125
0.100
0.075
0.050
0.025
0.000
INDEX
60
62
64
66
68
70
TRIAL PERIOD (MINUTES)

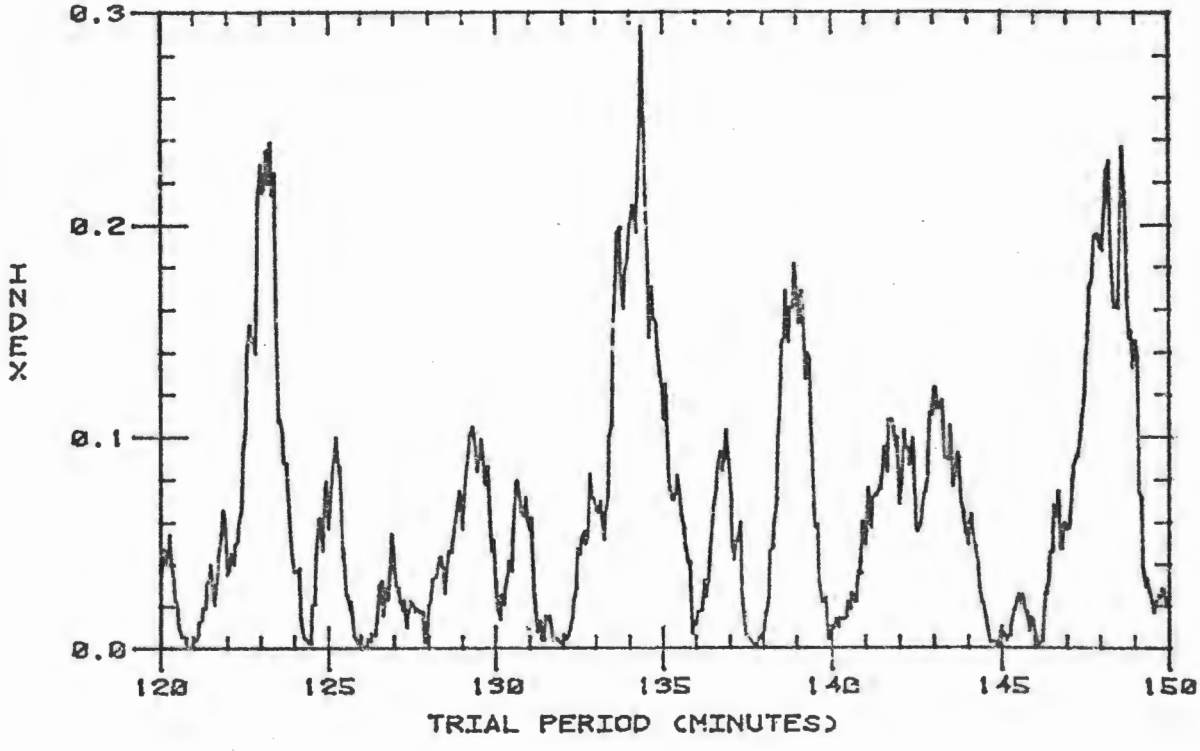
0.3
0.2
0.1
0.0
INDEX
120
125
130
135
140
145
150
TRIAL PERIOD (MINUTES)

Figure 4-10

Phase diagram of AI Scl for a period of 134.387 minutes.

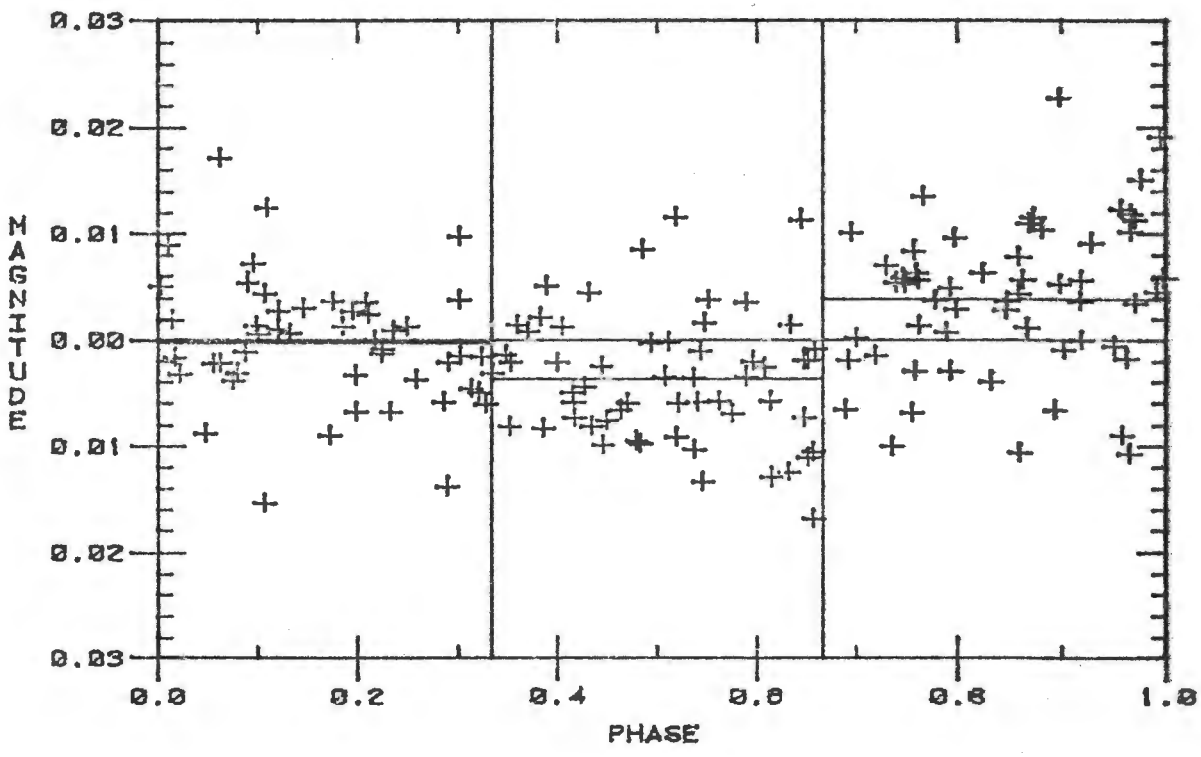
0.03
0.02
0.01
0.00
0.01
0.02
0.03
MAGNITUDE
0.0
0.2
0.4
0.6
0.8
1.0
PHASE

Figure 4-11

Observations of AI Scl on October 29. The solid curve was generated from the formula:

$f(t) = -3.1346 + .004\sin(67.32636t + 2.019)$,

corresponding to a period of 134.387 minutes. As can be seen, this curve does not fit the observations.

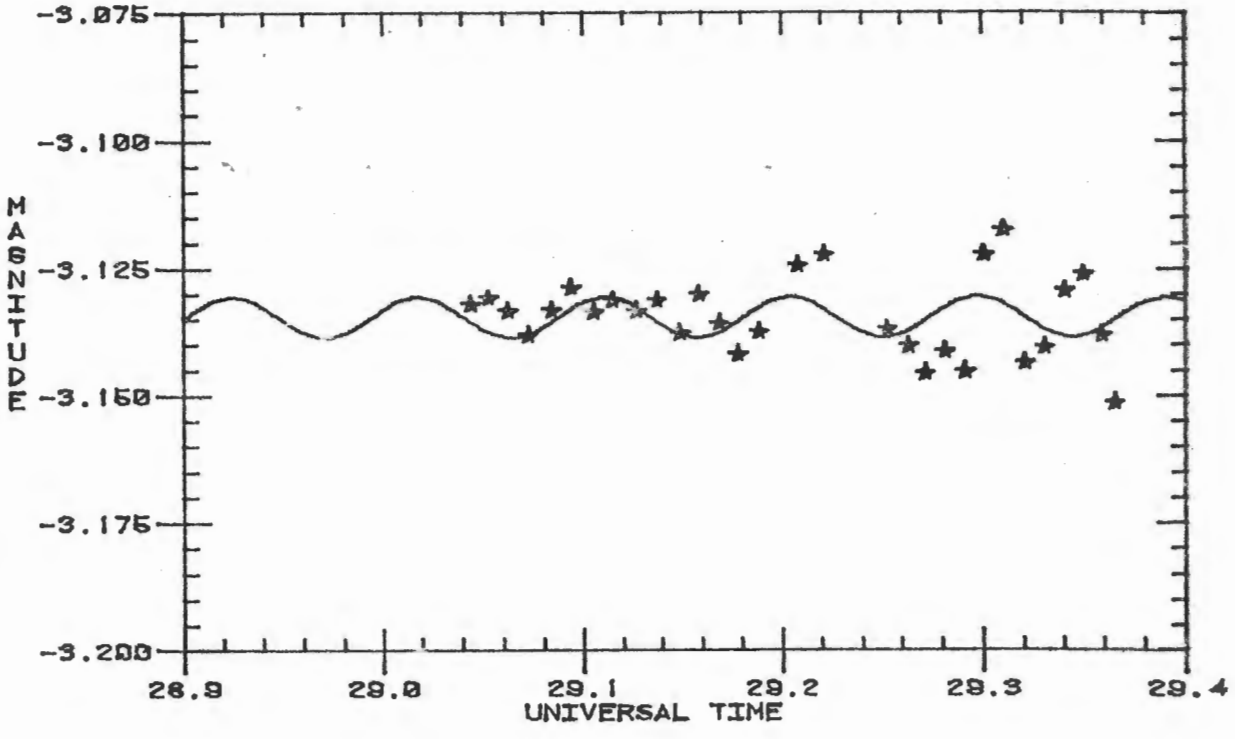
-3.075
-3.100
-3.125
-3.150
-3.175
-3.200
MAGNITUDE
28.9
29.0
29.1
29.2
29.3
29.4
UNIVERSAL TIME

As can be seen, the curve does not fit the observations, and this was true for the other nights as well.

In Section 3.3 it was concluded that if any strictly periodic fluctuations with half-amplitudes greater than 0.0017 were present, these periods would be detected in the Jurkevich periodogram. As the fluctuations in the data are much greater than this, it was concluded that AI Scl did not exhibit periodic behaviour during this observing run, based on Figure 4-9. However, many aperiodic δ Scuti stars are known to favour certain periods without following them exactly. Based on Figure 4-5 it was concluded that AI Scl did show some pulsations with periods of 64 and 134 minutes, but these pulsations were not strictly periodic over a time scale of a few days. Detailed observations of AI Scl at other epochs would be useful to investigate more completely this star's behaviour.

4.3 WZ Scl

A periodogram search for periods between 42 and 900 minutes found two very large peaks at 94.68 and 138.2 minutes, as seen in Figure 4-12. A remarkable feature of both these peaks is that they have a peak at each side of slightly less height, and that all the large peaks have a great number of small peaks at their base. In view of the discussion in Section 3-1 it seems likely that all these extra peaks are caused by aliasing. To verify this, the locations of the

Figure 4-12

Two periodograms of WZ Scl.

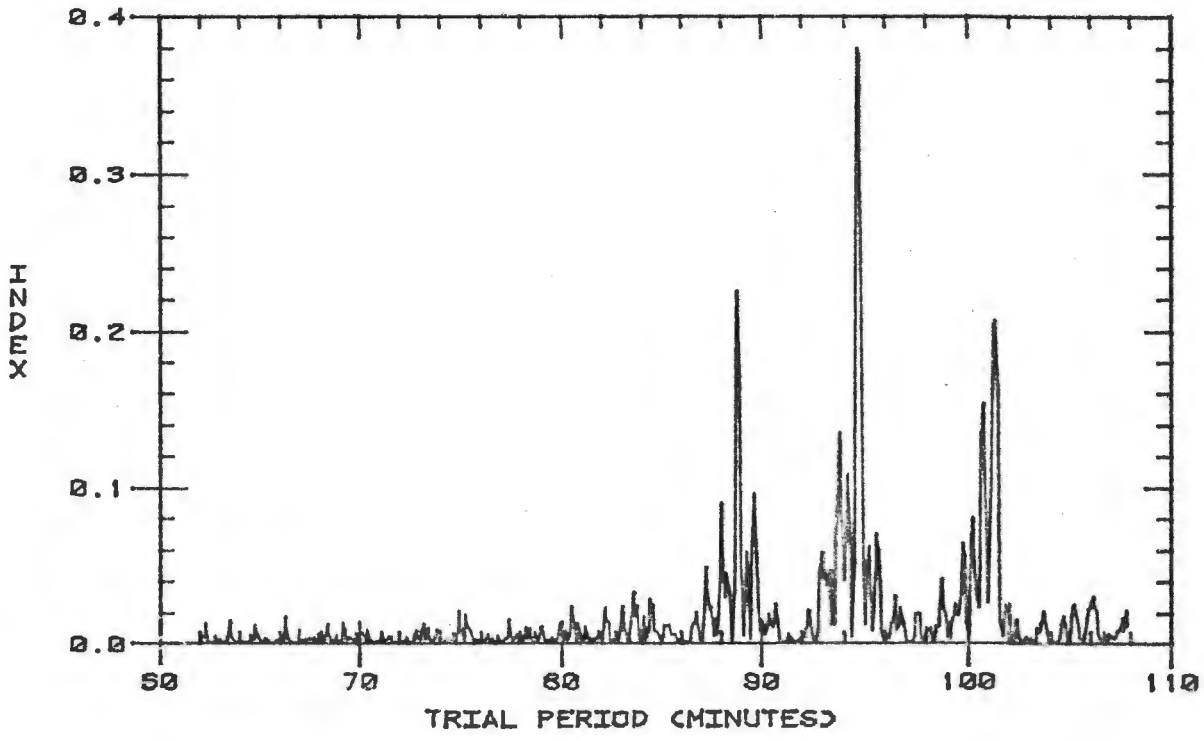
0.4
0.3
0.2
0.1
0.0
INDEX
50
70
80
90
100
110
TRIAL PERIOD (MINUTES)

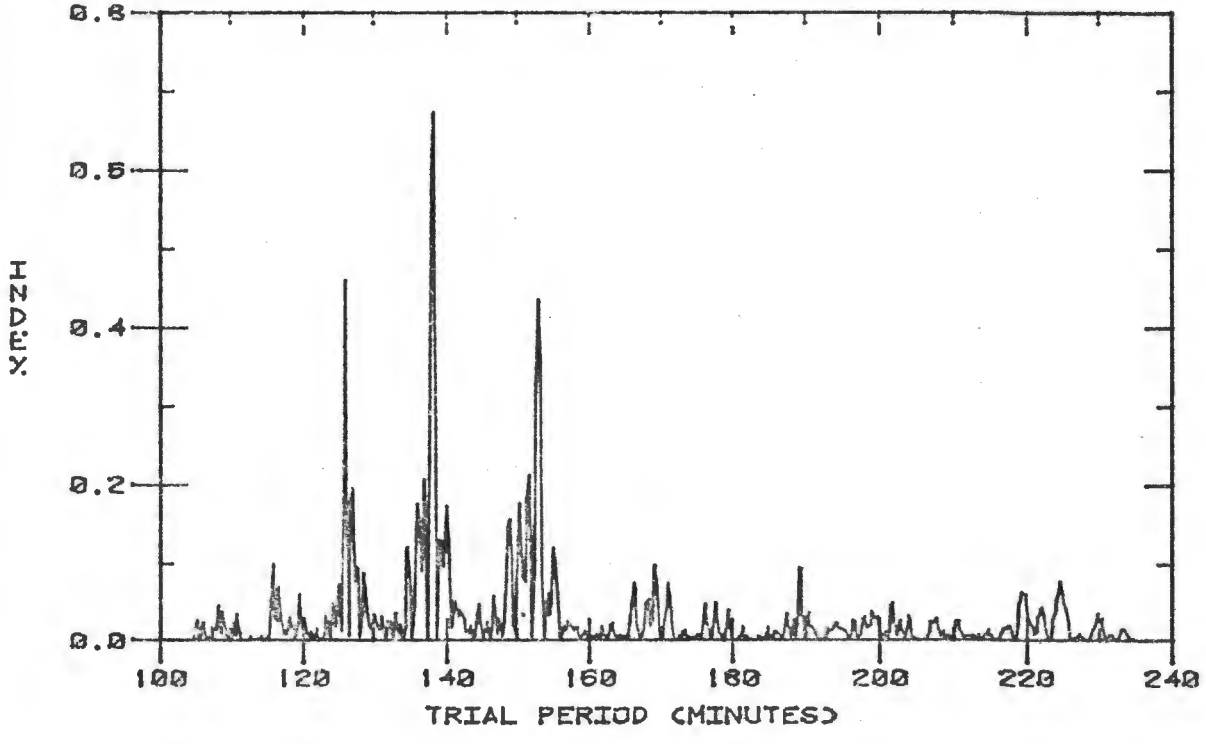
0.6
0.5
0.4
0.2
0.0
INDEX
100
120
140
160
180
200
220
240
TRIAL PERIOD (MINUTES)

two large peaks accompanying each peak at 94.68 and 138.2 minutes were found to be at 88.89, 101.36, 126.18 and 152.88 minutes, leading to beat periods of 1454 minutes (1.009 days), 1437 minutes (.9977 days), 1451 minutes (1.007 days) and 1439 minutes (.9995 days) respectively. Obviously, this aliasing is caused by the uncertainty of counting the cycles that take place during daylight hours. Similarly when the locations of the many small peaks were measured, they were found to generate a beat period of approximately 13 days. This can be explained by noticing that no data were obtained on the nights of October 17, 18, 20 and 21, because of non-photometric sky conditions. This split the data into two sections with the centres of both sections separated by about ten days. As the agreement between the two numbers is not exact, the problem was resolved by obtaining a periodogram for the data between October 22 and October 29. When this was done, the small peaks vanished, as expected.

The phase diagram for the period at 138.2 minutes was constructed, and the curve found in this diagram was subtracted from the data to create a new data file. This technique is known as prewhitening, and is very common in spectral analysis. The phase diagram for the period at 94.68 minutes, based on this new data file, will contain scatter due to noise but not scatter due to the other period; it is shown in Figure 4-13a. The process was repeated to obtain the prewhitened phase diagram for the period at 138.2 minutes, and this is shown in Figure 4-13b. The data were then pre-

Figure 4-13a

A prewhitened phase diagram of WZ Scl for a period of 94.68 minutes.

Figure 4-13b

A prewhitened phase diagram of WZ Scl for a period of 138.2 minutes.

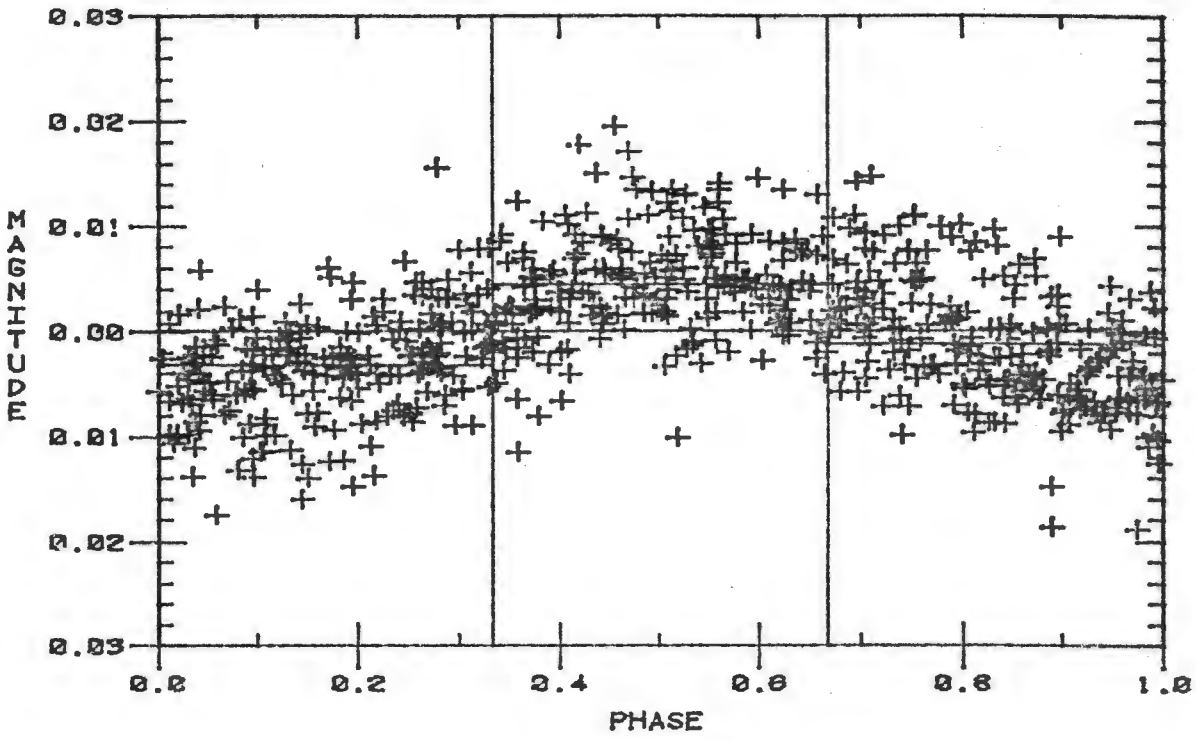
0.03
0.02
0.01
0.00
0.01
0.02
0.03
MAGNITUDE
0.0
0.2
0.4
0.6
0.8
1.0
PHASE

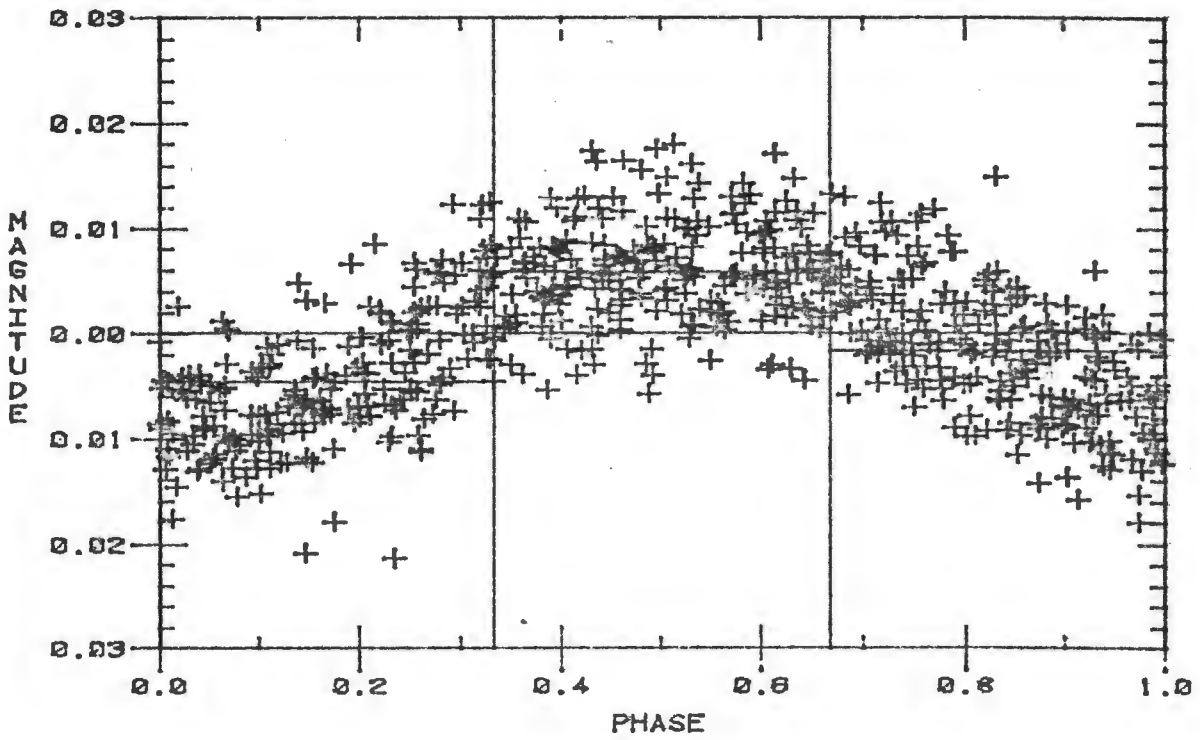
0.03
0.02
0.01
0.00
0.01
0.02
0.03
MAGNITUDE
0.0
0.2
0.4
0.6
0.8
1.0
PHASE

whitened for both periods, so that if any more periodicities existed in the data they would not be obscured by the two large-amplitude periodicities already found. As a period search did not show any large peaks, it was concluded that only two periods are present. It is quite common for δ Scuti stars to have two, but only two, periods present in their light curves. Only a few δ Scuti stars exhibit more than two periodicities (Hodson, Stellingwerf and Cox 1979). The amplitudes and x-intercepts in Figure 4-13 were measured by eye, and from this information the double-sine curve that would fit the observations was found to be:

$$f(t) = -2.5621 + .006\sin(95.58698t + .980) + .008\sin(65.44509t + 4.863),$$

where f(t) is the magnitude and t is the time of observation. The number -2.5621 was found by simply taking the average magnitude of all observations. Note that the sine function is in radians. The nightly data and the function were plotted together, and the agreement between them was found to be very good. Figure 4-14 shows this curve and the original data for the night of October 14. A slightly better curve is found in Section 5.2, based on the result of a least-squares fitting technique, and this slightly improved curve is used in Figures 2-12 to 2-21 where the results for all nights are given.

Figure 4-14

Observations of WZ Scl on October 14. The solid line was generated from the formula:

$$f(t) = -2.5621 + .006\sin(95.58698t + .980) + .008\sin(65.44509t + 4.863) .$$

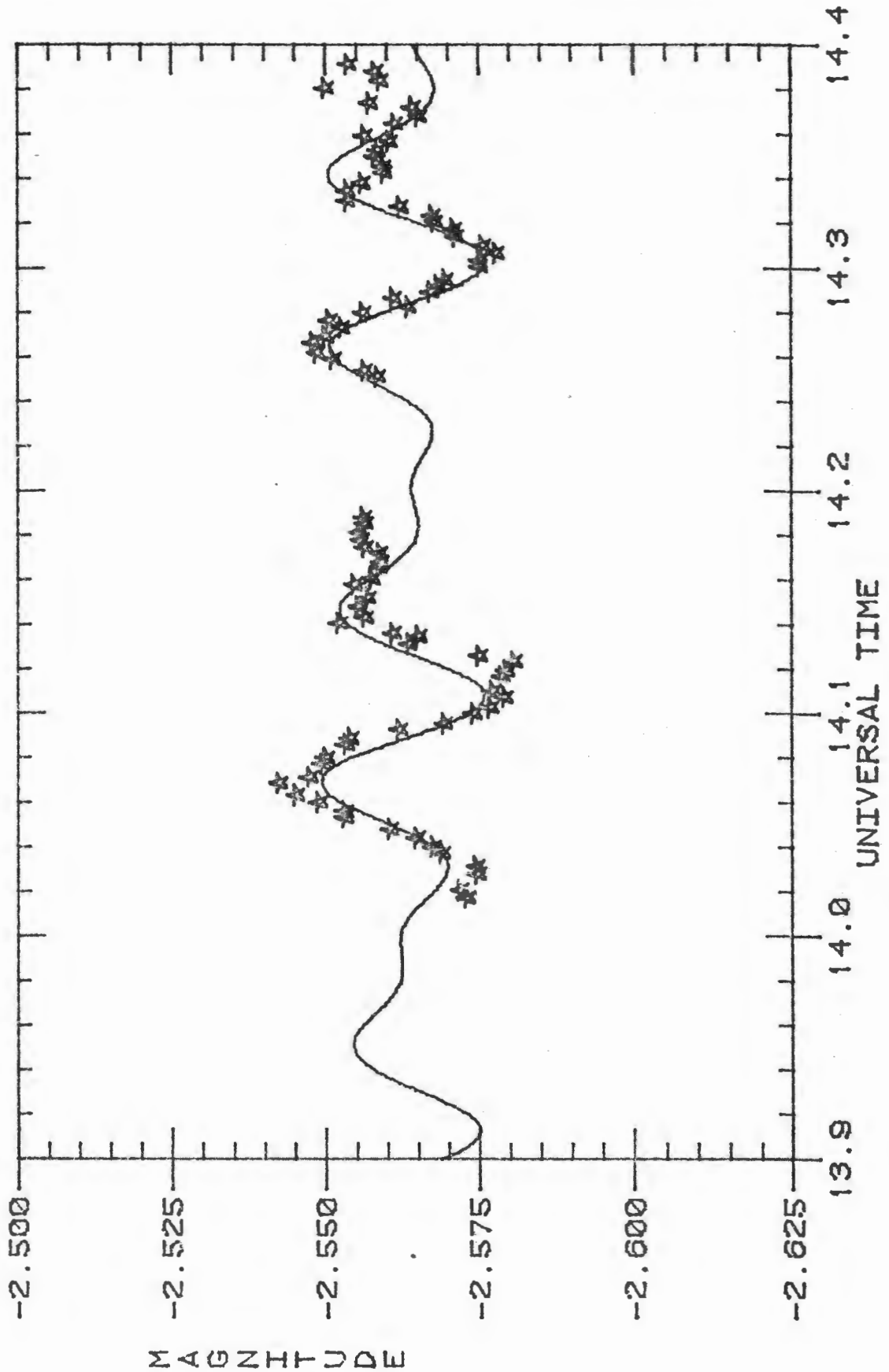
-2.500
-2.525
-2.550
-2.575
-2.600
-2.625
MAGNITUDE
13.9
14.0
14.1
14.2
14.3
14.4
UNIVERSAL TIME

4.4 XX Scl

It is clear from Figure 4-7 that only the region around 70 minutes needs to be searched, but as a precaution, a range from 45 to 170 minutes was searched using the entire data file. As expected, the only large peaks occurred near 70 minutes; these are shown in Figure 4-15. These periodograms are remarkable for the number of peaks present and their regular spacing. The small peaks around each of the large peaks, best seen in Figure 4-15b, were investigated and found to be caused by the gap in the data that had also caused small peaks in the WZ Scl periodograms. The presence of the large peaks is more troublesome. By examining the original data it can be seen that there seems to be only one period, but with a modulated amplitude. This can most easily be explained by the presence of two nearly-equal periods beating against each other. The most likely candidates are the periods at 67.155, 70.465 and 73.856 minutes, as deduced from expanded periodograms at these periods. However, it is very difficult to decide which pair are the correct periods. The problem is all the more difficult since adjacent periods have a beat period of about 1480 minutes (1.028 days), so that the same part of the beat cycle is observed every night. This appears to be a difficult case to analyze with the available data and particular care is required.

Figures 4-16, 4-17 and 4-18 show the phase diagrams for 67.1546, 70.465 and 73.856 minutes respectively. From these figures, it was found that these three periodicities

Figure 4-15a

Medium-resolution periodogram of XX Scl.

Figure 4-15b

High-resolution periodogram of XX Scl.

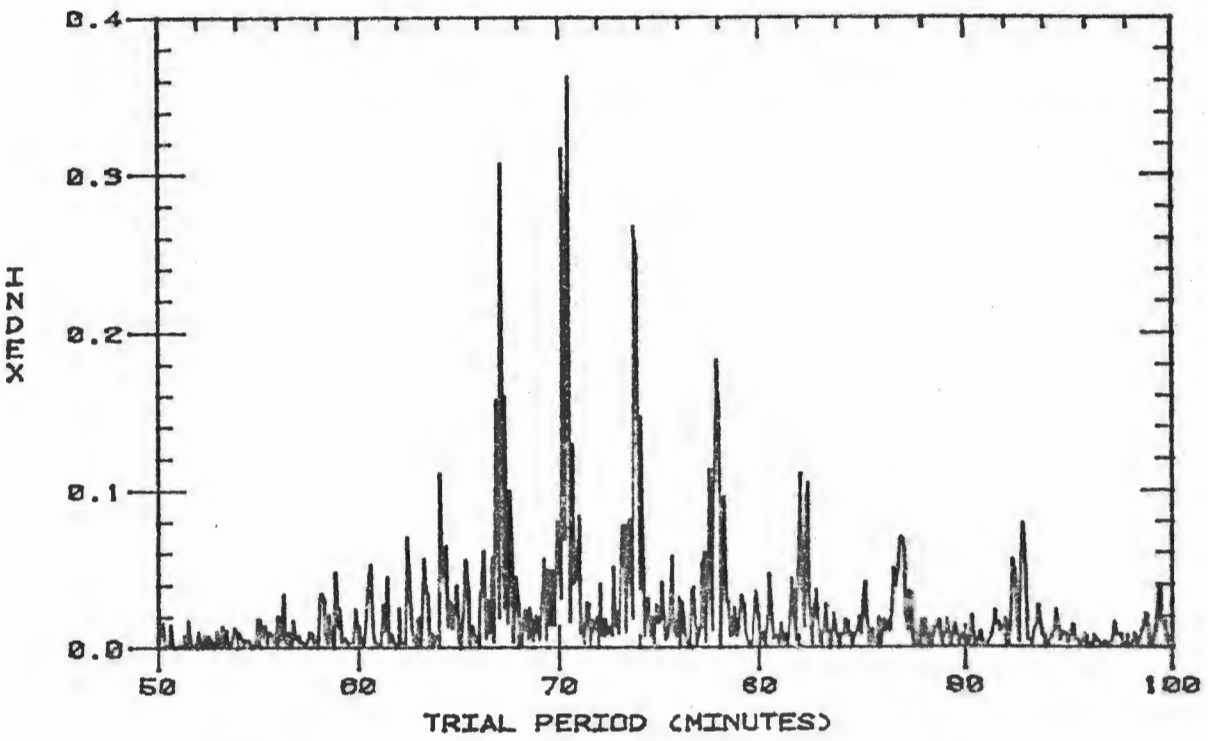
0.4
0.3
0.2
0.1
0.0
INDEX
50
60
70
80
90
100
TRIAL PERIOD (MINUTES)

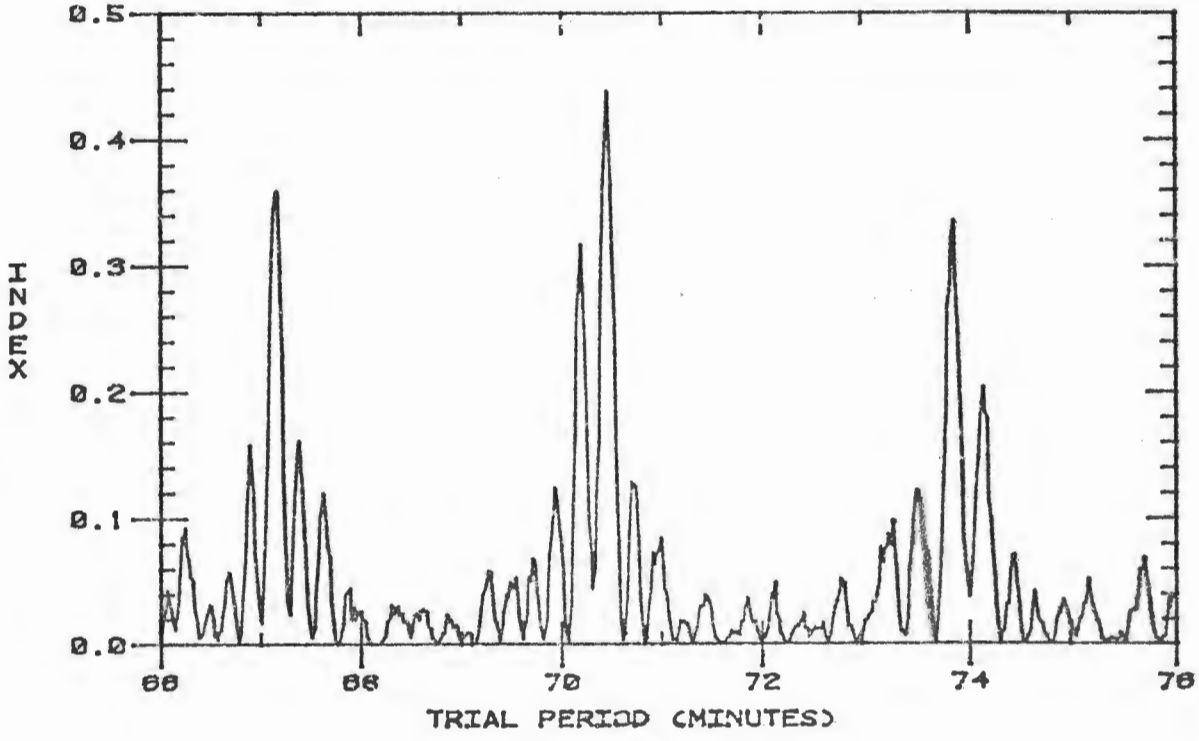
0.5
0.4
0.3
0.2
0.1
0.0
INDEX
64
66
70
72
74
76
TRIAL PERIOD (MINUTES)

Figure 4-16

Phase diagram of XX Scl for a period of 67.1546 minutes.

Figure 4-17

Phase diagram for XX Scl for a period of 70.465 minutes.

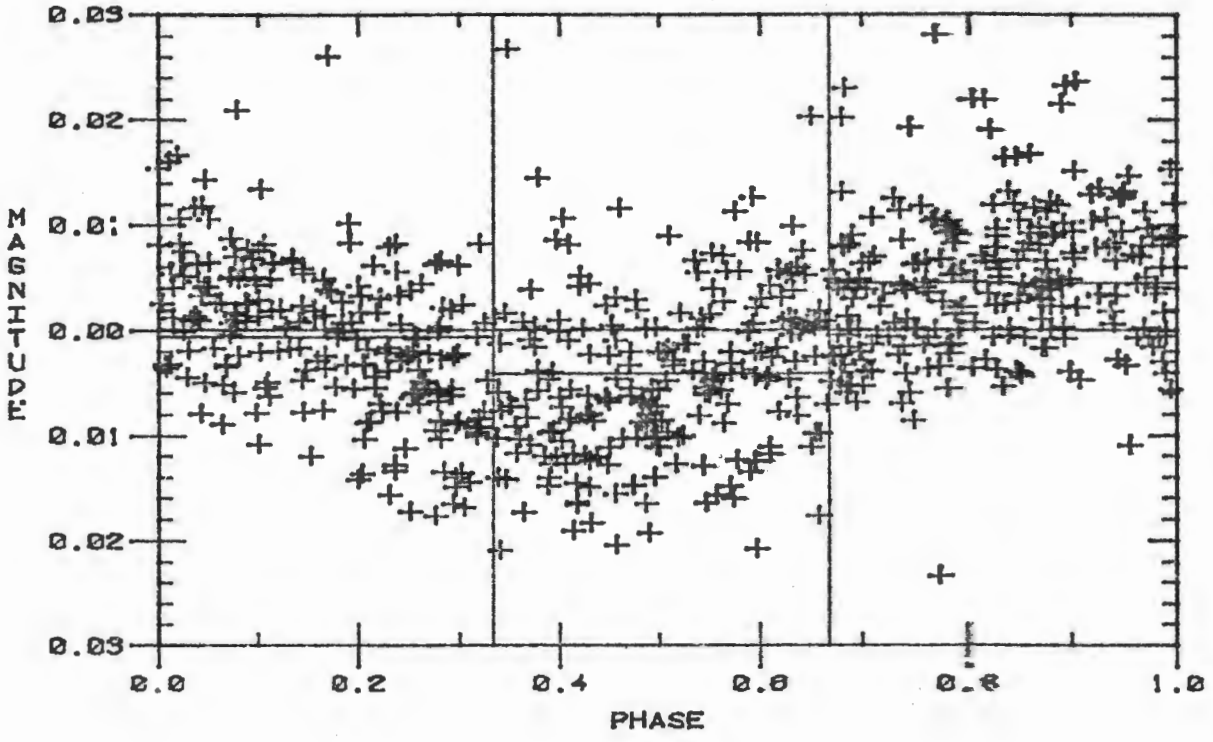
0.03
0.02
0.01
0.00
0.01
0.02
0.03
MAGNITUDE
0.0
0.2
0.4
0.6
0.8
1.0
PHASE

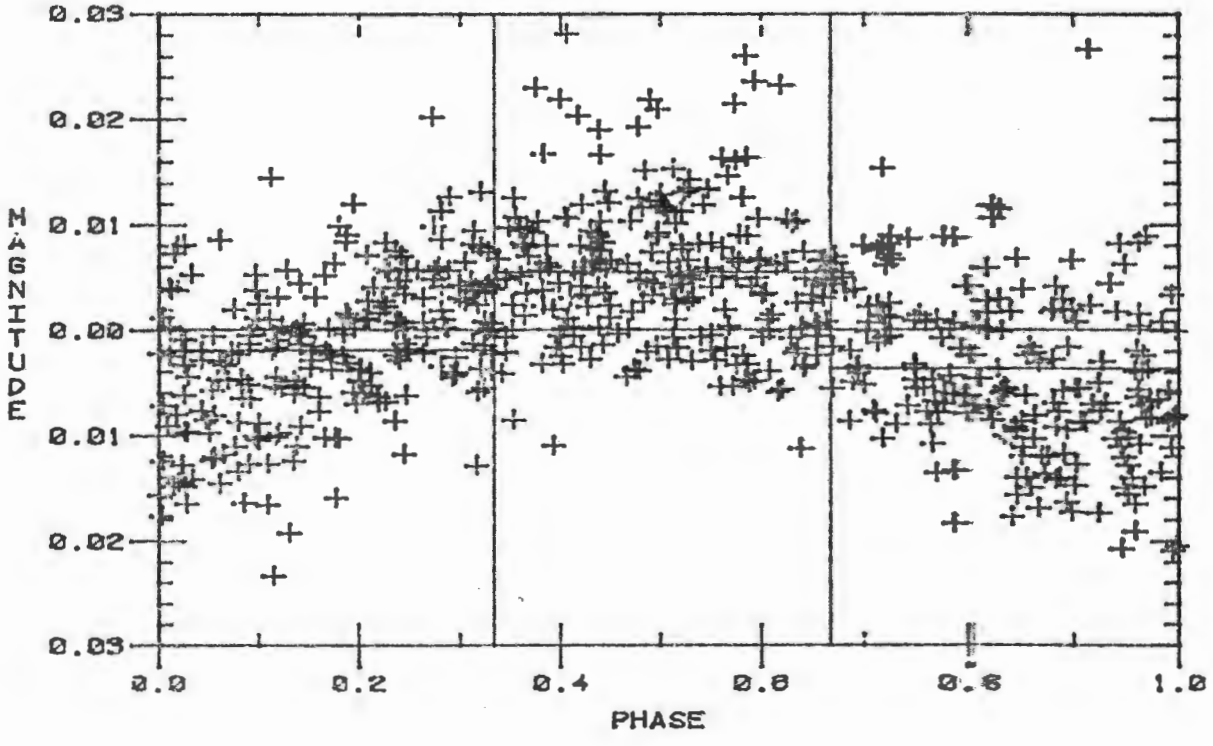
0.03
0.02
0.01
0.00
0.01
0.02
0.03
MAGNITUDE
0.0
0.2
0.4
0.6
0.8
1.0
PHASE

Figure 4-18

Phase diagram of XX Scl for a period of 73.856 minutes.

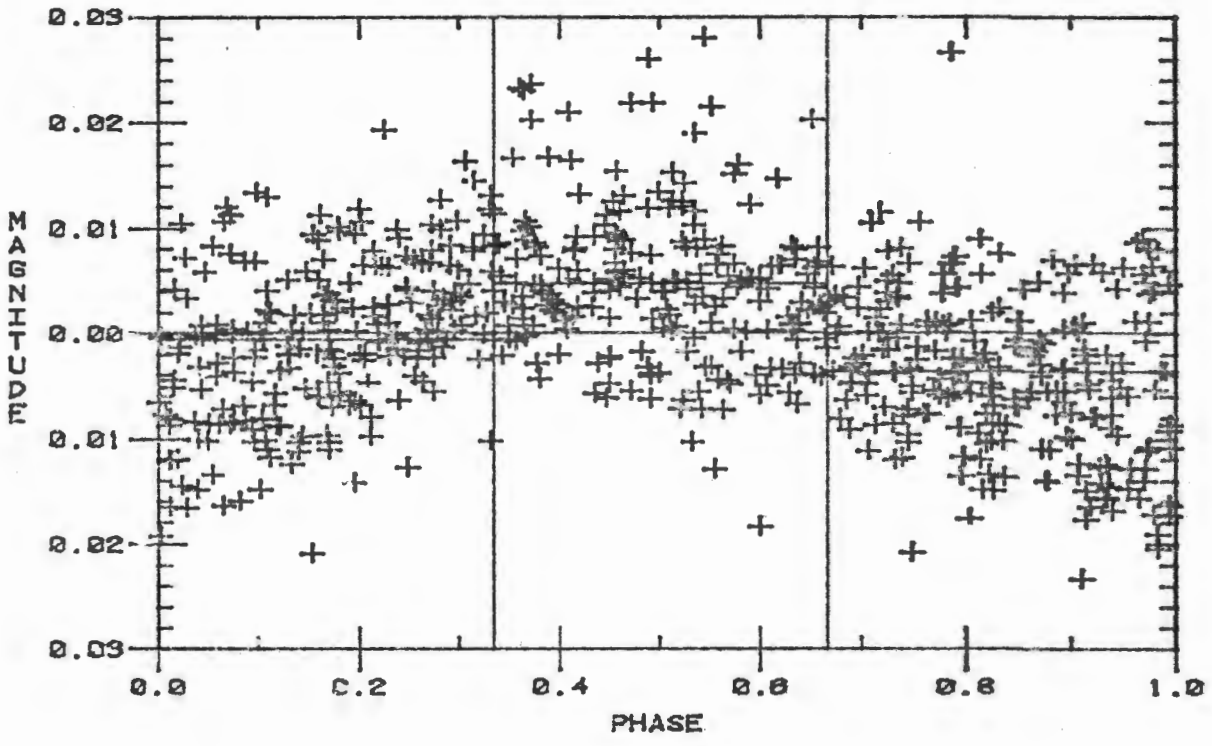
0.03
0.02
0.01
0.00
0.01
0.02
0.03
MAGNITUDE
0.0
0.2
0.4
0.6
0.8
1.0
PHASE

could be fitted by the formulae:

$f(t) = .0061\sin(134.745t - .45)$,

$f(t) = .0075\sin(128.405t + 1.95)$, and

$f(t) = .0056\sin(122.487t - 1.33)$.

It was found that by choosing any pair of these, a good fit to the data could be obtained. This is a case where only a least-squares fitting technique, as given in Section 5.2, can judge which periods are most likely present in the data.

For all three stars, Table 4-1 shows the periods that were found in this chapter.

CHAPTER FIVE

PERIOD-SEARCHING USING OTHER METHODS

5.1 The Maximum Entropy Method

In Section 3.4 it was shown that the maximum entropy method was capable of locating the correct periodicities in artificial data to within a few percent. Although the previous chapter contains accurate values of the periods found from the Jurkevich method, it was felt advisable to confirm these results using some other technique. Thus, the maximum entropy method was applied to the nightly data obtained for AI, WZ and XX Scl, and the resulting periods listed in Table 5-1. In general the high-resolution (dotted) curves contained too many peaks to be useful, and so only the moderate-resolution (solid) curves were examined for peaks. Figure 5-1 shows the periodogram obtained for XX Scl on October 14; the corresponding periodogram using the Jurkevich method is shown in Figure 4-4. Table 5-1 indicates that the maximum entropy method finds approximately the same peaks as the Jurkevich method when applied to the nightly data. By comparing the values in Table 5-1 with the more exact values in Table 6-1 found using the least-squares fitting technique, it may be seen that the maximum entropy method locates the correct period to within one or two percent, about the same accuracy as the Jurkevich method when applied to nightly data.

Because the data from different nights could not be linked together and searched for periodicities, the nightly

TABLE 5-1

PERIODS FOUND USING THE

MAXIMUM ENTROPY METHOD

Date (October)	AI Scl (minutes)	WZ Scl (minutes)	XX Scl (minutes)
14	———	58,69,94,139	68,76,158,257
15	———	65,93,141	54,69,75,97
16	———	95,140	79
22	———	55,91,138	66
23	82,131	90,132	65,96
25	60,145	97,127	68
26	52,66,140	62,97,128	67
27	60,78,119	56,92,136	70
28	52,70,111	90,142	56,72,86
29	62,135	96,147	68
All nights (stacked)	63,138	95,137	70,158

Figure 5-1

The maximum entropy periodogram for XX Scl on October 14. The solid line represents moderate resolution, and the dotted line represents high resolution.

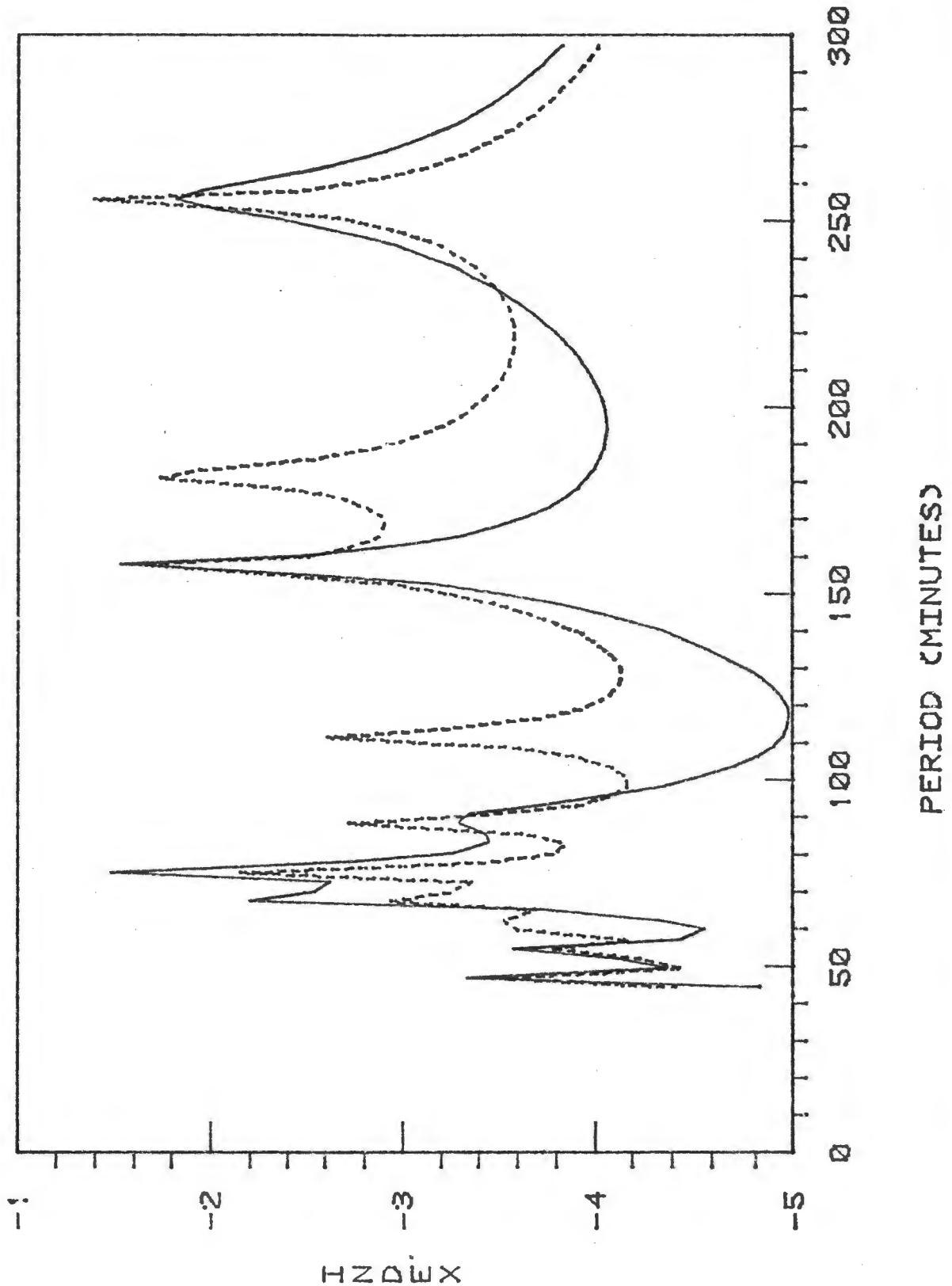
-1
-2
-3
-4
-5
0
50
100
150
200
250
300
PERIOD (MINUTES)

periodograms were averaged together (stacked) so that periodicities that occurred every night would become prominent. Figures 5-2, 5-3 and 5-4 show the stacked periodograms for AI, WZ and XX Scl respectively. The locations of the peaks in the moderate-resolution (solid) curves are listed in Table 5-1; these figures do locate the correct periods, but without great accuracy. Figures 5-2, 5-3 and 5-4 are similar in appearance to Figures 4-5, 4-6 and 4-7 which show the stacked periodograms from the Jurkevich method. In general, the results of the maximum entropy method agree with the results of the Jurkevich method, but do not increase the accuracy.

5.2 Non-Linear Least Squares

In Chapter 4 it was found that the light curves of both WZ and XX Scl could be fitted with the formula $f(t) = A + B\sin(Ct + D) + E\sin(Ft + G)$, where $f(t)$ is the magnitude and t is the Universal Time. In Chapter 4 the initial estimates were also found for the values of the seven parameters in this formula using the Jurkevich method. It is desirable to improve these values by fitting the function to the data using the method of least squares, to obtain the 'best' possible estimate of the parameters based on the available data. A non-linear least-square fitting program from the Dalhousie University computer library was used: the BMDP3R routine, which was part of the Biomedical Statistical Package from the University of California, Los

Figure 5-2

The stacked maximum entropy periodogram for AI Scl.

Figure 5-3

The stacked maximum entropy periodogram for WZ Scl.

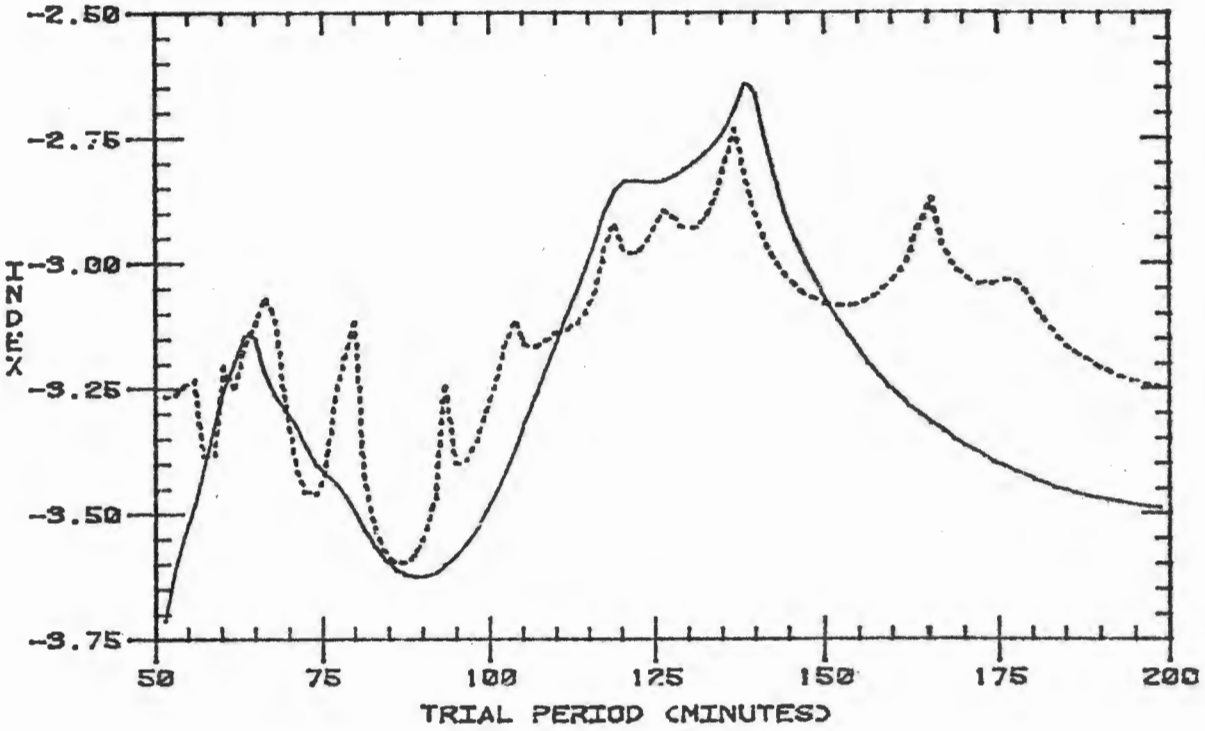
-2.50
-2.75
-3.00
-3.25
-3.50
-3.75
INDEX
50
75
100
125
150
175
200
TRIAL PERIOD (MINUTES)

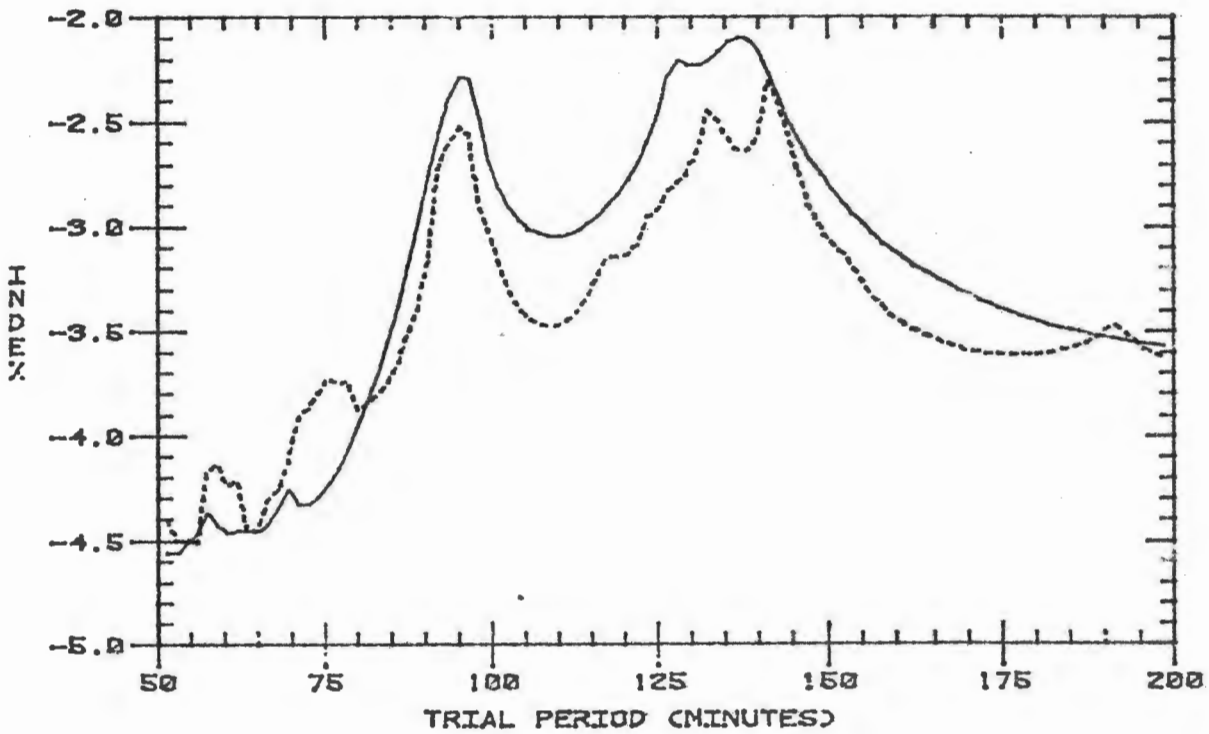
-2.0
-2.5
-3.0
-3.5
-4.0
-4.5
-5.0
INDEX
50
75
100
125
150
175
200
TRIAL PERIOD (MINUTES)

Figure 5-4

The stacked maximum entropy program for XX Scl.

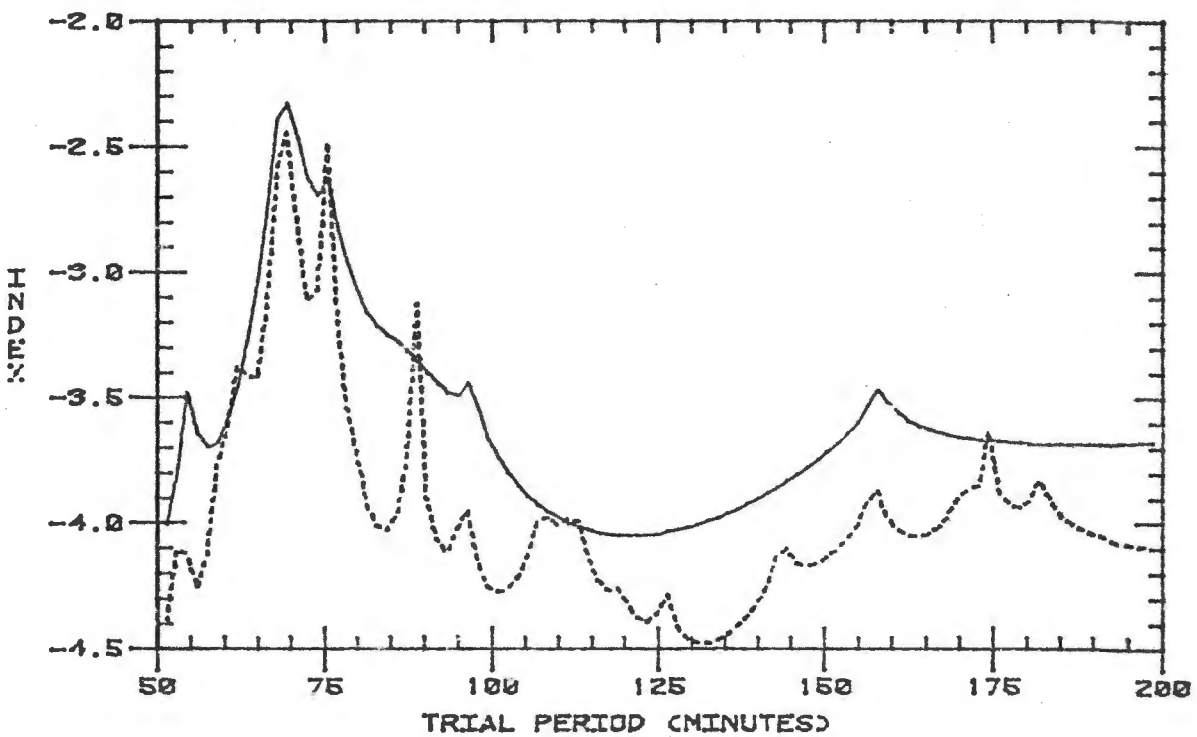
-2.0
-2.5
-3.0
-3.5
-4.0
-4.5
INDEX
50
75
100
125
150
175
200
TRIAL PERIOD (MINUTES)

Angeles. Appendix 7.5 contains all the information needed to use this program.

When this program was applied to the data for WZ Scl, it converged quickly to the values shown in Table 5.2 . The period P_1 in minutes is obtained from the parameter C using $P_1 = 2\pi x1440/C$, and the standard deviation of P is obtained from C and $\sigma(C)$ using $\sigma(P) = 2\pi x1440x\sigma(C)/C^2$. Similar relations hold between P_2 and F, giving rise to $P_1 = 94.69 \pm .01$ minutes and $P_2 = 138.16 \pm .01$ minutes. The period ratio $R = P_1/P_2$ is given by $R = F/C$, and its uncertainty is given by $\sigma(R) = F/Cx(\sigma^2(F)/F^2 + \sigma^2(C)/C^2)^{\frac{1}{2}}$. For WZ Scl, $R = 0.6853 \pm .0001$. Note that the errors quoted for the periods and period ratios are formal errors only, and are derived assuming the residuals are caused by Gaussian noise. Any other factors, such as changing periods or amplitudes, will make the true errors larger than the errors quoted here. The values of the parameters as given in Table 5-2 were then used to generate the light curves found in Figures 2-12 to 2-21.

The least-squares fitting technique used here is not capable of finding the absolute minimum of the hypersurface representing the partial derivatives of a function, but only a local minimum. It is of interest to ask whether the program will converge if any of the parameters are altered by a reasonable amount. To test this, the program was run several times using the data for WZ Scl, with one of the initial parameters slightly changed. The parameter A was tested first by adding the half-amplitudes B and E to it,

TABLE 5-2

LEAST-SQUARES PARAMETER VALUES FOR WZ SCL

	A	B	C	D	E	F	G	σ
No fitting attempted	———	———	———	——	———	———	———	.0085
Initial parameters	-2.5621	.0060	95.587	.98	.0080	65.445	4.863	.0049
Least-squares fitted parameters	-2.5623	.0057	95.554	1.8	.0078	65.485	4.0	.0047
Standard deviations for the least-squares fitted parameters	.0002	.0003	.008	.2	.0003	.006	.1	———

so that the new curve passed well above all the data points. The program converged correctly, and as an excellent initial value of A can always be found by simply taking the average of the y values of the data points (x_i, y_i), it was concluded that an initial value of A could always be estimated sufficiently well to ensure convergence.

The half-amplitude B was first doubled to B = .012, and then set to B = 0.0 . In both cases the results converged, and so it was concluded that B could be estimated well enought to allow convergence. Similarily the phase shift D was first set to 2.55 and then 4.12, corresponding to phase shifts of 90° and 180°, the most inaccurate value possible. In both cases the program converged, so it seems that the value of D will not cause divergence.

As could be expected, the parameter C associated with the period did not converge when the initial value of C was greatly altered. Figure 5-5 shows in detail the peak in the Jurkevich periodogram associated with this parameter and indicates which runs did, and did not, converge correctly. It is clear that the initial estimate of the period must be very good, or the least-squares approach will not converge correctly. Thus this approach may be used as a period-refinement method, but not a period-searching method. For the work in this thesis however, Figure 5-5 shows that the Jurkevich method provides a sufficiently narrow peak in the periodogram to locate sufficiently accurate initial periods. On this basis, it was concluded that the initial periods used

Figure 5-5

Detailed Jurkevich periodogram for WZ Scl. Solid lines indicate initial periods that converged correctly in the least-squares fitting method, broken lines indicate initial periods that converged incorrectly. The line labelled 'I' is the initial period obtained from the Jurkevich method, and 'F' is the final period obtained from the least-squares fitting routine.

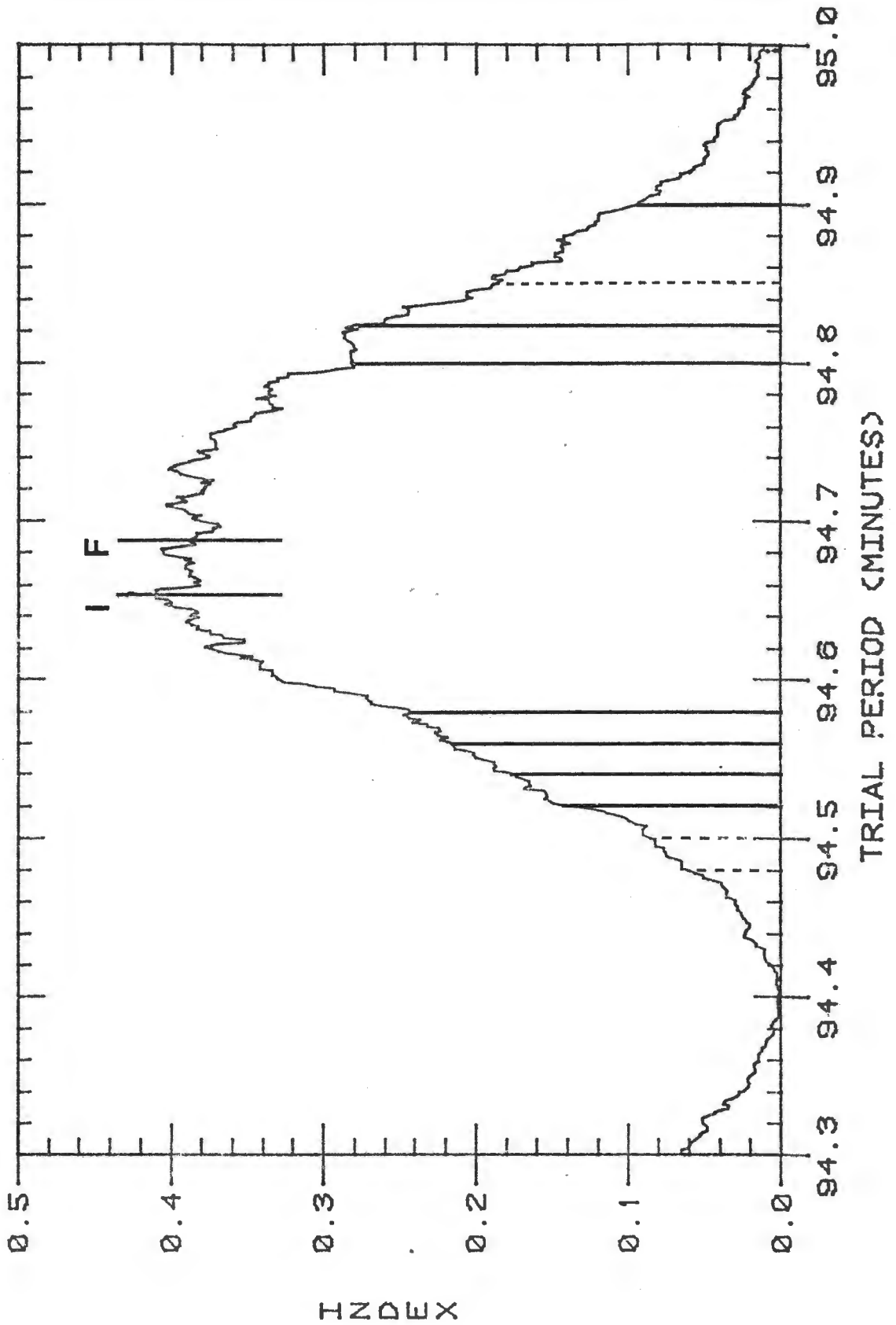
0.5
0.4
0.3
0.2
0.1
0.0
INDEX
94.3
94.4
94.5
94.6
94.7
94.8
94.9
95.0
TRIAL PERIOD (MINUTES)
I F

in this thesis were sufficiently accurate to locate the least-squares values for the parameters.

In Section 4.4, it was shown that the periods in XX Scl could not be unambiguously determined because of aliasing, but that three well-determined periods were the most likely candidates. To resolve this, the least-squares method was applied to all possible combinations, to find which combination gave the best fit to the data. To make sure that no possible candidates were overlooked, the amplitudes and phases for P = 64.133 and P = 77.940 minutes were measured and included, even though the Jurkevich method indicated that they were almost certainly aliases, and not true periods. Table 5-3 gives the initial values of the parameters for the different periods, and Table 5-4 gives the standard deviations for the least-squares fitting results. It is clear that while the combination of 70.413 and 73.944 minutes is favoured, the combinations of 67.136 and 73.873 minutes, and 70.455 and 77.955 minutes, cannot be ruled out. Values of the parameters and their uncertainties for the first combination is given in Table 5-5. The period ratio for the periods 70.413 and 73.944 minutes is R = .9522 ± .0001 and the beat period is 1474 ± 3.4 minutes.

It is unfortunate that the period ambiguity has not been clearly resolved. The only way to accomplish this is to look at two separate sections of the beat cycle. The periods of 1474 minutes and 1440 minutes (= 1 day) beat against each other with a period of 63000 ± 6000 minutes

TABLE 5-3

INITIAL PARAMETER VALUES FOR XX SCL

P (minutes)	B (or E)	C (or F)	D (or G)
64.133	.005	141.0785	3.07
67.1546	.007	134.7307	5.92
70.463	.007	128.4048	1.89
73.856	.006	122.5058	4.78
77.940	.005	116.0866	2.52

TABLE 5-4

LEAST-SQUARES FITTING RESULTS FOR XX SCL

Least- Squares Value of P_1	Least-Squares Value of P_2	Standard Deviation of Residuals
64.215	67.174	.00672
67.112	70.498	.00675
70.413	73.944	.00594
73.823	77.995	.00714
64.098	70.475	.00679
67.136	73.873	.00623
70.445	77.955	.00624

TABLE 5-5

LEAST-SQUARES PARAMETER VALUES FOR XX SCL

	A	B	C	D	E	F	G	σ
No fitting attempted	———	——	———	——	——	———	——	.0084
Initial parameters	-.24452	.007	128.4048	1.89	.006	122.5058	4.78	.0069
Least-squares fitted parameters	-.2445	.0088	128.50	0.0	.0075	122.36	1.3	.00594
Standard deviations for the least-squares fitted parameters	.0002	.0005	.01	.2	.0005	.01	.3	———
Least-squares fitted parameters with R=20/21 exactly	-.2445	.0082	128.49	0.1	.0071	122.37	1.1	.00595
Standard deviations for least-squares fitted parameters with R=20/21 exactly	.0002	.0004	.01	0.2	.0004	.01	.2	———

(= 44 ± 4 days). Thus observations on two nights separated by approximately 22 days should resolve the ambiguity: if XX Scl is in the same part of the beat cycle on these two nights, the correct periods are either 67.136 and 73.873 minutes or 70.445 and 77.955 minutes; if the beat cycles are 180° out of phase on the two nights, the correct periods are 70.413 and 73.944 minutes.

The inverse of the period ratio is 1.05016 ± .0001 which is very close to 21/20 = 1.05 . To investigate this, the least-squares program was run with the constraint that 1/R = 1.05 exactly. The resulting values for the seven parameters and their standard deviations are listed in Table 5-5. The resulting periods are P_1 = 70.416 ± .005 and P_2 = 73.937 ± .005 minutes, with a beat period of 1478 ± 3 minutes (= 1.027 ± .002 days). The standard deviations for the residuals increases only slightly with this constraint, so that it is a possibility that the periods are locked together in this ratio. However, as the time span of the data is not long enough to demonstrate this conclusively, the values of the unconstrained parameters will be assumed correct for the remainder of this thesis. Figures 2-12 to 2-21 show the data for XX Scl and the light curve based on these parameters.

CHAPTER SIX

CONCLUSIONS

6.1 Analysis of the Colours of AI, WZ and XX Scl

Table 6-1 lists all the available absolute photometry of AI, WZ and XX Scl. The V, B-V and U-B values were taken from Section 2.2 . The spectral classifications for AI and WZ Scl were taken from the Catalogue of Bright Stars (Hoffleit 1964), and for XX Scl from the Henry Draper Catalogue (Cannon and Pickering 1918). For AI and WZ Scl, the values of the absolute magnitude M_V were taken from Eggen (1976) and Breger (1979), and the quoted uncertainty is the one suggested by Breger (1979). Unfortunately, no published values of M_V exist for XX Scl and so the only method available now to obtain M_V is by using the method of spectroscopic parallaxes. Therefore, for the purpose of deriving the interstellar extinction only, a luminosity class III-IV was assumed and $M_V = 1.8$ obtained (Allen, 1973).

With these absolute magnitudes, the visual extinction A_V and the de-reddened UBV colours could be obtained. The values of A_V were found using the standard relation $\log r = (V - A - M_V + 5)/5$ and the cosecant law given by Parenago (1945), and calibrated by Sharov (1964) on 1500 OB stars: $A_V = \alpha_0 \beta \csc|b| \left\{ 1 - \exp(-r\sin|b|/\beta) \right\}$, where r is the distance to the star in parsecs, α_0 is the line of sight extinction in magnitudes per parsec, and β is the scale height in parsecs. The values of these scale parameters for

TABLE 6-1

Parameter	AI Scl	WZ Scl	XX Scl
V	5.89±.03	6.52±.03	8.84±.03
B-V	0.31±.02	0.34±.02	0.26±.02
U-B	0.12±.03	0.06±.03	0.15±.03
b	-78°.37	-79°.59	-79°.72
Spec. Class	A7 III	F0 IV	F0
M_V	2.3±.2	1.55±.2	———
A_V	.066±.005	.10±.01	.16±.02
r(parsecs)	50±4	94±10	230±100
$(B-V)_o$	.29±.02	.31±.02	.21±.02
$(U-B)_o$	.11±.03	.04±.03	.11±.03
b-y	.176	.217	.15
$(b-y)_o$	.162	.199	.11
m_1	.190	.144	———
β	2.781	2.722	———
c_1	.809	.764	———
P_1(min.)	64	94.69±.01	70.413±.005
P_2(min.)	134	138.16±.01	73.944±.005
R	.5	.6853±.0001	.9522±.0002
Δc_1	.05	.16	———
log g	4.2	3.8	———
T	7700°K	7200°K	———
M	1.8	1.8	———
Q_1	.025	.052	———
Q_2	.019	.027	———

the Sculptor region are α_o = .0016 magnitudes per parsec and β = 114 parsecs. A few iterations of these formulae gave the values of A_v and r found in Table 6-1 . As may be seen from the small uncertainty quoted for A_v , the values of A_v are not strongly dependent on the assumed values of M_v. The errors quoted for r are formal errors only, and will be larger if the calibrations used to derive M_v are incorrect. The un-reddened colours were obtained using the ratio of total to selective extinction of R = 3.3 (Herbst 1975) to obtain the colour excesses E(B-V) = A/3.3 and E(U-B) = 0.72 E(B-V) (Allen 1973). The unreddened colours were then found from $(B-V)_o$ = (B-V) - E(B-V) and $(U-B)_o$ = (U-B) - E(U-B). The values of (b-y), m_1, β and c_1 were taken from Section 1.2 . As no unreddened value of (b-y) was available for AI Scl, the relation given by Crawford & Barnes (1970) between the colour corrections for (B-V) and (b-y) were used to obtain $(b-y)_o$ = (b-y) - 0.7E(B-V). For XX Scl, it was possible to transform the values of B-V and $(B-V)_o$ to b-y and $(b-y)_o$ using the information in Crawford and Perry (1966), but no accurate transformations exist for m_1, β and c_1. The periods and period ratios were taken from Section 5.2 . For AI and WZ Scl, the formulae given by Petersen and Jorgensen (1972) were used to find the values of log g, T_e, the mass M in units of the solar mass and the pulsation constant Q for each period.

Figure 6.1 shows the positions of AI and WZ Scl on the HR diagram along with all other δ Scuti stars with accurate

Figure 6-1

An HR diagram showing all δ Scuti stars with accurate photometry (Breger 1979).

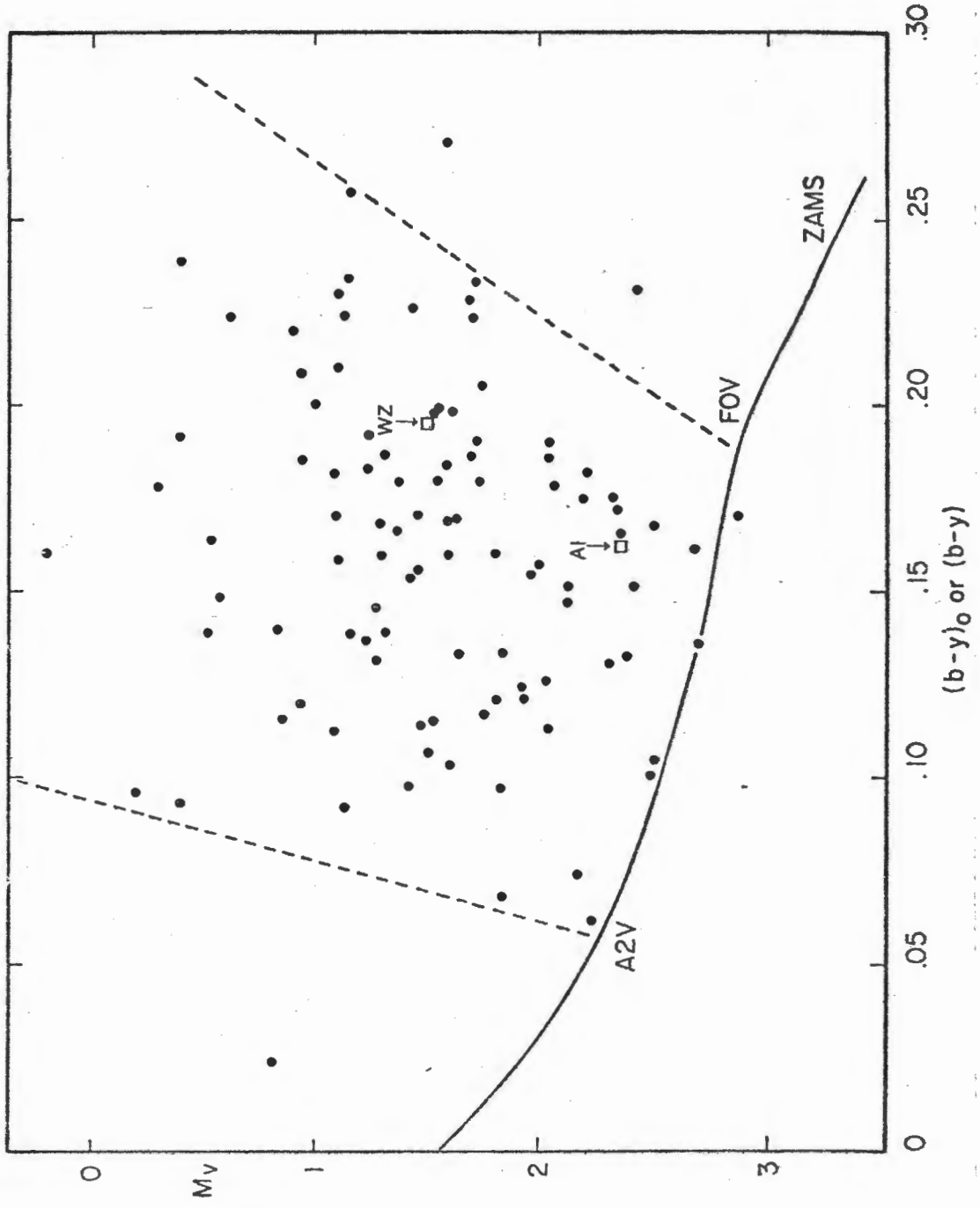
ZAMS
FOV
A2V
WZ
AI
M_V
$(b-y)_o$ or $(b-y)$
0
1
2
3
.05
.10
.15
.20
.25
.30

photometry (Breger 1979). Both stars are within the instability strip indicated by dashed lines and are near the cooler edge, where δ Scuti stars are expected to pulsate in their fundamental modes (Breger 1975). Many authors (Leung 1970) have given period-luminosity and period-luminosity-colour relations over the years. The most recent one, by Breger (1979), is: $M_v = -3.052\log P + 8.456(b-y) - 3.121$, where P is in days. For AI, WZ and XX Scl, this relation predicts periods of 80 ± 30 minutes, 180 ± 50 minutes and 100 ± 40 minutes respectively, where the uncertainties are based on the scatter in the diagram used to derive the relation. The observed periodicities for WZ and XX Scl lie within the error bars, and the periods found in this study for AI Scl are so tentative that one cannot say that AI Scl violates this relation.

From the catalogue of δ Scuti stars given by Petersen and Jorgensen (1972), it may be seen that the value of log g, T and M derived here for AI and WZ Scl are all consistent with values found for other δ Scuti stars. According to their log g, log T graph, AI Scl is very close to the zero-age main sequence and is still in the central hydrogen-burning phase, while WZ Scl is in the shell hydrogen-burning phase. Petersen and Jorgensen find from their model calculations that values of Q accurate to better than 10% can only be found for stars with amplitudes less than .08 magnitudes, and point out that at the time their paper was written, only twelve stars with amplitudes less than .08 magnitudes

had their periods determined to an accuracy of better than 10%. For these stars, the observed values of Q fall very close to the theoretical values of Q for the fundamental mode and the first three overtones at Q_0=.0333, Q_1=.0252, Q_2=.0201 and Q_3=.0170 . Although AI Scl was found to pulsate in an unstable manner, it is of interest to note that one of the observed values of Q falls very close to the value of Q for the first overtone. For WZ Scl, the observed value of Q=.027 lies very close to the expected value of the first overtone. The value of Q=.019 lies close to both the second and third overtone, and on this basis alone it cannot be said which overtone is excited. Unfortunately, nothing can be said about the colours of XX Scl, except that the U-B and B-V colours place this star very close to the zero-age main sequence.

6.2 Analysis of the Periods of AI, WZ and XX Scl

For AI Scl, it was found in Section 4.2 that while the star's brightness did fluctuate with an amplitude of .02 magnitudes, the periods of 64 and 134 minutes were not strict, but were present in a statistical sense. As was pointed out in Chapter 1, there is some evidence to indicate that AI Scl is a spectroscopic binary, and that it has been suggested that tidal modulation or magnetic coupling will inhibit pulsational stability. Thus neither the periods nor the period ratio of R = 0.5 can be considered meaningful.

For WZ Scl, the period ratio R = 0.6853 ± 0.0001

indicates that the star is not pulsating in the fundamental radial mode. Petersen (1975) has published a very useful list of theoretical period ratios for radial and non-radial modes, based on his assumed models for δ Scuti stars. In the previous section it was suggested that, based on the value of Q, WZ Scl was pulsating in the first radial overtone, and the second or third radial overtone. From Petersen's work, these two alternatives correspond to theoretical period ratios of .806 and .675, respectively. No other theoretical period ratios close to .685 have realistic values for WZ Scl, and so the best explanation for the observed behaviour of this star is that it is pulsating in the first and third radial overtone, corresponding to Petersen's predicted values of Q_1 = .0252, Q_3 = .0170 and R = .675 . Petersen states that his theoretical ratios for radial mode pulsations are accurate to 1% for δ Scuti stars, and so the difference between the observed and theoretical ratios of .6853 ± .0001 and .675 ± .007 is not considered objectionable.

The period ratio for XX Scl of .9522 ± .0001 is surprising but not inexplicable. Petersen's tables show that for a zero-age main-sequence δ Scuti star, pulsation in the first-overtone radial mode and the lowest-order non-radial mode will give the values R = .950, Q_1(radial) = .0252 and Q_0(non-radial) = .0240 . Petersen does not give uncertainties for these values, but notes that non-radial modes depend critically on the internal structure of the star. Thus the observed value of R for this star may serve as a useful test

of δ Scuti star models. XX Scl is not unique in its large value of R. Michael and Seeds (1974) observed the δ Scuti star τ Pegasi and found the periods .05433 and .04895 days, giving R = .9010 . They do not give any analysis of this ratio. Shobbrook and Stobie (1976) claim to have found three equally-spaced frequencies in the star 1 Monocerotis, with a period ratio of .98 for adjacent frequencies, and they suggest that this is caused by a degenerate non-radial mode splitting due to stellar rotation. This could also be the cause in XX Scl; only a detailed study of the rotational broadening of the spectrum of XX Scl and a mathematical prediction of the rotational velocity based on the ratio of the observed periodicities will be able to demonstrate whether or not this phenomenon is occurring in XX Scl.

6.3 Future Work

For AI Scl, it would be advisable to obtain several consecutive or closely-spaced nights of observation, working only on this star to get a very well-determined light curve, to demonstrate conclusively whether or not this star contains strict periodicities. It would also be useful to determine whether or not this star is a spectroscopic binary. For XX Scl, it has already been pointed out that two nights of observation spaced 22 nights apart are necessary to thoroughly resolve the aliasing problem that exists for this star. Four-colour photometry is needed to calculate the Q values for the observed periods, to test if the non-radial modes chosen on the basis of the value of R are correct. As was pointed out in the previous paragraph, a study of the rotation velocity of XX Scl would confirm the nature of the period ratio for this star. For WZ Scl, the periods found in this research seem well-enough determined that another extended analysis does not seem necessary, except to look for changes in the pulsation. However, if a series of short observing sessions on this star spaced judiciously across several years were carried out, it would be able to demonstrate long-term stability or gradual change in this star's period. If the star is strictly periodic, a period ratio accurate to several decimal places could be obtained.

APPENDIX 7.1

DATA FOR AI SCULPTORIS

UNIVERSAL TIME	MAGNITUDE	UNIVERSAL TIME	MAGNITUDE	UNIVERSAL TIME	MAGNITUDE
23.0035	-3.1441	25.1438	-3.1395	27.1694	-3.1336
23.0160	-3.1475	25.1535	-3.1230	27.1785	-3.1346
23.0313	-3.1309	25.1694	-3.1412	27.1882	-3.1395
23.0424	-3.1119	25.1792	-3.1375	27.2097	-3.1308
23.0528	-3.1256	25.1889	-3.1293	27.2264	-3.1276
23.0632	-3.1319	25.1979	-3.1155	27.2424	-3.1356
23.0729	-3.1359	26.0104	-3.1344	27.2535	-3.1378
23.0826	-3.1407	26.0194	-3.1250	27.2639	-3.1340
23.0924	-3.1428	26.0271	-3.1242	27.2736	-3.1337
23.1021	-3.1382	26.0375	-3.1300	27.2840	-3.1360
23.1125	-3.1365	26.0465	-3.1358	27.2931	-3.1445
23.1229	-3.1283	26.0556	-3.1334	27.3021	-3.1405
23.1333	-3.1231	26.0653	-3.1484	27.3118	-3.1232
23.1431	-3.1195	26.0757	-3.1367	27.3215	-3.1293
23.1694	-3.1384	26.0861	-3.1348	27.3306	-3.1318
23.1799	-3.1338	26.0951	-3.1372	27.3417	-3.1454
23.1965	-3.1329	26.1056	-3.1361	27.3493	-3.1434
23.2229	-3.1386	26.1153	-3.1284	27.3549	-3.1500
23.2340	-3.1351	26.1250	-3.1254	28.0590	-3.1365
23.2444	-3.1368	26.1410	-3.1341	28.0688	-3.1262
23.2549	-3.1310	26.1535	-3.1414	28.0792	-3.1237
23.2667	-3.1248	26.1653	-3.1332	28.0917	-3.1295
23.2785	-3.1390	26.1750	-3.1412	28.1014	-3.1302
23.2889	-3.1449	26.1854	-3.1416	28.1125	-3.1354
23.3000	-3.1452	26.2028	-3.1333	28.1243	-3.1428
23.3097	-3.1290	26.2542	-3.1392	28.1354	-3.1406
23.3189	-3.1302	26.2639	-3.1419	28.1465	-3.1311
23.3265	-3.1364	26.2736	-3.1406	28.1563	-3.1245
23.3389	-3.1385	27.0104	-3.1405	28.1660	-3.1317
25.0090	-3.1232	27.0201	-3.1438	28.1771	-3.1310
25.0201	-3.1292	27.0306	-3.1470	28.1861	-3.1327
25.0299	-3.1319	27.0403	-3.1446	28.2563	-3.1210
25.0389	-3.1367	27.0507	-3.1310	28.2653	-3.1290
25.0479	-3.1430	27.0618	-3.1227	28.2743	-3.1436
25.0569	-3.1444	27.0722	-3.1377	28.2833	-3.1368
25.0674	-3.1366	27.0833	-3.1379	28.2917	-3.1316
25.0764	-3.1365	27.0951	-3.1362	28.3014	-3.1334
25.0854	-3.1339	27.1007	-3.1324	28.3111	-3.1367
25.0951	-3.1412	27.1111	-3.1349	28.3201	-3.1422
25.1049	-3.1288	27.1222	-3.1404	28.3292	-3.1480
25.1139	-3.1274	27.1389	-3.1297	28.3396	-3.1354
25.1236	-3.1414	27.1507	-3.1290	28.3472	-3.1292
25.1333	-3.1361	27.1597	-3.1363	28.3583	-3.1268

APPENDIX 7.1, CONTINUED

UNIVERSAL TIME	MAGNITUDE	UNIVERSAL TIME	MAGNITUDE	UNIVERSAL TIME	MAGNITUDE
28.3639	-3.1346	29.1375	-3.1311	29.2722	-3.1457
29.0444	-3.1321	29.1493	-3.1377	29.2819	-3.1415
29.0528	-3.1307	29.1583	-3.1301	29.2917	-3.1453
29.0625	-3.1334	29.1688	-3.1357	29.3007	-3.1223
29.0722	-3.1381	29.1785	-3.1419	29.3104	-3.1175
29.0840	-3.1331	29.1889	-3.1375	29.3208	-3.1436
29.0944	-3.1288	29.2083	-3.1244	29.3313	-3.1405
29.1056	-3.1335	29.2215	-3.1222	29.3410	-3.1295
29.1153	-3.1312	29.2528	-3.1371	29.3500	-3.1261
29.1271	-3.1333	29.2639	-3.1403	29.3597	-3.1381
				29.3660	-3.1514

APPENDIX 7.2

DATA FOR WZ SCULPTORIS

UNIVERSAL TIME	MAGNITUDE	UNIVERSAL TIME	MAGNITUDE	UNIVERSAL TIME	MAGNITUDE
14.0174	-2.5729	14.1854	-2.5561	15.0014	-2.5461
14.0208	-2.5719	14.1882	-2.5559	15.0042	-2.5479
14.0285	-2.5747	14.2514	-2.5584	15.0097	-2.5553
14.0319	-2.5744	14.2542	-2.5563	15.0125	-2.5607
14.0375	-2.5688	14.2597	-2.5512	15.0160	-2.5602
14.0403	-2.5673	14.2625	-2.5485	15.0188	-2.5608
14.0444	-2.5647	14.2667	-2.5479	15.0229	-2.5616
14.0486	-2.5603	14.2694	-2.5499	15.0250	-2.5586
14.0535	-2.5530	14.2736	-2.5524	15.0292	-2.5616
14.0563	-2.5529	14.2771	-2.5505	15.0313	-2.5590
14.0604	-2.5487	14.2806	-2.5559	15.0368	-2.5590
14.0639	-2.5450	14.2833	-2.5633	15.0389	-2.5556
14.0688	-2.5423	14.2868	-2.5610	15.0431	-2.5615
14.0715	-2.5472	14.2896	-2.5670	15.0444	-2.5544
14.0778	-2.5494	14.2924	-2.5681	15.0507	-2.5566
14.0806	-2.5498	14.2951	-2.5695	15.0535	-2.5585
14.0861	-2.5532	14.3007	-2.5752	15.0569	-2.5574
14.0889	-2.5539	14.3035	-2.5751	15.0597	-2.5644
14.0931	-2.5619	14.3069	-2.5777	15.0632	-2.5676
14.0958	-2.5692	14.3104	-2.5756	15.0667	-2.5660
14.1000	-2.5741	14.3146	-2.5712	15.0701	-2.5648
14.1028	-2.5766	14.3174	-2.5707	15.0736	-2.5711
14.1076	-2.5791	14.3208	-2.5678	15.0771	-2.5751
14.1104	-2.5771	14.3236	-2.5672	15.0799	-2.5693
14.1167	-2.5786	14.3278	-2.5620	15.0833	-2.5732
14.1194	-2.5793	14.3306	-2.5534	15.0861	-2.5726
14.1236	-2.5806	14.3347	-2.5534	15.0917	-2.5687
14.1264	-2.5748	14.3382	-2.5558	15.0938	-2.5676
14.1319	-2.5633	14.3431	-2.5594	15.1042	-2.5588
14.1347	-2.5648	14.3458	-2.5592	15.1083	-2.5525
14.1361	-2.5607	14.3500	-2.5580	15.1125	-2.5514
14.1410	-2.5520	14.3528	-2.5583	15.1153	-2.5514
14.1438	-2.5562	14.3569	-2.5604	15.1194	-2.5513
14.1486	-2.5550	14.3597	-2.5562	15.1222	-2.5512
14.1521	-2.5567	14.3653	-2.5612	15.1271	-2.5552
14.1583	-2.5544	14.3681	-2.5651	15.1285	-2.5521
14.1611	-2.5572	14.3722	-2.5640	15.1313	-2.5555
14.1660	-2.5585	14.3743	-2.5571	15.1368	-2.5628
14.1681	-2.5589	14.3813	-2.5499	15.1403	-2.5660
14.1722	-2.5585	14.3840	-2.5589	15.1438	-2.5696
14.1750	-2.5561	14.3882	-2.5579	15.1465	-2.5712
14.1785	-2.5556	14.3917	-2.5536	15.1507	-2.5726
14.1819	-2.5554	14.9979	-2.5504	15.1535	-2.5743

APPENDIX 7.2, CONTINUED

UNIVERSAL TIME	MAGNITUDE	UNIVERSAL TIME	MAGNITUDE	UNIVERSAL TIME	MAGNITUDE
15.1563	-2.5764	15.3646	-2.5777	16.1840	-2.5562
15.1590	-2.5775	15.3674	-2.5725	16.1868	-2.5572
15.1632	-2.5816	15.3708	-2.5704	16.2451	-2.5617
15.1660	-2.5803	15.3736	-2.5666	16.2479	-2.5623
15.1708	-2.5759	15.3799	-2.5616	16.2576	-2.5591
15.1736	-2.5755	15.3826	-2.5614	16.2604	-2.5573
15.2243	-2.5529	15.9931	-2.5602	16.2667	-2.5601
15.2264	-2.5576	15.9965	-2.5588	16.2694	-2.5593
15.2319	-2.5577	16.0028	-2.5686	16.2771	-2.5573
15.2347	-2.5559	16.0056	-2.5664	16.2799	-2.5607
15.2382	-2.5567	16.0125	-2.5670	16.2868	-2.5629
15.2417	-2.5599	16.0153	-2.5689	16.2896	-2.5656
15.2451	-2.5564	16.0215	-2.5654	16.3028	-2.5647
15.2479	-2.5580	16.0313	-2.5643	16.3049	-2.5683
15.2514	-2.5624	16.0340	-2.5629	16.3111	-2.5691
15.2542	-2.5613	16.0403	-2.5608	16.3146	-2.5730
15.2583	-2.5683	16.0431	-2.5611	16.3208	-2.5739
15.2611	-2.5696	16.0514	-2.5644	16.3236	-2.5731
15.2646	-2.5683	16.0542	-2.5701	16.3299	-2.5748
15.2674	-2.5744	16.0611	-2.5634	16.3326	-2.5749
15.2729	-2.5760	16.0632	-2.5626	16.3382	-2.5698
15.2750	-2.5742	16.0694	-2.5617	16.3417	-2.5754
15.2792	-2.5706	16.0722	-2.5659	16.3493	-2.5604
15.2813	-2.5711	16.0792	-2.5648	16.3528	-2.5581
15.2854	-2.5701	16.0819	-2.5670	16.3590	-2.5601
15.2896	-2.5643	16.0882	-2.5637	16.3611	-2.5563
15.2931	-2.5606	16.0910	-2.5588	16.3688	-2.5509
15.2958	-2.5591	16.0972	-2.5554	16.3715	-2.5533
15.2993	-2.5543	16.1000	-2.5540	22.0042	-2.5770
15.3014	-2.5522	16.1049	-2.5621	22.0083	-2.5623
15.3056	-2.5581	16.1090	-2.5608	22.0132	-2.5564
15.3076	-2.5534	16.1153	-2.5638	22.0167	-2.5438
15.3125	-2.5544	16.1188	-2.5608	22.0208	-2.5367
15.3153	-2.5515	16.1243	-2.5669	22.0236	-2.5417
15.3201	-2.5576	16.1278	-2.5748	22.0271	-2.5416
15.3236	-2.5554	16.1354	-2.5762	22.0319	-2.5465
15.3271	-2.5631	16.1375	-2.5747	22.0375	-2.5529
15.3299	-2.5630	16.1444	-2.5702	22.0403	-2.5498
15.3361	-2.5684	16.1472	-2.5680	22.0444	-2.5584
15.3382	-2.5731	16.1535	-2.5648	22.0472	-2.5599
15.3424	-2.5721	16.1556	-2.5629	22.0521	-2.5647
15.3451	-2.5759	16.1618	-2.5579	22.0549	-2.5599
15.3486	-2.5782	16.1639	-2.5489	22.0583	-2.5631
15.3563	-2.5792	16.1694	-2.5499	22.0611	-2.5652
15.3590	-2.5836	16.1722	-2.5549	22.0660	-2.5775

APPENDIX 7.2, CONTINUED

UNIVERSAL TIME	MAGNITUDE	UNIVERSAL TIME	MAGNITUDE	UNIVERSAL TIME	MAGNITUDE
22.0701	-2.5773	22.2736	-2.5681	23.0792	-2.5478
22.0743	-2.5731	22.2778	-2.5677	23.0861	-2.5491
22.0785	-2.5712	22.2806	-2.5514	23.0903	-2.5489
22.0806	-2.5704	22.2854	-2.5543	23.0951	-2.5496
22.0847	-2.5681	22.2875	-2.5616	23.0993	-2.5515
22.0875	-2.5659	22.2917	-2.5584	23.1056	-2.5580
22.0917	-2.5596	22.2944	-2.5607	23.1097	-2.5658
22.0944	-2.5626	22.2993	-2.5627	23.1160	-2.5652
22.1000	-2.5565	22.3021	-2.5637	23.1201	-2.5679
22.1021	-2.5524	22.3063	-2.5639	23.1257	-2.5648
22.1069	-2.5486	22.3090	-2.5598	23.1299	-2.5682
22.1097	-2.5519	22.3139	-2.5563	23.1368	-2.5608
22.1153	-2.5602	22.3167	-2.5564	23.1403	-2.5652
22.1188	-2.5542	22.3222	-2.5577	23.1660	-2.5588
22.1229	-2.5508	22.3257	-2.5600	23.1729	-2.5514
22.1264	-2.5533	22.3306	-2.5644	23.1771	-2.5535
22.1319	-2.5555	22.3333	-2.5640	23.1924	-2.5544
22.1354	-2.5603	22.3375	-2.5680	23.2201	-2.5686
22.1472	-2.5596	22.3403	-2.5617	23.2271	-2.5718
22.1500	-2.5608	22.3451	-2.5610	23.2313	-2.5744
22.1542	-2.5623	22.3479	-2.5569	23.2375	-2.5760
22.1563	-2.5623	22.3521	-2.5555	23.2417	-2.5701
22.1604	-2.5638	22.3556	-2.5544	23.2472	-2.5670
22.1646	-2.5615	22.3597	-2.5605	23.2521	-2.5657
22.1681	-2.5633	22.3632	-2.5660	23.2576	-2.5587
22.1722	-2.5726	22.3660	-2.5649	23.2639	-2.5523
22.1778	-2.5637	22.3681	-2.5650	23.2715	-2.5465
22.1819	-2.5776	22.3708	-2.5772	23.2764	-2.5485
22.1868	-2.5754	22.3750	-2.5738	23.2819	-2.5514
22.1903	-2.5722	22.3778	-2.5783	23.2861	-2.5542
22.1958	-2.5649	22.9965	-2.5539	23.2924	-2.5594
22.1986	-2.5637	23.0007	-2.5559	23.2965	-2.5644
22.2042	-2.5650	23.0076	-2.5465	23.3028	-2.5715
22.2090	-2.5558	23.0125	-2.5556	23.3063	-2.5706
22.2174	-2.5512	23.0215	-2.5570	23.3125	-2.5714
22.2222	-2.5533	23.0257	-2.5574	23.3160	-2.5729
22.2319	-2.5552	23.0347	-2.5660	23.3215	-2.5716
22.2354	-2.5572	23.0389	-2.5715	23.3243	-2.5737
22.2444	-2.5679	23.0458	-2.5711	23.3319	-2.5601
22.2479	-2.5714	23.0500	-2.5736	23.3361	-2.5546
22.2521	-2.5770	23.0563	-2.5653	23.3417	-2.5632
22.2549	-2.5771	23.0597	-2.5648	23.3465	-2.5602
22.2590	-2.5772	23.0660	-2.5514	25.0021	-2.5603
22.2625	-2.5725	23.0701	-2.5452	25.0049	-2.5603
22.2701	-2.5694	23.0757	-2.5403	25.0125	-2.5592

APPENDIX 7.2, CONTINUED

UNIVERSAL TIME	MAGNITUDE	UNIVERSAL TIME	MAGNITUDE	UNIVERSAL TIME	MAGNITUDE
25.0167	-2.5608	26.0403	-2.5569	27.0417	-2.5642
25.0229	-2.5619	26.0438	-2.5600	27.0458	-2.5650
25.0264	-2.5632	26.0486	-2.5579	27.0549	-2.5747
25.0326	-2.5640	26.0528	-2.5546	27.0583	-2.5786
25.0361	-2.5585	26.0576	-2.5567	27.0653	-2.5730
25.0417	-2.5626	26.0611	-2.5601	27.0694	-2.5720
25.0451	-2.5655	26.0681	-2.5603	27.0757	-2.5637
25.0507	-2.5597	26.0722	-2.5636	27.0806	-2.5602
25.0549	-2.5654	26.0792	-2.5574	27.0882	-2.5569
25.0611	-2.5712	26.0833	-2.5589	27.0917	-2.5532
25.0646	-2.5723	26.0889	-2.5565	27.0979	-2.5520
25.0701	-2.5666	26.0924	-2.5608	27.1042	-2.5536
25.0736	-2.5722	26.0986	-2.5574	27.1083	-2.5581
25.0799	-2.5703	26.1028	-2.5608	27.1146	-2.5604
25.0826	-2.5693	26.1083	-2.5608	27.1194	-2.5653
25.0889	-2.5656	26.1125	-2.5677	27.1319	-2.5678
25.0924	-2.5660	26.1188	-2.5680	27.1368	-2.5648
25.0979	-2.5582	26.1222	-2.5676	27.1431	-2.5665
25.1014	-2.5563	26.1278	-2.5734	27.1479	-2.5648
25.1076	-2.5507	26.1375	-2.5720	27.1535	-2.5697
25.1111	-2.5466	26.1438	-2.5641	27.1569	-2.5670
25.1181	-2.5559	26.1486	-2.5550	27.1632	-2.5752
25.1215	-2.5584	26.1569	-2.5486	27.1667	-2.5718
25.1271	-2.5568	26.1625	-2.5506	27.1715	-2.5725
25.1306	-2.5652	26.1681	-2.5459	27.1750	-2.5714
25.1361	-2.5649	26.1722	-2.5537	27.1813	-2.5674
25.1410	-2.5730	26.1785	-2.5626	27.1861	-2.5682
25.1472	-2.5793	26.1819	-2.5574	27.1993	-2.5630
25.1507	-2.5773	26.1965	-2.5733	27.2056	-2.5547
25.1618	-2.5726	26.2007	-2.5787	27.2160	-2.5532
25.1660	-2.5672	26.2465	-2.5431	27.2222	-2.5507
25.1722	-2.5588	26.2514	-2.5444	27.2306	-2.5594
25.1764	-2.5546	26.2569	-2.5528	27.2396	-2.5735
25.1826	-2.5507	26.2611	-2.5556	27.2465	-2.5770
25.1861	-2.5454	26.2667	-2.5634	27.2507	-2.5785
25.1917	-2.5499	26.2708	-2.5684	27.2569	-2.5807
25.1951	-2.5449	26.2764	-2.5697	27.2674	-2.5732
26.0035	-2.5628	27.0035	-2.5651	27.2715	-2.5688
26.0076	-2.5713	27.0076	-2.5547	27.2778	-2.5629
26.0132	-2.5722	27.0139	-2.5523	27.2813	-2.5600
26.0167	-2.5690	27.0174	-2.5464	27.2868	-2.5480
26.0208	-2.5664	27.0236	-2.5529	27.2958	-2.5499
26.0243	-2.5566	27.0278	-2.5521	27.3000	-2.5485
26.0299	-2.5609	27.0333	-2.5543	27.3049	-2.5551
26.0347	-2.5562	27.0375	-2.5570	27.3090	-2.5530

APPENDIX 7.2, CONTINUED

UNIVERSAL TIME	MAGNITUDE	UNIVERSAL TIME	MAGNITUDE	UNIVERSAL TIME	MAGNITUDE
27.3146	-2.5625	28.2681	-2.5479	29.1347	-2.5566
27.3188	-2.5631	28.2722	-2.5490	29.1403	-2.5542
27.3236	-2.5634	28.2771	-2.5530	29.1438	-2.5561
27.3278	-2.5653	28.2806	-2.5569	29.1514	-2.5626
27.3347	-2.5613	28.2854	-2.5616	29.1556	-2.5685
27.3389	-2.5640	28.2889	-2.5669	29.1611	-2.5633
27.3444	-2.5624	28.2944	-2.5664	29.1660	-2.5682
27.3514	-2.5722	28.2986	-2.5676	29.1715	-2.5668
28.0521	-2.5621	28.3042	-2.5823	29.1757	-2.5642
28.0563	-2.5544	28.3083	-2.5828	29.1813	-2.5637
28.0625	-2.5567	28.3139	-2.5728	29.1861	-2.5647
28.0660	-2.5581	28.3174	-2.5704	29.1993	-2.5576
28.0722	-2.5560	28.3229	-2.5668	29.2042	-2.5595
28.0764	-2.5555	28.3264	-2.5642	29.2125	-2.5587
28.0847	-2.5528	28.3319	-2.5481	29.2160	-2.5617
28.0889	-2.5588	28.3361	-2.5750	29.2444	-2.5613
28.0944	-2.5649	28.3417	-2.5635	29.2493	-2.5636
28.0986	-2.5714	28.3451	-2.5596	29.2569	-2.5547
28.1042	-2.5657	28.3507	-2.5650	29.2618	-2.5531
28.1083	-2.5733	28.3549	-2.5615	29.2667	-2.5578
28.1167	-2.5709	28.3604	-2.5713	29.2701	-2.5599
28.1208	-2.5774	29.0458	-2.5663	29.2750	-2.5594
28.1278	-2.5677	29.0500	-2.5565	29.2799	-2.5648
28.1319	-2.5662	29.0556	-2.5553	29.2847	-2.5679
28.1382	-2.5642	29.0597	-2.5570	29.2889	-2.5752
28.1431	-2.5607	29.0653	-2.5626	29.2944	-2.5677
28.1493	-2.5609	29.0694	-2.5654	29.2979	-2.5628
28.1528	-2.5585	29.0771	-2.5679	29.3035	-2.5636
28.1590	-2.5636	29.0813	-2.5649	29.3069	-2.5564
28.1632	-2.5685	29.0875	-2.5657	29.3132	-2.5622
28.1688	-2.5714	29.0917	-2.5694	29.3174	-2.5525
28.1743	-2.5718	29.0972	-2.5669	29.3250	-2.5404
28.1799	-2.5725	29.1021	-2.5600	29.3292	-2.5421
28.1833	-2.5725	29.1083	-2.5583	29.3340	-2.5431
28.2493	-2.5625	29.1125	-2.5548	29.3382	-2.5539
28.2535	-2.5588	29.1194	-2.5529	29.3431	-2.5526
28.2590	-2.5520	29.1243	-2.5482	29.3472	-2.5540
28.2632	-2.5497	29.1299	-2.5526	29.3528	-2.5659
				29.3569	-2.5695
				29.3625	-2.5694

APPENDIX 7.3

DATA FOR XX SCULPTORIS

UNIVERSAL TIME	MAGNITUDE	UNIVERSAL TIME	MAGNITUDE	UNIVERSAL TIME	MAGNITUDE
14.0194	-.2366	14.1896	-.2322	15.0174	-.2390
14.0222	-.2425	14.2528	-.2579	15.0201	-.2444
14.0306	-.2508	14.2556	-.2585	15.0236	-.2451
14.0340	-.2575	14.2611	-.2636	15.0264	-.2379
14.0389	-.2242	14.2639	-.2593	15.0299	-.2396
14.0417	-.2484	14.2681	-.2534	15.0326	-.2373
14.0472	-.2355	14.2708	-.2414	15.0382	-.2427
14.0500	-.2396	14.2750	-.2375	15.0403	-.2424
14.0549	-.2359	14.2785	-.2351	15.0458	-.2412
14.0576	-.2403	14.2819	-.2278	15.0521	-.2441
14.0625	-.2425	14.2847	-.2342	15.0542	-.2393
14.0660	-.2483	14.2882	-.2292	15.0583	-.2463
14.0701	-.2450	14.2938	-.2380	15.0604	-.2490
14.0729	-.2300	14.2965	-.2409	15.0653	-.2425
14.0792	-.2473	14.3021	-.2507	15.0681	-.2422
14.0819	-.2486	14.3042	-.2547	15.0750	-.2403
14.0875	-.2415	14.3097	-.2601	15.0785	-.2378
14.0903	-.2383	14.3118	-.2557	15.0813	-.2364
14.0944	-.2449	14.3160	-.2580	15.0847	-.2438
14.0972	-.2484	14.3188	-.2556	15.0875	-.2376
14.1014	-.2486	14.3229	-.2514	15.0931	-.2464
14.1049	-.2535	14.3250	-.2467	15.0951	-.2467
14.1090	-.2565	14.3319	-.2338	15.1063	-.2390
14.1118	-.2532	14.3368	-.2328	15.1097	-.2402
14.1181	-.2587	14.3396	-.2394	15.1139	-.2382
14.1208	-.2572	14.3403	-.2396	15.1167	-.2459
14.1250	-.2547	14.3444	-.2402	15.1208	-.2378
14.1285	-.2465	14.3514	-.2517	15.1236	-.2492
14.1333	-.2397	14.3549	-.2565	15.1299	-.2525
14.1375	-.2378	14.3583	-.2556	15.1326	-.2553
14.1424	-.2415	14.3611	-.2602	15.1382	-.2514
14.1458	-.2412	14.3667	-.2498	15.1410	-.2549
14.1500	-.2464	14.3694	-.2468	15.1451	-.2454
14.1535	-.2499	14.3729	-.2375	15.1479	-.2468
14.1597	-.2522	14.3771	-.2371	15.1514	-.2466
14.1625	-.2532	14.3826	-.2279	15.1542	-.2417
14.1667	-.2543	14.3854	-.2235	15.1576	-.2385
14.1694	-.2510	14.3896	-.2184	15.1604	-.2396
14.1736	-.2443	14.9993	-.2473	15.1646	-.2392
14.1764	-.2362	15.0021	-.2420	15.1674	-.2484
14.1806	-.2364	15.0056	-.2483	15.1722	-.2479
14.1826	-.2320	15.0111	-.2442	15.1743	-.2502
14.1868	-.2255	15.0139	-.2487	15.2257	-.2401

APPENDIX 7.3, CONTINUED

UNIVERSAL TIME	MAGNITUDE	UNIVERSAL TIME	MAGNITUDE	UNIVERSAL TIME	MAGNITUDE
15.2278	-.2421	15.9944	-.2389	16.2618	-.2537
15.2333	-.2482	15.9972	-.2369	16.2681	-.2513
15.2361	-.2537	16.0042	-.2354	16.2708	-.2542
15.2403	-.2529	16.0069	-.2341	16.2785	-.2470
15.2431	-.2465	16.0139	-.2357	16.2813	-.2438
15.2465	-.2443	16.0160	-.2327	16.2882	-.2422
15.2486	-.2447	16.0229	-.2362	16.2910	-.2362
15.2535	-.2404	16.0257	-.2408	16.3042	-.2521
15.2556	-.2360	16.0326	-.2509	16.3063	-.2500
15.2597	-.2349	16.0417	-.2466	16.3132	-.2608
15.2625	-.2326	16.0444	-.2470	16.3160	-.2547
15.2660	-.2400	16.0528	-.2498	16.3222	-.2556
15.2688	-.2362	16.0556	-.2453	16.3243	-.2543
15.2743	-.2437	16.0625	-.2435	16.3313	-.2438
15.2764	-.2438	16.0646	-.2386	16.3333	-.2418
15.2799	-.2515	16.0708	-.2427	16.3403	-.2324
15.2826	-.2545	16.0736	-.2446	16.3424	-.2412
15.2882	-.2566	16.0806	-.2400	16.3438	-.2393
15.2910	-.2517	16.0833	-.2443	16.3507	-.2415
15.2944	-.2465	16.0896	-.2437	16.3542	-.2535
15.2965	-.2462	16.0924	-.2478	16.3604	-.2594
15.3000	-.2354	16.0986	-.2472	16.3625	-.2592
15.3028	-.2442	16.1014	-.2462	16.3701	-.2527
15.3063	-.2421	16.1076	-.2481	16.3729	-.2465
15.3090	-.2352	16.1104	-.2478	22.0063	-.2532
15.3139	-.2427	16.1167	-.2427	22.0104	-.2482
15.3160	-.2435	16.1201	-.2383	22.0153	-.2461
15.3222	-.2481	16.1257	-.2360	22.0181	-.2252
15.3243	-.2532	16.1285	-.2414	22.0222	-.2281
15.3285	-.2581	16.1361	-.2389	22.0250	-.2212
15.3326	-.2585	16.1389	-.2483	22.0299	-.2291
15.3375	-.2585	16.1458	-.2482	22.0333	-.2358
15.3396	-.2527	16.1479	-.2462	22.0389	-.2437
15.3438	-.2491	16.1542	-.2479	22.0417	-.2509
15.3465	-.2497	16.1569	-.2496	22.0458	-.2521
15.3507	-.2417	16.1625	-.2446	22.0486	-.2551
15.3528	-.2451	16.1646	-.2461	22.0535	-.2493
15.3576	-.2410	16.1708	-.2437	22.0563	-.2389
15.3604	-.2385	16.1729	-.2455	22.0597	-.2447
15.3660	-.2363	16.1854	-.2404	22.0632	-.2450
15.3688	-.2395	16.1875	-.2410	22.0688	-.2420
15.3722	-.2389	16.2465	-.2474	22.0715	-.2441
15.3750	-.2384	16.2493	-.2495	22.0757	-.2450
15.3813	-.2532	16.2507	-.2504	22.0792	-.2419
15.3840	-.2501	16.2590	-.2506	22.0826	-.2463

APPENDIX 7.3, CONTINUED

UNIVERSAL TIME	MAGNITUDE	UNIVERSAL TIME	MAGNITUDE	UNIVERSAL TIME	MAGNITUDE
22.0861	-.2477	22.2931	-.2392	23.1174	-.2363
22.0889	-.2495	22.2958	-.2473	23.1215	-.2364
22.0931	-.2536	22.3000	-.2445	23.1271	-.2458
22.0958	-.2563	22.3028	-.2488	23.1313	-.2387
22.1007	-.2547	22.3076	-.2555	23.1375	-.2531
22.1042	-.2439	22.3111	-.2489	23.1417	-.2442
22.1083	-.2367	22.3153	-.2464	23.1674	-.2485
22.1125	-.2339	22.3181	-.2446	23.1736	-.2458
22.1174	-.2333	22.3250	-.2492	23.1785	-.2433
22.1201	-.2367	22.3278	-.2491	23.1944	-.2394
22.1250	-.2398	22.3319	-.2416	23.2215	-.2493
22.1278	-.2432	22.3354	-.2430	23.2285	-.2497
22.1333	-.2499	22.3389	-.2392	23.2319	-.2480
22.1368	-.2501	22.3417	-.2449	23.2389	-.2412
22.1486	-.2499	22.3465	-.2430	23.2431	-.2405
22.1514	-.2493	22.3493	-.2411	23.2486	-.2381
22.1556	-.2444	22.3535	-.2439	23.2535	-.2363
22.1576	-.2402	22.3569	-.2478	23.2597	-.2407
22.1632	-.2362	22.3611	-.2465	23.2653	-.2517
22.1660	-.2316	22.3646	-.2498	23.2736	-.2493
22.1708	-.2339	22.3694	-.2441	23.2771	-.2434
22.1736	-.2469	22.3722	-.2457	23.2833	-.2407
22.1799	-.2488	22.3764	-.2524	23.2875	-.2365
22.1833	-.2507	22.9979	-.2327	23.2938	-.2312
22.1917	-.2479	23.0021	-.2280	23.2979	-.2344
22.1972	-.2445	23.0090	-.2355	23.3042	-.2438
22.2007	-.2436	23.0139	-.2416	23.3076	-.2446
22.2063	-.2501	23.0229	-.2470	23.3139	-.2484
22.2104	-.2434	23.0278	-.2435	23.3174	-.2489
22.2201	-.2435	23.0361	-.2332	23.3229	-.2450
22.2257	-.2453	23.0410	-.2408	23.3250	-.2444
22.2340	-.2503	23.0472	-.2381	23.3340	-.2375
22.2375	-.2440	23.0514	-.2208	23.3375	-.2383
22.2465	-.2439	23.0576	-.2432	23.3431	-.2473
22.2493	-.2483	23.0618	-.2441	23.3472	-.2558
22.2535	-.2389	23.0681	-.2400	25.0035	-.2397
22.2563	-.2451	23.0715	-.2433	25.0063	-.2326
22.2604	-.2472	23.0771	-.2455	25.0139	-.2365
22.2674	-.2376	23.0813	-.2505	25.0181	-.2444
22.2722	-.2501	23.0875	-.2468	25.0243	-.2533
22.2750	-.2450	23.0910	-.2444	25.0278	-.2580
22.2792	-.2428	23.0965	-.2416	25.0340	-.2611
22.2826	-.2403	23.1007	-.2451	25.0375	-.2548
22.2868	-.2355	23.1069	-.2377	25.0431	-.2471
22.2889	-.2406	23.1111	-.2417	25.0465	-.2432

APPENDIX 7.3, CONTINUED

UNIVERSAL TIME	MAGNITUDE	UNIVERSAL TIME	MAGNITUDE	UNIVERSAL TIME	MAGNITUDE
25.0521	-.2399	26.0736	-.2338	27.0701	-.2367
25.0556	-.2405	26.0806	-.2352	27.0771	-.2466
25.0618	-.2391	26.0847	-.2319	27.0813	-.2542
25.0653	-.2436	26.0903	-.2480	27.0896	-.2546
25.0708	-.2549	26.0938	-.2492	27.0931	-.2477
25.0750	-.2594	26.1000	-.2540	27.0993	-.2407
25.0806	-.2591	26.1042	-.2511	27.1056	-.2313
25.0840	-.2638	26.1097	-.2511	27.1097	-.2311
25.0896	-.2563	26.1139	-.2605	27.1167	-.2375
25.0931	-.2504	26.1201	-.2380	27.1208	-.2431
25.0993	-.2410	26.1236	-.2342	27.1340	-.2574
25.1028	-.2344	26.1292	-.2371	27.1375	-.2545
25.1090	-.2370	26.1389	-.2494	27.1444	-.2469
25.1125	-.2369	26.1458	-.2504	27.1493	-.2377
25.1194	-.2469	26.1500	-.2178	27.1542	-.2356
25.1229	-.2521	26.1521	-.2054	27.1583	-.2332
25.1278	-.2507	26.1590	-.2433	27.1639	-.2419
25.1319	-.2573	26.1632	-.2448	27.1681	-.2451
25.1382	-.2437	26.1694	-.2409	27.1729	-.2531
25.1424	-.2460	26.1736	-.2400	27.1764	-.2562
25.1486	-.2378	26.1792	-.2452	27.1826	-.2526
25.1521	-.2314	26.1840	-.2431	27.1875	-.2489
25.1632	-.2478	26.1979	-.2461	27.2028	-.2367
25.1674	-.2502	26.2014	-.2469	27.2076	-.2393
25.1736	-.2502	26.2479	-.2421	27.2194	-.2512
25.1778	-.2531	26.2528	-.2372	27.2243	-.2565
25.1833	-.2522	26.2583	-.2388	27.2333	-.2568
25.1875	-.2458	26.2625	-.2405	27.2410	-.2486
25.1931	-.2394	26.2681	-.2444	27.2479	-.2421
25.1965	-.2351	26.2722	-.2442	27.2521	-.2404
26.0049	-.2574	26.2778	-.2418	27.2583	-.2425
26.0083	-.2590	26.2924	-.2518	27.2625	-.2412
26.0139	-.2569	27.0049	-.2365	27.2688	-.2504
26.0181	-.2429	27.0090	-.2342	27.2729	-.2527
26.0215	-.2319	27.0153	-.2376	27.2792	-.2503
26.0257	-.2216	27.0188	-.2461	27.2826	-.2474
26.0313	-.2226	27.0250	-.2508	27.2882	-.2382
26.0354	-.2230	27.0292	-.2587	27.2917	-.2387
26.0417	-.2446	27.0347	-.2529	27.2972	-.2351
26.0451	-.2523	27.0389	-.2533	27.3007	-.2382
26.0500	-.2582	27.0431	-.2465	27.3063	-.2386
26.0542	-.2610	27.0479	-.2415	27.3097	-.2384
26.0590	-.2566	27.0563	-.2352	27.3160	-.2517
26.0632	-.2536	27.0604	-.2364	27.3194	-.2443
26.0701	-.2435	27.0667	-.2419	27.3250	-.2474

APPENDIX 7.3, CONTINUED

UNIVERSAL TIME	MAGNITUDE	UNIVERSAL TIME	MAGNITUDE	UNIVERSAL TIME	MAGNITUDE
27.3292	-.2408	28.2785	-.2450	29.1417	-.2503
27.3361	-.2460	28.2819	-.2418	29.1424	-.2479
27.3403	-.2398	28.2868	-.2469	29.1479	-.2346
27.3458	-.2445	28.2903	-.2439	29.1528	-.2331
27.3528	-.2461	28.3000	-.2557	29.1569	-.2367
28.0535	-.2520	28.3056	-.2593	29.1625	-.2320
28.0576	-.2617	28.3097	-.2543	29.1674	-.2381
28.0639	-.2593	28.3146	-.2481	29.1729	-.2407
28.0674	-.2549	28.3188	-.2369	29.1771	-.2452
28.0736	-.2423	28.3243	-.2348	29.1833	-.2572
28.0778	-.2399	28.3278	-.2403	29.1875	-.2533
28.0861	-.2328	28.3333	-.2397	29.2014	-.2346
28.0903	-.2298	28.3382	-.2467	29.2056	-.2347
28.0958	-.2395	28.3424	-.2548	29.2139	-.2302
28.0993	-.2482	28.3458	-.2629	29.2194	-.2442
28.1056	-.2472	28.3521	-.2515	29.2465	-.2504
28.1097	-.2554	28.3535	-.2653	29.2514	-.2486
28.1181	-.2506	28.3563	-.2622	29.2590	-.2433
28.1222	-.2509	28.3618	-.2679	29.2625	-.2368
28.1292	-.2363	29.0410	-.2655	29.2681	-.2463
28.1333	-.2387	29.0472	-.2501	29.2715	-.2423
28.1396	-.2285	29.0514	-.2374	29.2771	-.2339
28.1444	-.2382	29.0569	-.2314	29.2806	-.2425
28.1507	-.2469	29.0611	-.2164	29.2861	-.2569
28.1521	-.2505	29.0667	-.2401	29.2903	-.2496
28.1549	-.2585	29.0708	-.2410	29.2958	-.2481
28.1604	-.2650	29.0785	-.2522	29.2993	-.2397
28.1618	-.2610	29.0826	-.2602	29.3049	-.2385
28.1646	-.2609	29.0889	-.2528	29.3083	-.2448
28.1701	-.2515	29.0931	-.2491	29.3146	-.2478
28.1715	-.2513	29.0993	-.2361	29.3181	-.2379
28.1757	-.2458	29.1035	-.2243	29.3264	-.2329
28.1813	-.2423	29.1097	-.2226	29.3299	-.2378
28.1847	-.2357	29.1139	-.2294	29.3354	-.2441
28.2507	-.2541	29.1208	-.2340	29.3396	-.2408
28.2549	-.2514	29.1222	-.2397	29.3444	-.2325
28.2604	-.2465	29.1257	-.2433	29.3486	-.2426
28.2639	-.2448	29.1313	-.2623	29.3542	-.2462
28.2694	-.2423	29.1326	-.2614	29.3583	-.2391
28.2729	-.2415	29.1354	-.2618	29.3639	-.2493

APPENDIX 7.4

A FORTRAN VERSION OF THE JURKEVICH METHOD

```
      PROGRAM JURK(DATA,INPUT=DATA,OUTPUT)
C     THIS PROGRAM READS IN A SET OF X,Y VALUES AND FOR A SET OF PERIODS
C     CALCULATES A MODIFIED JURKEVICH INDEX.  THE ORIGINAL JURKEVICH INDEX
C     IS DESCRIBED IN JURKEVICH, I. 1971, ASTROPHYSICS AND SPACE SCIENCE
C     VOL. 13, PAGE 154.  THE MODIFICATIONS TO THIS INDEX ARE DESCRIBED IN
C     SECTION 3.2 OF THIS THESIS.  AS NOTED IN SECTION 3.2, THE BEST VALUE
C     FOR NTOTAL IS 3, AND THE BEST VALUE OF CONST IS 8*PI**2/27/NPOINTS
C     = 2.92433/NPOINTS .
C     TO TEST THIS PROGRAM, RUN IT ON THE FOLLOWING FIVE DATA POINTS:
C     (1.,1.),(2.,2.),(3.,3.),(4.,4.),(5.,5.) .  SET THE FOLLOWING VALUES
C     OF THE PARAMETERS IN THE PROGRAM:  NPOINTS=5, PSTART=1.0, PDELTA=0.25,
C     NPERIOD=10 .  THE OUTPUT SHOULD BE:
C     .1000E+01   0.
C     .1250E+01    .8773E+00
C     .1500E+01    .3509E+01
C     .1750E+01    .3509E+01
C     .2000E+01   0.
C     .2250E+01    .3509E+01
C     .2500E+01    .3509E+01
C     .2750E+01    .3509E+01
C     .3000E+01    .4874E+00
C     .3250E+01    .8773E+00
C
C     NPOINTS   NUMBER OF DATA POINTS TO BE READ IN.
C     X         X-VALUES OF THE DATA.
C     Y         Y-VALUES OF THE DATA.
C     PHI       PHASE OF EACH DATA POINT.
C     XAVE      AVERAGE OF THE VALUES OF X.
C     YAVE      AVERAGE OF THE VALUES OF Y.
C     PSTART    INITIAL PERIOD.
C     PDELTA    SPACING BETWEEN PERIODS.
C     NPERIOD   NUMBER OF PERIODS TO BE SEARCHED.
C     PERIOD    PERIOD.
C     RESULT    INDEX FOR THE PERIOD.
C     NTOTAL    TOTAL NUMBER OF BINS IN THE PHASE DIAGRAM.
```

```
C  BINDEX     VALUE OF THE INDEX IN EACH BIN.
C  CONST      MULTIPLICATIVE FACTOR FOR THE INDEX.
C  NBIN       INDICATES WHICH BIN EACH DATA POINT FALLS INTO.
C  ICOUNT     NUMBER OF DATA POINTS IN EACH BIN.
C  IA         COUNTER FOR DO LOOPS.
C  IB         COUNTER FOR NESTED DO LOOPS.
C
      INTEGER IA,IB,NBIN,NPERIOD,NPOINTS,NTOTAL,ICOUNT(20)
      REAL CONST,PDELTA,PSTART,XAVE,YAVE
      REAL BINDEX(20),PERIOD(500),PHI(700),RESULT(500),X(700),Y(700)
C
C       INITIALIZE THE VALUES, AND READ IN AND AVERAGE THE DATA POINTS.
C
      NPOINTS=654
      PSTART=.05
      PDELTA=.00005
      NPERIOD=500
      NTOTAL=3
      CONST=2.92433/FLOAT(NPOINTS)
      XAVE=0.0
      YAVE=0.0
      DO 2 IA=1,NPOINTS
      READ 1,X(IA),Y(IA)
 1    FORMAT(2X,F7.4,F7.4)
      XAVE=XAVE+X(IA)
 2    YAVE=YAVE+Y(IA)
      XAVE=XAVE/FLOAT(NPOINTS)
      YAVE=YAVE/FLOAT(NPOINTS)
      DO 3 IA=1,NPOINTS
      X(IA)=X(IA)-XAVE
 3    Y(IA)=Y(IA)-YAVE
C
C  FOR EACH PERIOD, CALCULATE THE INDEX.
C
      DO 8 IA=1,NPERIOD
```

APPENDIX 7.4, CONT.

```
      PERIOD(IA)=PSTART+PDELTA*FLOAT(IA-1)
      DO 4 IB=1,NTOTAL
      ICOUNT(IB)=0
      BINDEX(IB)=0.0
      DO 5 IB=1,NPOINTS
      PHI(IB)=AMOD(X(IB)/PERIOD(IA),1.0)
      IF(PHI(IB).LT.0.0) PHI(IB)=PHI(IB)+1.0
      NBIN=IFIX(FLOAT(NTOTAL)*PHI(IB))+1
      IF(NBIN.EQ.(NTOTAL+1)) NBIN=NBIN-1
      ICOUNT(NBIN)=ICOUNT(NBIN)+1
      BINDEX(NBIN)=BINDEX(NBIN)+Y(IB)
      DO 6 IB=1,NTOTAL
      IF (ICOUNT(IB).NE.0) BINDEX(IB)=BINDEX(IB)**2/FLOAT(ICOUNT(IB))
      RESULT(IA)=0.0
      DO 7 IB=1,NTOTAL
      RESULT(IA)=RESULT(IA)+BINDEX(IB)
      RESULT(IA)=RESULT(IA)*CONST
C
C     PRINT OUT THE RESULTS.
C
      DO 10 IA=1,NPERIOD
      PRINT 9,PERIOD(IA),RESULT(IA)
      FORMAT(E12.4,E12.4)
      CONTINUE
      STOP
      END
```

APPENDIX 7.5

THE NON-LINEAR LEAST-SQUARES PROGRAM

This appendix gives instructions on how to fit the equation $y(x) = A + B\sin(Cx + D) + E\sin(Fx + G)$ to a set of data using the method of least squares. First, ask the computer centre to make available the non-linear regression program BMDP3R, a library program in the Biomedical Statistical Package from the University of California, Los Angeles. Put it into a data file called BMDP3R. Then create the following six files:

NONLIN :

```
/JOB
/NOSEQ
ATFN,CM200000,T20.
/READ,MYACCT
MODE(0)
/READ,MYFILE
ATTACH,BMDPLIB/UN=LIB.
GET,BMDP3R/UN=SMGR151.
FTN,L=OUT,PL=15000,A.
LDSET,PRESET=0.
LDSET,LIB=BMDPLIB.
LOAD,LGO.
BMDP3R.
GOTO,1.
EXIT.
1,DAYFILE,DF.
REPLACE,DF/NA.
IFE,EF.EQ.0,THEN.
NOTIFY. JOB SUCCESSFUL.
ELSE,THEN.
NOTIFY. JOB FAILED.
ENDIF, THEN.
REPLACE,OUT/NA.
REPLACE,OUTPUT=RESULT/NA.
/EOR
/READ,FUN
/EOR
/READ,CNTRL
/EOF
```

FUN:

```
      SUBROUTINE FUN(F,D,P,X,N)
       DIMENSION D(7),P(7),X(7)
       F=P(1)+P(2)*SIN(P(3)*X(1)+P(4))+P(5)*SIN(P(6)*X(1)+P(7))
       D(1)=1.
       D(2)=SIN(P(3)*X(1)+P(4))
       D(3)=P(2)*X(1)*COS(P(3)*X(1)+P(4))
       D(4)=P(2)*COS(P(3)*X(1)+P(4))
       D(5)=SIN(P(6)*X(1)+P(7))
       D(6)=P(5)*X(1)*COS(P(6)*X(1)+P(7))
       D(7)=P(5)*COS(P(6)*X(1)+P(7))
       RETURN
       END
```

CNTRL:

```
PROBLEM     TITLE IS "PERIOD SEARCH"./
INPUT       VARIABLES ARE 2.
         UNIT IS 9.
            CASES ARE 654.
            FORMAT IS "(2X,2F7.4)"./
VARIABLE    NAMES ARE TIME,AMP./
REGRESSION  TITLE IS "AMP VERSUS TIME".
             HALVING IS 50.
             ITERATION IS 30
            DEPENDENT IS AMP.
            NUMBER IS 1.
            PARAMETERS ARE 7./
PARAMETER   NAMES ARE A,B,C,D,E,F,G.
            INITIAL ARE -.2,.01,128.42,1.57,.005,116.07,2.6.
          MINIMUMS ARE -10.,-10.,-10.,-10.,-10.,-10.,-10.0.
        MAXIMUMS ARE 200.,200.,200.,200.,200.,200.,200.0./
/END
/FINISH
```

MYACCT:

```
            USER(SMGR151,ARGHH)
```

MYFILE:

```
              GET,PTAPE=IN.
```

IN:

```
XX14.0194 -.2366
XX14.0222 -.2425
XX14.0306 -.2508
XX14.0340 -.2575
XX14.0389 -.2242
XX14.0417 -.2484
XX14.0472 -.2355
  :       :      :
  :  646 lines   :
  :       :      :
XX29.3639 -.2493
```

NONLIN calls all the other data files and the BMDP3R program. FUN contains the function and its partial derivatives. CNTRL gives the number of data points to be fitted (654 in this case), the format of the data and the initial values for the parameters. These lines must be changed to suit the data as given in IN and to suit the estimated values of the parameters. MYACCT lists the user's account name and password, and MYFILE gives the name of the file containing the input. IN contains the data.

To run the program, type:

```
OLD,NONLIN.
SUBMIT,NONLIN.
```

The output will appear in a file called RESULT. A file called DF will also be created, containing the dayfile for the computer run. If the program doesn't work, DF will contain diagnostics of the problem.

REFERENCES

Allen, C.W. 1973, Astrophysical Quantities (3rd Edition) Univ. of London, The Althone Press.

Andersen, N. 1974, Geophys. 39, 69.

———————— 1978, private communication to J. R. Percy.

Baglin, A., Breger, M., Chevalier, C., Hauck, B., le Contel, J.M., Sareyan, J.P., and Valtier, J.C. 1973, Astron. and Astrophys. 23, 221.

Breger, M. 1975, Variable Stars and Stellar Evolution, IAU Colloq. No. 67, p. 231.

———————— 1979, P.A.S.P. 91, 5.

Burg, J.P. 1967, Paper presented at the 37th Annual International Society of Exploration Geophysics Meeting, Oklahoma.

Cannon, A.J., and Pickering, E.C. 1918, The Henry Draper Catalogue, Annals of the Astronomical Observatory of Harvard College 91.

Crawford, D.L., and Barnes, J.V. 1970, A.J. 75, 978.

Crawford, D.L., and Perry, C.L. 1966, A.J. 71, 206.

Deeming, T.J. 1975, Astrophys. Space Sci. 36, 137.

———————— 1976, Astrophys. Space Sci. 42, 257.

Demers, S. 1969, P.A.S.P. 81, 861.

Eggen, O.J. 1976, P.A.S.P. 88, 402.

Fitch, W.S. 1975, Multiple Periodic Variable Stars, IAU Colloq. No. 29, p. 167.

Gray, D.F., and Desikachary, K. 1973, Ap. J. 181, 523.

Herbst, W. 1975, A.J. 80, 498.

Hodson, S.W., Stellingwerf, R.F., and Cox, A.N. 1979, Ap. J. 229, 642.

Hoffleit, D. 1964, Catalogue of Bright Stars, Yale University Observatory.

Iriarte, B., Johnson, H.L., Michell, R.I., and Wisniewski, W.K. 1965, Sky and Telescope 30, 21.

Jurkevich, I. 1971, Astrophys. and Space Sci. 13, 154.

Kukarkin, B.V., Kholopov, P.N., Fedorovich, V.P., Frolov, M.S., Kukarkina, N.P., Kurochrin, N.E., Medvedeva, G.L., Perova, N.B., and Pskovsky, Yu.P. 1976, The Third Supplement to the Third Edition of the General Catalogue of Variable Stars, The Academy of Sciences of the U.S.S.R., Moscow.

Leung, K. 1970, A.J. 75, 643.

Michael, J.L., and Seeds, M.A. 1974, A.J. 79, 1091.

Nather, R.E. 1978, P.A.S.P. 90, 477.

Parenago, P.P. 1945, Astronomical Journal U.S.S.R. 22, 129.

Percy, J.R. 1975, Astron. and Astrophys. 43, 469.

———————— 1977, M.N.R.A.S. 181, 647.

Petersen, J.O. 1975, Multiple Periodic Variable Stars, IAU Colloq. No. 29, p. 195.

Petersen, J.O., and Jorgensen, H.E. 1972, Astron. and Astrophys. 17, 367.

Seeds, M.A., and Yanchak, G.A. 1972, The Delta Scuti Stars,

Bartol Research Foundation of the Franklin Institute, Swathmore, Pennsylvania.

Sharov, A.S. 1964, Sov. Astron. A.J. 7, 689.

Shobbrook, R.R., and Stobie, R.S. 1976, M.N.R.A.S. 174, 401.

Stellingwerf, R.F. 1978, Ap. J. 224, 953.

Stokes, N.R. 1972, M.N.R.A.S. 160, 155.

Swingler, D.N. 1979a, A Modified Burg Algorithm for Maximum Entropy Spectral Analysis, to be published in Proc. IEEE.

———————— 1979b, Burg's Maximum Entropy Algorithm vs. The Discrete Fourier Transform as a Frequency Estimator for Truncated Real Sinusoids, preprint.